UNIVERSITY OF CALGARY

Settling Rate of Asphaltenes and Solids from Diluted Bitumen

by

Yoshinori Casas

A THESIS

SUBMITTED TO THE FACULTY OF GRADUATE STUDIES

IN PARTIAL FULFILMENT OF THE REQUIREMENTS FOR THE

DEGREE OF MASTER OF SCIENCE

GRADUATE PROGRAM IN CHEMICAL ENGINEERING

CALGARY, ALBERTA

AUGUST, 2017

Abstract

One method to remove fine solids from bitumen prior to transportation is to add a paraffinic solvent to precipitate asphaltenes, which flocculate with the fine solids and enhance the settling rate. The process conditions, solvent type, and ratio of solvent to bitumen must be optimized to achieve practical settling rates while minimizing solvent and bitumen losses. A settling model was developed that requires the size distribution, density, and fractal dimension of the flocculated asphaltene/solids, and the density and viscosity of the fluid as inputs. Settling rates were measured using visual and sampling methods for three diluted bitumen mixtures: *n*-pentane/WC-B-A3, *n*-heptane/WC-B-A3 and *n*-heptane/WC-B-B2. The floc size distributions were measured using micrography and the Focused Beam Reflectance Method. Densities and viscosities were calculated from the component properties. The fractal dimension was determined from sediment volumes. The settling model predicted the settling rates to within 15%, except near the onset of precipitation.

Acknowledgements

Harvey Yarranton gave me one of the best opportunities and experiences in my life. I am extremely thankful for the opportunity to join his research group and to work under his supervision. His guidance and support have contributed to my professional and personal growth, from just answering silly questions to figuring out messy ideas and converting them into more logical sentences. I like his guidance using the right questions to show me the way. He is an amazing teacher that actually takes care of the wellbeing of his students.

To Elaine and Florian for their support in the lab. Elaine specially for helping me convert my Spanish-like English into more organized and grammatically correct English sentences. My writing process would have been much harder without her help. Florian was always willing to help me in my experiments with challenging questions and accepting our particle size analyzer where it should not be. I feel proud of you both. Thanks to you I could present better results to Harvey.

To my friends in the research group, especially Jairo Duran who was an important contributor in this work. We had many discussions about this project trying to understand what was going on with the data. Sharing ideas with him, I could better understand the meaning of my results. To Michaela, for always being there to listen to my ideas, failed translations and always helping me to improve my English. To the rest of you guys for always being there to have fun and laugh.

Thank you to Imperial Oil for providing the funding to develop this project. I hope all this information will be useful in future projects. To the Department of Chemical and Petroleum Engineering at the Schulich School of Engineering for providing the academic environment to perform my graduate studies. I want to recognize the support of former professor Alexander De Visscher who helped me solve problems in hard times and gave me a hand organizing events for graduate students in our department. To my evaluation committee for taking the time to evaluate what I have done.

This amazing achievement was possible with the support of all my family and friends. Although this thesis was a lot of "individual" work, I was able to do it because I had amazing people around me. They are always wishing me the best and expecting me to exceed my goals.

Dedication

To Isatlema, to challenge her to do something bigger than this.

To Carmenza, who has always loved me and felt proud of me.

To Jairo, for teaching me realistic lessons in life.

Table of Contents

List of Tables

List of Figures

ix

xii

List of Symbols and Nomenclature

Symbol	Definition
A	Area.
$°C$	Celsius degree.
$c_{2,mix}$	Viscosity parameter specific for each mixture.
d	Solid diameter (2-5).
d_i	Diameter of ith bin.
d_{imp}	Impeller diameter.
d_{floc}	Maximum diameter of the floc.
d_{LN}	Log number mean diameter.
d_m	Diameter of encasing sphere, maximum diameter.
d_n	Number mean diameter (2-18).
d_p	Diameter of primary particle in the floc.
d_v	Volume mean diameter (2-19).
D_f	Fractal dimension.
D_{f1}	Fractal dimension of the perimeter.
f_i	Number frequency of ith bin.
$f_{N,i}$	Calibrated number frequency.
$F(\alpha_f)$	Hindering effect as a function of the volume fraction of the fluid.
g	Gravitational constant 9.8 m/s^2.
h	Height.
h_t	Height of the floc at t time.
$h_{t+\Delta t}$	Height of the floc at t+Δt time.
L	Thickness of the layer.
m_A	Mass of precipitated asphaltene.
m_i	Mass of ith bin or ith floc.
m_j	Asphaltene mass in layer j.
m_{ij}	Mass of flocs of size i in layer j.
n	Number of sides of irregular polygon (2-1).
n	Hindering exponent in equation (2-16).
n	Number of layers in equation (5-1).
n_f	Number of particles in the floc (2-3).
n_i	Number of primary chord measurements in the ith bin.
n_{ij}	Number of flocs is size i in layer j.
n_{ij}^{mod}	Modeled number of flocs of size i in layer j.
n_T	Total number of primary chord measurements.
N	Total number of channels in equation 3-5.
N_f	Total number of flocs in the experiment.
P	Perimeter.
r_v	Ratio between the solid volume fraction in the void layer and the initial solid volume fraction.
T	Temperature.

t	Time.
u	Settling rate from Stokes' law.
u_h	Settling rate including floc porosity, drag coefficient and hindering effect.
u_i	Settling rate of ith floc.
u_0	Settling rate including floc porosity.
u_p	Settling rate including floc porosity and drag coefficient.
V_{act}	Actual volume of the particles in the floc.
V_{floc}	Spherical volume of the floc.
$V_{f,j}$	Volume occupied by the flocs in layer j.
V_i	Volume of ith bin or floc.
V_j	Volume of layer j.
V_{sed}	Uncompacted sediment volume.
w	Mass fraction.
w_i	Weighting factor.
$wt\%$	Percentage by weight.
$\#/sec$	Number of particles counted by the FBRM in one second.

Greek letters

α_f	Volume fraction of the fluid in layer j.
β_{12}	Binary interaction parameter equation 3-1.
β_{mix}	Correlation parameter between density and viscosity in the expanded fluid model.
γ	Particle size distribution calibration exponent.
Δ	Difference.
ε_j	Volume fraction of the particles not flocs in layer j.
$\varepsilon_{exp,j}$	Experimental volume fraction of the particles not flocs in layer j.
$\varepsilon_{model,j}$	Modeled volume fraction of the particles not flocs in layer j.
λ	Side length of irregular polygon.
κ	Brinkman permeability.
μ	Viscosity.
μ_0	Viscosity of diluted gas.
μ_m	Mixture viscosity.
v	Specific volume.
Ω	Drag coefficient.
$\bar{\phi}$	Average volume fraction in each experiment.
ϕ_{exp}	Experimental asphaltene volume fraction.
ϕ_{floc}	Porosity of the floc.
ϕ_{model}	Asphaltene volume fraction calculated with settling model.
ϕ_{void}	Solid volume fraction in the void layer.
ϕ_0	Initial solid volume fraction in the layer.
ρ_A	Asphaltene density.
ρ_{eff}	Effective density of the floc.

ρ_i	Density of ith floc.
ρ_s	Solid density.
ρ_m	Mixture density.
ρ_p	Primary particle density.
σ_d	Standard deviation.

Abbreviations

AARD	Average Absolute Relative Deviation.
EF	Expanded Fluid model.
FBRM	Focused Beam Reflectance Measurement.
H/C	Hydrogen / Carbon ratio.
OF	Optimization function to iterate D_f.
ppm	Parts per million.
RCF	Relative centrifugal force.
RD	Relative difference.

Chapter One: Introduction

1.1 Background

Oil is the world's main source of energy and as the population grows, the oil demand also increases. To supply the increasing demand, oil exploitation has moved from conventional to non-conventional oils. The latter includes heavy oils, extra heavy oils and oil sands (Gray, 2015). Oil sands are a mixture of viscous, high molar mass oil, referred to as bitumen, sand, and water (Gray, 2015; Masliyah *et al.*, 2004; Speight, 2013). One of the biggest oil sand deposits is found in Canada (BP, 2014).

The commercial processes in Canada for separating bitumen from the oil sands use two steps: hot water extraction followed by solvent froth treatment. The water extraction process, developed by Clark (1951), mixes hot water with the oil sands to separate bitumen from the sand matrix. A bitumen froth is obtained which is a mixture of bitumen, water, and fine solids (Masliyah *et al*., 2004). The typical composition of bitumen froth is 60 wt% bitumen, 30 wt% water, and 10 wt% solids (Long *et al.*, 2004; Zahabi *et al*, 2010). In solvent froth treatment, the froth is mixed with either a naphthenic or a paraffinic solvent. The addition of a naphthenic solvent reduces the viscosity and density of the bitumen to facilitate the separation of water and solids from the froth by centrifugation. After centrifugation, the diluted bitumen still contains approximately 1.0 wt% fine solids, mostly clays (Gray, 2015). The addition of a paraffinic solvent precipitates asphaltenes, the heaviest fraction of bitumen. The precipitated asphaltenes flocculate and collect the fine solids and water droplets from the froth (Long *et al*., 2002). The aggregates of asphaltenes, water, and solids settle and produce a pipeline quality bitumen with a water and solids content below 0.5 wt%. Although commercially successful, the aqueous extraction process requires a high amount of energy to heat the oil sands and water, and large tailings ponds are required to settle the suspended solids rejected from the process.

An alternative to aqueous extraction is a solvent based extraction process. A solvent based process requires no water and relatively little heat and therefore potentially reduces energy consumption and the need for tailings ponds. Solvent based extraction processes have been proposed since the

mid-1950s with different solvents and configurations (Speight, 1999). Recent studies in solvent extraction processes have increased the bitumen recovery up to 95 wt%. Nevertheless, solvent based extraction processes have not been commercialized because the solvent recovery is poor (Nikakhtari *et al.*, 2013; Osacky *et al.*, 2013) and the fine solids content in the bitumen product exceeds pipeline specifications (Pal *et al*., 2015).

Imperial Oil Ltd. proposed a non-aqueous process to extract bitumen from oil sands (Adeyinka and Speirs, 2010). The proposed process consists of two stages: coarse solids separation and fine solids separation. In the first stage, the oil sand is mixed with a solvent to decrease viscosity and density of the bitumen and to allow coarse solids and water to settle. In the second stage, a paraffinic solvent is added to precipitate asphaltenes and collect the fine solids. The flocs of asphaltenes and solids are then removed by gravity settling. The optimum conditions for the gravity settling have not yet been identified. If insufficient solvent is added, no asphaltenes will precipitate and consequently there will be no fine solids separation. However, if excess solvent is added, there will be high asphaltene precipitation and a large sediment with a corresponding loss of bitumen and solvent trapped in the sediment. Therefore, the target is a choice of solvent and an optimum amount of solvent that precipitates just enough asphaltenes to settle the flocs without significant bitumen and solvent losses. In other words, a rapid and complete separation must be achieved near the onset of asphaltene precipitation. The solvent must also be sufficiently volatile to recover most of the solvent from the rejected asphaltene and solids with an evaporation based method.

The factors controlling the settling of flocs are the diameter of the flocs, the porosity of the flocs, and the properties of the liquid medium. The viscosity and density of diluted bitumen have been investigated thoroughly and can be accurately modeled using the Expanded Fluid Model (Ramos-Pallares *et al.*, 2016; Saryazdi *et al.*, 2013). The size and structure of the flocculated material is less established. Asphaltenes precipitate as primary particles of approximately 1 μm but tend to immediately aggregate into flocs tens to hundreds of micrometers in diameter (Ferworn *et al.*, 1993; Rastegari *et al.*, 2004; Calles *et al.*, 2008; Daneshvar, 2005; Shafiee, 2014). These flocs are composed of asphaltenes, fine solids, and water, if present (Long *et al.*, 2002). The flocs have

irregular shapes (Ferworn *et al.*, 1993; Rahmani *et al.*, 2005; Shafiee, 2014) and follow a fractal relationship with size (Rahmani *et al.*, 2005a). The porosity of the flocs has been studied for model oils (Rahmani *et al.*, 2005a; Rahmani *et al.*, 2005b) and calculated for diluted bitumen (Daneshvar, 2005; Shafiee, 2014) using the fractal dimension. However, the porosity of flocs from diluted bitumen has not been systematically evaluated as a function of the solvent content and solvent type. Also, most of the size measurements have been performed at high solvent contents, far from the onset of asphaltene precipitation. Hence, size measurements close to the onset of asphaltene precipitation are required to study the effect of the solvent content and solvent type.

The settling rate of asphaltene flocs has been measured in model oils (Rahmani *et al.*, 2005b; Zahabi *et al.*, 2010) and bitumen froth (Kosior *et al.*, 2016; Long *et al.*, 2002, 2004; Zawala *et al.*, 2012). Rahmani *et al*. (2005b) studied the effect of mixing speed on the settling rate of individual flocs from a model oil. Zahabi *et al*. (2010) investigated the effect of the content of silica particles and solvent/bitumen (S/B) ratio on the settling rate of asphaltene flocs and found that the settling rate increased as either silica content or S/B ratio increased. Long *et al*. (2004) and Kosior *et al.* (2016) observed that the settling rate of asphaltene flocs increased with lighter solvents used to dilute bitumen froth and at higher temperature. The studies mentioned above were developed to treat froth bitumen from aqueous bitumen extraction.

While settling rate data for asphaltene flocs from model oil and diluted bitumen froth are available, there are no data for asphaltene flocs from diluted bitumen. The asphaltene flocs from diluted bitumen may behave differently than asphaltenes in solvent or diluted froth because the flocs in the froth contain water droplets and a large amount of solids and therefore they may have a different structure, flocculation rate, and settling rate than the asphaltene flocs in diluted bitumen. In addition, there are not data for the size and porosity of asphaltene flocs near the onset of precipitation in different solvents. Such data are essential for the development of new solvent based extraction methods.

1.2 Objectives of this Thesis

This thesis is part of a larger project investigating the precipitation of asphaltenes and flocculation and settling of asphaltenes and fine solids from solvent diluted bitumen. The thesis focuses on the measurement and modeling of the settling of flocculated asphaltenes and fine solids. The size distribution and porosity of the flocs, and the properties of the liquid medium are either measured or reported as required to model settling. Two different bitumens and two paraffinic solvents (*n*-pentane and *n*-heptane) are evaluated. These solvents were selected because the industrial solvents commonly used to precipitate asphaltenes from bitumen are a mixture of paraffinic solvents predominantly consisting of components from carbon number 5 to 7. The emphasis is towards conditions near the onset of asphaltene precipitation.

Specific objectives are:

- to measure the onset of asphaltene precipitation (precipitate mass/bitumen mass) of two bitumen samples diluted with *n*-pentane and *n*-heptane with the asphaltenes precipitated at different solvent contents.
- to determine the particle size distributions of the flocs from the same systems.
- to determine the fractal dimensions of the flocs from the same systems.
- to measure and model the settling rate of asphaltene flocs from the same systems.
- to evaluate if asphaltene flocs and fine solids settle together close to the onset of asphaltene precipitation.
- to develop a settling model for flocculated asphaltenes in diluted bitumen.

The settling model must be suitable for industrial application based on data that can be collected for those systems.

Note: The floc size and fractal dimension were measured at a single fixed mixing condition. The effect of shear rate was not investigated because it was only necessary to obtain the size and fractal dimension for input into the settling model.

1.3 Thesis Structure

This thesis is organized into six chapters. Chapter 2 reviews oil sands composition and how bitumen is extracted from the oil sands using aqueous and non-aqueous processes. This chapter also discusses the precipitation of asphaltenes and their flocculation into fractal structures. Finally, fundamentals of the settling of solids in liquids are introduced and the literature on the settling of asphaltene flocs is reviewed.

Chapter 3 describes the experimental methods starting with the chemicals and materials used. The following procedures are described: the measurement of asphaltene yield curves and toluene insoluble (fine solids) content; the preparation of mixtures of solvent and bitumen for the flocculation and settling experiments; the measurement of the floc size distribution using both micrography and Focused Beam Reflectance Measurement (FBRM); the measurement of settling from direct observation and with a sampling method.

Chapter 4 presents the settling model adapted from Valinasad (2006) and Saadatmand (2008) and its main assumptions. The settling process was modeled using Stokes' Law, modified to include polydisperse particles, porous particles and hindered settling. The porosity of the flocs was related to the fractal dimension. The density and viscosity of the medium were determined from the bitumen and solvent properties, density mixing rules, and the Expanded Fluid viscosity model. The model algorithm uses Euler's method and can be fitted to either settling data to determine the fractal dimension of the flocs or used to predict the settling rate given a known fractal dimension.

Chapter 5 presents the results and discussion for two bitumen samples diluted with *n*-pentane and *n*-heptane. Yield curves, floc size distributions, and settling rates in diluted bitumen are reported and their relation to solvent type, solvent content, and bitumen sample is discussed. The settling model is used to determine the fractal dimension and the results are compared with independent measurements.

Chapter 6 summarizes the main findings of this work and presents recommendations for the next steps in this project and for modifications to the settling model.

Chapter Two: Literature Review

This thesis is concerned with settling fine solids from a non-aqueous oil sands extraction process with the aid of asphaltenes precipitated from diluted bitumen. This chapter provides a background on oil sands composition and bitumen chemistry with a focus on asphaltenes, including self-association, precipitation, and flocculation. The fractal nature of asphaltene flocs is an important factor in settling and is also discussed. Bitumen extraction processes are summarized with a focus on the challenges in developing non-aqueous extraction methods, in particular the removal of fine solids. Finally, the principles of settling particles are reviewed considering variables such as porosity, permeability, particle concentration, and size polydispersity. The literature related to settling flocculated asphaltenes is reviewed.

2.1 Oil Sands

Alberta's bitumen resources are the third largest proven oil deposit in the world and are located in three main geological zones: Athabasca, Peace River, and Cold Lake (Masliyah *et al*., 2004; Tan *et al*., 2016). The deposit contains 28 billion cubic meters of recoverable bitumen reserves, of which 6 billion are shallow enough to be mined (AER, 2015). The deeper deposits are recovered with *in situ* methods such as steam assisted gravity drainage and cyclic steam stimulation (Brandt *et al.*, 2013; Speight, 2006).

This thesis is concerned with mineable bitumen commonly referred to as oil sands. Oil sands are a complex, naturally-occurring mixture of bitumen, sand, fine solids and clays, other minerals and water (Gray, 2015) with typical compositions shown in Table 2.1. The Alberta's oil sands are generally believed to contain hydrophilic solid grains surrounded with a thin layer of water separating them from the bitumen (Masliyah *et al*., 2004; Czarnecki *et al*., 2005; Speight, 2013). The bitumen and solids are relevant for the thesis and are discussed in more detail below.

Table 2.1. Oil sands composition (Gray, 2015; Hooshiar *et al.*, 2012)

Component	Composition (wt%)
Bitumen	4-18
Sand	55-80
Fine solids (<44 µm)	5-34
Water	2-15

2.1.1 Bitumen

Bitumen is a naturally occurring highly viscous material that is immobile under reservoir conditions and cannot be recovered from a well by conventional techniques. By definition, bitumen has a specific gravity greater than unity and a viscosity above 100,000 mPa.s at ambient conditions (Gray, 1994). Bitumen is a complex mixture of hydrocarbon based species, many of which include nitrogen, oxygen, and sulfur groups and metallic constituents (Speight, 2013). The carbon content of bitumen ranges from 80 to 85 wt% and the hydrogen content ranges from 5 wt% in heavy fractions to 12-14 wt% in light fractions. The remaining elemental composition includes nitrogen, oxygen, sulfur and metals such as vanadium, nickel and iron present within organic structures (Gray, 2015; Speight, 1998). The elemental composition of three Canadian bitumens are presented Table 2.2.

Table 2.2. Elemental composition (*wt*%) and H/C molar ratio of three Canadian bitumens (Gray, 2015).

Bitumen	Origin	C	H	N	O	S	H/C molar ratio
Athabasca	Syncrude	83.1	10.6	0.4	1.1	4.8	1.53
Athabasca	Suncor	83.9	10.5	0.4	1.0	4.2	1.50
Cold Lake	-	83.7	10.4	0.4	1.1	4.4	1.49

The number of chemical species in bitumen is vast, more than tens or perhaps hundreds of thousands (McKenna *et al*., 2013). Hence, a complete molecular description is challenging.

However, the functional groups that constitute these species have been identified. The hydrocarbon groups are straight chain and branched paraffins, mono and polynuclear naphthenes, and mono and polynuclear aromatics. The heteroatomic groups in bitumen include, but are not limited to, sulfur within aromatic rings, organic sulfides, derivatives of pyrrole and pyridine, carboxylic acid, and esters. The metals include vanadium and nickel compounds occurring mainly as substituted porphyrins (Gray, 2015).

While conventional crude oils are often characterized based on their boiling point or carbon number distributions, only 20 to 30 wt% of a bitumen can be characterized with these methods (Castellanos *et al.*, 2014). The remainder is non-distillable nor can it be fractionated using gas chromatography. Instead, bitumen is commonly characterized based on solubility and adsorption classes, specifically the SARA fractions: saturates, aromatics, resins, and asphaltenes (Gray, 2015; Nomura *et al.*, 2004). The saturate fraction contains only aliphatic compounds such as paraffins and naphthenes. The aromatic fraction contains structures with at least one aromatic group which may also incorporate saturated and heteroatomic groups. Saturates and aromatics are the lowest molecular weight fractions of the crude oil. The resins and asphaltenes are similar to the aromatics but have progressively higher molecular weight, aromaticity, polarity, heteroatom content, and metallic content (Gray, 2015). The aromatics, resins, and asphaltenes are a continuum of polynuclear aromatic species and the division between each fraction depends on the method used to separate the fractions. The asphaltenes, or at least some of their constituents, are known to self-associate. Asphaltenes are relevant for this thesis and are discussed in more detail later.

2.1.2 Inorganic Solids

The inorganic matrix of the oil sands is a mixture of sand and clay particles ranging in size from less than 0.2 μm to more than 100 μm. The particles are classified as coarse (> 44 μm), fine (0.2 to 44 μm) and ultrafine (< 0.2 μm) loosely based on their ease of processing. The coarse solids consist mainly of coarse grained quartz particles. The fine solids are a mixture of fine grained quartz (2 to 44 μm diameter) and clays (0.2 to 2 μm), (Kaminsky *et al.*, 2008). The ultrafines are clays (Tu *et al*., 2005). The composition of the clays in oil sands vary across the deposit but the main mineral structures are kaolinite, illite, smectite and chlorite. Kaolinite and illite are the most

abundant making up approximately 30 and 45 wt% of the clay material, respectively (Hooshiar *et al*., 2012; Osacky *et al.*, 2013).

The coarse solids in oil sands are believed to be water-wet at least *in situ* (Dang-Vu *et al.*, 2009). The fine solids in the oil sands appear to have an intermediate wettability. For example, fine solids recovered from the oil sands using a solvent based process have contact angles of 80-88°. SEM-FIB analysis suggests a partial organic coating on the surface of the solids (Nikakhtari *et al.*, 2014). The coating can be partially removed with toluene washing suggesting that the fine solids are covered with asphaltenes (Pal *et al.*, 2015). The greater the bitumen-solids interaction, the more organics adsorb, and the higher the hydrophobicity of the solids. Note that the wettability of the solids may be altered during processing and when they are removed from the oil sands because the organics may adsorb or desorb depending on the surrounding medium and temperature.

2.2 Asphaltenes

Asphaltenes are the most complex fraction of bitumen. They are defined as the components of a crude oil insoluble in *n*-alkanes such as *n*-pentane and *n*-heptane, and soluble in toluene. Asphaltenes are a solubility fraction, not a pure component, and contain tens or hundreds of thousands of molecular species (Gray, 2015; Powers *et al*., 2016; Yarranton, 2005). Asphaltenes consist of approximately 80 wt% carbon and 7.5 wt% hydrogen (Fenistein *et al.*, 1998). While the functional groups that make up an asphaltene molecule are known, the range of structures in the asphaltenes is a matter of speculation. Two main structures have been proposed: 1) the continental structure, a polynuclear aromatic core surrounded by small alkyl chains; 2) the archipelago structure, dispersed aromatic clusters linked with alkyl chains. It is likely that both structural motifs exist in crude oils (Mullins *et al.*, 2007; Podgorski *et al*., 2013; Speight, 2007; Yarranton *et al*., 2013).

Asphaltenes from different sources have similar elemental composition, functional groups, and density. The apparent molecular weight of the asphaltenes varies between different sources because they self-associate (Yarranton, 2005). The molar mass of the non-associated asphaltenes measured with vapor pressure osmometry (VPO) suggest a monomer molecular weight between

700 and 2,000 g/mol (Barrera *et al.*, 2013). FT-ICR mass spectrometry for the most abundant basic species span a range of 350 to 3000 g/mol (McKenna *et al.*, 2013). Mullins *et al.* (2008) reports monomer molecular weights for the asphaltenes between 500 and 1200 g/mol, based on a variety of methods.

2.2.1 Asphaltene Self-Association

Asphaltenes self-associate into nano-structures of tens of nanometers in diameter. VPO data gives number average molecular weights for asphaltene nano-aggregates between 2,000 to 10,000 g/mol (Agrawala and Yarranton, 2001; Barrera *et al*., 2013; Powers *et al*., 2016). SAXS experiments provide mass average molecular weights between 24,000 and 1.5 million g/mol (Fenistein and Barré, 2001;Yarranton *et al.*, 2013). The methods mentioned above confirm the broad distribution of asphaltene nano-aggregate molecular weights. However, the difference in the average asphaltene molecular weight between VPO and SAXS experiments is approximately 20 times. This discrepancy is beyond the difference between a number and a mass average and the source of the discrepancy is unknown. Yarranton *et al.*, (2013) speculated that the nano-aggregates may flocculate into larger structures detectable by SAXS but having no impact on VPO measurements.

Due to self-association, the molar mass of asphaltenes is not constant and depends on the asphaltene concentration, asphaltene cut, solvent, and temperature. (Agrawala and Yarranton, 2001; Barrera *et al*., 2013; McKenna *et al.*, 2013). As asphaltene concentration increases, the apparent molecular weight increases because there are more asphaltene molecules to self-associate. However, the molecular weight reaches an asymptote ranging from 1600 to 16000 g/mol at concentrations above 30 kg/m^3 (Barrera *et al*., 2013; Powers *et al.*, 2016). Asphaltenes precipitated with *n*-heptane have higher molar mass than those precipitated with *n*-pentane. Increasing temperature or using a better solvent for the asphaltenes decreases the self-association, reducing the apparent molecular weight of the asphaltenes. (Agrawala and Yarranton, 2001; Barrera *et al.*, 2013; Powers *et al*., 2016).

There are two main views on the nature of asphaltene self-association: the colloidal model and the oligomer model. The colloidal perspective considers that asphaltene molecules are held together

with π-π bonds as a nano-aggregate. This asphaltene core is surrounded by resins which peptize the core and maintain the asphaltenes in a colloidal dispersion within the bitumen. In some versions, it is proposed that the resin layer is covered by another layer of lighter molecules and it is these progressive layers which disperse the asphaltenes in the bitumen (Mullins *et al.*, 2007; Yudin *et al.*, 1998). When the bitumen is mixed with aliphatic solvents, the resin and light components are removed and the asphaltenes start to aggregate and precipitate (Chacón-Patiño *et al.*, 2015; Mostowfi *et al.*, 2009). This model fails to explain asphaltene dispersion in solvents like toluene and also the reversibility of asphaltene precipitation.

The oligomer view is an analogy to a polymer where the aggregate is held together by intermolecular forces (π-π bonds, acid-base interactions and hydrogen bonds) rather than covalent bonds. Agrawala and Yarranton (2001) assumed the self-associated asphaltene molecules were linked by van der Waals forces. They proposed that asphaltenes and resins consist of two classes of molecules: propagators and terminators. Propagators have multiple active sites, capable of linking with other molecules or aggregates. Terminators have a single active site, capable of linking with just one molecule and preventing further association. Asphaltenes consist primarily of propagators while resins consist primarily of terminators. The terminator/propagator aggregates act like macromolecules just like a polymer in a solution. This model is consistent with the solubilization of asphaltenes in solvents observed in VPO measurements. Further explanation and formulation of this model can be found elsewhere (Agrawala and Yarranton, 2001; Barrera *et al.*, 2013; Merino-Garcia *et al.*, 2004; Yarranton *et al.*, 2013).

2.2.2 Asphaltene Precipitation

Asphaltenes can precipitate with changes in pressure, temperature or composition (Hirschberg *et al.*, 1984; Maqbool *et al.*, 2009; Powers *et al.*, 2016). For the purposes of phase behavior modeling, asphaltenes are usually treated as macromolecules in solution with the oil and asphaltene precipitation as a conventional phase transition. At ambient temperatures, this phase transition corresponds to a sudden appearance of approximately 1 µm diameter particles (Ferworn *et al.*, 1993; Rastegari *et al.*, 2004; Shafiee, 2014) and is termed the onset of asphaltene precipitation. At temperatures above approximately 100°C, the asphaltenes separate as an asphaltene-rich liquid

phase (Agrawal *et al.*, 2012; Johnston *et al.*, 2017). Nevertheless, the onset of asphaltene precipitation changes very little with temperature. (Agrawal *et al.*, 2012)

Asphaltenes precipitate when bitumen or model oils are diluted with paraffinic solvents. The amount of precipitation decreases as: pressure increases (Akbarzadeh *et al*., 2005; Hirschberg *et al.*, 1984), the carbon chain in the paraffinic solvents increases from C5 to C9 (Akbarzadeh *et al.*, 2005; Alboudwarej *et al*., 2003; Wiehe *et al,* 2005), and temperature increases up to approximately 100°C (Akbarzadeh *et al.*, 2005; Calles *et al.*, 2008). There is some evidence that the amount of precipitation decreases above 100°C (Johnston *et al.*, 2017).

Asphaltene precipitation has been modeled with regular solution theory (Akbarzadeh *et al*., 2005; Alboudwarej *et al.*, 2003; Barrera *et al.*, 2013; Hirschberg *et al.*, 1984; Wang and Buckley, 2001). Regular solution theory has had success in modeling asphaltene precipitation from heavy oils diluted with solvent and from depressurized live oils. However, it is not applicable to other phase behavior encountered in these systems such as vapor-liquid equilibria. Cubic equations of state are often applied to crude oil phase behavior but, while they can be tuned to match the onset of precipitation, they fail to predict asphaltene yields (Agrawal *et al*., 2012; Castellanos *et al*., 2011; Johnston *et al.*, 2017). The Cubic Plus Association equation of state (CPA) has been able to predict asphaltene precipitation from model solutions and heavy oils diluted with *n*-alkanes (Arya *et al.*, 2017; Li and Firoozabadi, 2010). Finally, Statistical Associating Fluid Theory (SAFT) has been used to model asphaltene phase behavior (Panuganti *et al.*, 2013; Ting *et al.*, 2003). Although asphaltenes were modeled as a monodisperse species, the SAFT equation successfully predicted asphaltene instability and mixture bubble points from model oil and recombined oils (Ting *et al.*, 2003).

2.2.3 Asphaltene Flocculation
When asphaltenes precipitate as particles, the primary particles (approximately 1 µm diameter particles) tend to rapidly flocculate to form flocs with diameters up to several hundred micrometers (Daneshvar, 2005; Rastegari *et al.*, 2004; Shafiee, 2014), Figure 2.1. The asphaltene flocs are porous aggregates with irregular structures (Jarvis *et al.*, 2005; Rahmani *et al*., 2005a; Rastegari

et al., 2004; Seifried *et al.*, 2013). The spherical volume each floc occupies can be related to the number (or mass) of particles within the floc using a fractal relationship, as will be discussed in more detail later.
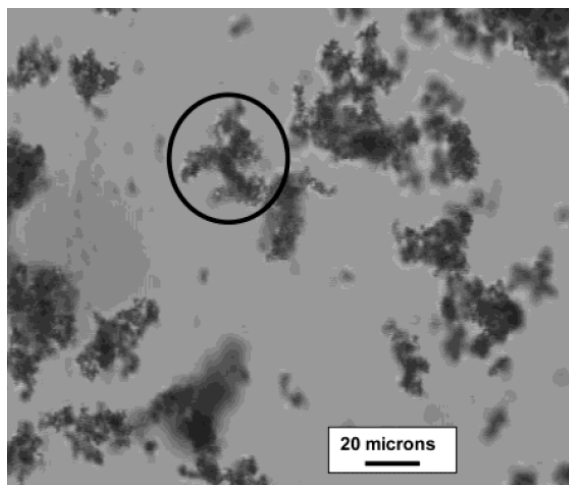
Figure 2.1. Asphaltene flocs from a solution of 0.1 g/L of asphaltenes in a mixture of 70 wt% heptane and 30 wt% toluene (Rastegari *et al.*, 2004).

Asphaltene floc size distributions have been measured using time of transmission (Ferworn *et al.*, 1993; Rastegari *et al.*, 2004), Focused Beam Reflectance Measurement (FBRM) (Calles *et al.*, 2008; Daneshvar, 2005; Shafiee, 2014), and Confocal Laser-Scanning Microscopy (Seifried *et al*., 2013) methods. The time of transmission and FBRM studies used raw data from the measurement technique (a chord length distribution) without calibration. Calles *et al*. (2008) used a probabilistic method to estimate the particle diameter distribution of the chord length distribution from the FBRM technique, assuming a spherical shape for the asphaltene flocs. The chord length distribution was shifted to longer sizes by a factor of 1.5 to 2.5. Comparing absolute results from different studies is challenging due to the difference between chord length and diameter distributions but also because number mean diameters are reported in some studies and volume mean diameters in other studies. Hence, the discussion below focuses on trends.

Ferworn *et al.* (1993) studied asphaltene particle sizes from six heavy crude oils diluted with *n*-heptane at 22°C and observed almost instantaneous asphaltene precipitation and unimodal floc size

distributions. The floc diameters in the volume distribution ranged from 4.5 to 291 μm. For *n*-heptane contents between 79 and 97 wt%, the average particle size increased as the solvent content increased. The asphaltene flocs were larger for oils with higher asphaltene content and molar mass.

Daneshvar (2005) measured the size of asphaltene flocs from bitumen diluted with *n*-heptane and *n*-pentane and observed significantly larger diameters in the poorer solvent, *n*-pentane. The volume mean diameter increased from 50 to 110 μm for *n*-heptane solvent contents ranging from 77 to 95 wt% and it was around 320 μm at 92 wt% solvent content for *n*-pentane. Seifried *et al.* (2013) confirmed this trend for crude oil diluted with *n*-hexane and *n*-heptane. They related the average floc size to the solubility parameter of the solvent. Their floc diameters ranged from 10 to 90 μm in *n*-hexane and from 10 to 30 μm in *n*-heptane. Shafiee (2014) measured floc sizes in *n*-heptane diluted bitumen and found that the volume mean diameter increased up to 170 μm as the *n*-heptane content increased to 85 wt% but decreased to 120 μm as the *n*-heptane content increased from 85 to 95 wt%.

Similarly, Calles *et al*. (2008) reported that the asphaltene floc sizes from a 190°C+ residue of a 31 API crude oil diluted with either *n*-pentane, *n*-hexane or *n*-heptane increased with increasing solvent content. They also found that the lighter the aliphatic solvent, the bigger the asphaltene flocs. Their particle number mean diameters ranged from 10 to 80 μm. Rastegari *et al.* (2004) obtained similar results for asphaltene flocs in model systems of asphaltenes/*n*-heptane and toluene. The floc diameters in the distribution ranged from 1 to 100 μm, increasing with asphaltene concentration, *n*-heptane content, and mixing rate.

Daneshvar (2005) found that the volume mean diameter increased with increasing temperature up to a maximum at 40-50 °C in *n*-heptane and then decreased at higher temperatures. They speculated that temperature had two effects: 1) the amount of precipitated asphaltenes decreased with increasing temperature tending to smaller flocs; 2) the stickiness of the flocs increased with temperature tending to larger flocs.

Both Daneshvar (2005) and Shafiee (2014) reported that the method used to dilute the bitumen affected the asphaltene floc size distribution. To avoid potential artifacts related to poor mixing, Shafiee (2014) recommended adding the solvent to the bitumen in two stages of mixing. For *n*-heptane diluted bitumen, Shafiee (2014) could not measure the particle size distribution close to the onset of asphaltene precipitation (55 wt% *n*-heptane), probably due to the opacity and stickiness of the asphaltene particles.

Asphaltene flocculation has been modeled with a Smoluchowski population balance coupled with a kinetic model (Rastegari *et al.*, 2004; Shafiee, 2014), diffusion-limited and reaction-limited aggregation (Burya *et al.*, 2001; Seifried *et al.*, 2013), and geometric population balance equations (Maqbool *et al.*, 2011; Rahmani, *et al.*, 2004).

2.3 Asphaltene Floc Structure and Fractal Dimension

Asphaltene flocs have been shown to follow a fractal relationship with size rather than having a constant porosity (Rahmani *et al.*, 2005a). Before discussing asphaltene flocs, the concept of the fractal dimension is presented.

In Euclidean geometry, the area occupied by a circle is the square of its diameter and the volume of a sphere is the cube of its diameter. Euclidean geometry does not apply to certain irregular solids such as coastlines and clouds. To describe irregular patterns, Mandelbrot introduced the fractal dimension, known initially as the Hausdorff-Besicovitch dimension (Mandelbrot, 1977). Irregular patterns described by the fractal dimension are called fractals. A more recent, straightforward definition by Mandelbrot clarified this concept: "A fractal is a shape made of parts similar to the whole in some way" (Feder, 1988). For example, to measure the perimeter of an irregular shape in two dimensions (coast of an island), it is possible to define a length, λ, to surround the perimeter n times, analogous to a polygon with n sides. The perimeter is related to this length as follows:

$$P_\lambda = \lambda n \tag{2-1}$$

For irregular shapes like a coastline, the measured perimeter increases as the λ length is reduced. Mandelbrot (1977) and Feder (1988) found that for different coasts and land frontiers, the λ length and the perimeter have a linear log-log relationship as follows.

$$\log(P) = (1 - D_{f1})\log(\lambda) + \log(k) \tag{2-2}$$

where D_{f1} is the fractal dimension for a perimeter. The fractal dimension defined by Equation 2.2 is for a line and can be considered as a one-dimensional (1D) fractal dimension.

Flocs are also considered as fractal objects if, for a large number of flocs, the mass plotted against size in a log-log plot has linear tendency (Elimenech *et al.*, 1998; Jarvis *et al.*, 2005). In this case, the fractal dimension is for an object and can be considered as a 3D fractal dimension. Note, only the 3D fractal dimension is used in this thesis and for convenience it is referred to simply as the fractal dimension. The fractal relationship for a floc is commonly expressed between the number of particles in the floc (proportional to the mass) and a floc diameter scaled to the particle size diameter as follows (Elimenech *et al.*, 1998; Jarvis *et al.*, 2005; Li and Logan, 2001; Rogak and Flagan, 1990):

$$\log n_f = D_f \log\left(\frac{d_{floc}}{d_p}\right) \tag{2-3}$$

or

$$n_f = \left(\frac{d_{floc}}{d_p}\right)^{D_f} \tag{2-4}$$

where n_f is the number of particles in the floc, and d_{floc} and d_p are the diameters of the floc and each primary particle within the floc, respectively. Note, if the flocs had constant porosity, the mass would be proportional to the size and would follow a linear log-log relationship with a fractal dimension of 3. If the fractal dimension is lower than 3, the porosity of the floc varies with size.

Rastegari *et al.* (2004) determined the fractal dimension of asphaltene flocs in solutions of toluene and *n*-heptane by fitting the measured floc size distribution and mass of asphaltene particles with a mass balance that included Equation (2-4). The fitted fractal dimension was 1.6. Rahmani *et al.* (2005a) determined the fractal dimension of asphaltene flocs in solutions of toluene and *n*-heptane from the slope of a log-log plot of aggregate settling velocity versus the longest dimension. The fractal dimension was between 1.06 and 1.41. In a follow-up study, Rahmani *et al.* (2005b) included the permeability of the asphaltene flocs and the projected area diameter instead of the

longest distance and estimated fractal dimensions between 1.3 and 2.0. Daneshvar (2005) and Shafiee (2014) determined the fractal dimension of asphaltene flocs in *n*-heptane diluted Athabasca bitumen based on the mass of precipitated asphaltenes and the volume occupied by the settled flocs. They reported fractal dimensions above 2 (Daneshvar, 2005) and up to 2.3 ± 0.1 with a slight dependence on *n*-heptane content (Shafiee, 2014).

2.4 Bitumen Extraction Processes

The nature of the particles or flocs to be settled depends on the type of process used to extract bitumen from the oil sands. The water based process is a well-established commercial process to extract bitumen from mined oil sands. This process has been used since 1967 when Suncor Oil Sand Division developed the Clark process at the commercial scale (Speight, 1999). While commercially successful, this technology has three negative impacts: it is energy intensive, has high water consumption, and creates tailings ponds (Osacky *et al.*, 2013; Speight, 1999). Non-aqueous extraction is an alternative process that can overcome these issues but has not yet been commercialized (Hooshiar *et al.*, 2012a; Hooshiar *et al.* , 2012b; Nikakhtari *et al.*, 2013, 2014; Wang *et al.*, 2013). Both aqueous and non-aqueous extraction methods are reviewed below.

2.4.1 Water Based Extraction Process

The Alberta oil sands up to 75 meters deep are shovelled from open mines and transported in trucks to the extraction plant (Speight, 2006; Wiehe, 2008). The oil sands are crushed at the plant inlet and mixed with hot water and in some cases with additives to create an alkaline environment. Hydrotransport may be used when the mines are further removed from the processing plant (Gray, 2015). In this case, the oil sand is slurried with water near the mine site and transported in a pipeline to the processing plant. Some conditioning of the bitumen occurs in the pipeline allowing for a more efficient separation of bitumen, water, and solids in the processing plant.

Once at the plant, the slurry is agitated and aerated to decrease the size of lumps and to liberate bitumen from sand grains. The liberated bitumen attaches to the air bubbles, floats to form a froth, and is separated from the slurry in large gravity separation vessels. The treatment temperature for the slurry process is 40 to 55°C. Typical bitumen recovery is about 88 to 95%. The composition

of recovered bitumen froth is typically 60 wt% bitumen, 30 wt% water and 10 wt% solids (Long *et al*., 2004; Speight, 2006; Zahabi *et al.,* 2010).

The bitumen froth is mixed with a solvent to facilitate the separation of bitumen from water and solids. There are two commercial processes: naphtha-based froth treatment used by Syncrude and paraffinic froth treatment used by Shell and Imperial Oil. Syncrude dilutes froth with naphtha to create a density difference between the bitumen and water, and to decrease the bitumen viscosity. The mixture is centrifuged to remove the water and solids. The diluted bitumen product is distilled to recover naphtha. The bitumen product contains approximately 1.0 wt% of fine solids and is an acceptable feed for an on-site coker-based plant (Gray, 2015; Romanova *et al.*, 2004). Paraffinic froth treatment takes advantage of the precipitation of asphaltene from bitumen diluted with *n*-hexane or similar paraffins. The precipitated asphaltene particles flocculate and collect the suspended solids and water droplets (Long *et al.*, 2002) which are readily separated by gravity, eliminating the use of cyclones or centrifuges (Masliyah *et al.*, 2004). After froth treatment, the bitumen meets the pipeline requirements of solids and water content below 0.5 wt% and has a substantially lower asphaltene content (Gray, 2015; Romanova *et al.*, 2004).

One issue in oil sands processing is the handling of poorer quality oil sands; that is, oil sands with high content of fine solids (<44 μm). There is a strong correlation between bitumen recovery and fine solid content; the higher the fine solid content, the lower the bitumen recovery (Dai and Chung, 1995; Dang-Vu *et al.*, 2009; Hooshiar *et al.*, 2012; Masliyah *et al.*, 2004; Nikakhtari *et al*., 2014). Coarse solids are readily removed during the extraction process, mostly in the primary separation stage (Hooshiar *et al.*, 2012; Kaminsky *et al*., 2008). However, fine solids are more difficult to separate because they are small but also because they can interact with the solvent, bitumen, and water in the extraction process (Hooshiar *et al*., 2012; Masliyah *et al.*, 2004; Osacky *et al.*, 2013). Fine solids can adsorb at the water-oil interface where they stabilize water droplets (Sztukowski and Yarranton, 2004; Yan and Masliyah, 1993). They can also modify the adhesion of bitumen to air bubbles in the presence of calcium ions (Masliyah *et al*., 2004). Some native minerals also affect the pH of the oil sands during aqueous extraction these include carbonates (*e.g.*, calcite, siderite) and iron-sulfur compounds (Bowman, 1967). pH is known to affect oil sands

processability and particle interactions (Wallace *et al.*, 2004). The separation of hydrophobic solids from bitumen is more difficult than hydrophilic solids since hydrophobic fine solids can migrate into the bitumen phase (Dang-Vu *et al.*, 2009).

2.4.2 Solvent Based Extraction Process

Non-aqueous extraction processes reduce the density and viscosity of the bitumen by solvent dilution and moderate heating. These processes have potential advantages including high bitumen recovery, little or no water consumption, less energy consumption, and the elimination of tailings ponds. Solvent based extraction processes have been studied at the lab scale since the mid-1950s with different solvents and process configurations (Speight, 1999). In most cases, the proposed process uses at least two stages. In the first stage, solvent is added to the oil sands to create a slurry from which the coarse solids and some fine solids are settled. In the second stage, the settled solids are contacted with more solvent to recover more bitumen. More stages can be added if necessary to obtain higher bitumen recovery.

Adeyinka and Speirs (2010) patented a non-aqueous process to extract bitumen from mineable oil sands using two solvents at 30℃ and atmospheric pressure. The main stages of the process are initial slurry preparation, agglomeration, agglomerate separation, and solvent recovery. They depicted several processes for the addition of the two solvents: the first solvent was always added to prepare the initial slurry and the second solvent could be added in the agglomeration or agglomerates separation stages. Both produce at least one bitumen product that meets pipeline specifications. Both solvents have low boiling points, below 100 °C, and the first solvent has a similar or slightly higher boiling point than the second solvent. The first solvent may be a low boiling point cycloalkane, paraffin or a blend. The second solvent could be *n-* or iso-alkane or alcohols or alcohol blends. With alkanes, asphaltenes precipitation can be controlled with the solvent to bitumen ratio. Using cyclohexane as first solvent at a ratio of oil sand/solvent of 1.6/1, and pentane beyond onset of asphaltene precipitation as second solvent, they obtained a partially de-asphalted diluted bitumen with solids and water content less than 400 ppm and 200 ppm on a dry bitumen basis.

Hooshiar *et al*. (2012) developed a solvent extraction process using toluene/*n*-heptane blends at several mass ratios 70/30, 30/70, 10/90 and 0/100. Mixtures of oil sand ore and solvent at a ratio of 100 g solvent/150 g oil sand were agitated 10 minutes and left to settle for 30 minutes to separate the water and solids. The diluted bitumen was decanted. The remaining slurry was mixed again with 50 g of solvent, agitated for 10 minutes and filtered through a 45 μm sieve. They reported a bitumen recovery higher than 80 wt% and a solid content in the diluted bitumen below 0.5 wt% on a solvent free basis. The ratio of toluene to *n*-heptane did not affect the solvent recovery. Mixtures with high *n*-heptane content caused asphaltene precipitation as expected but surprisingly resulted in higher solids content in the diluted bitumen product. The authors speculated that there was a transition zone of incompletely settled flocs between the supernatant and the separated water and solids that contributed to a high solids content in the recovered diluted bitumen.

Nikakhtari *et al*. (2013) used a variety of solvents (aromatics, cycloalkanes, and biologically derivate solvents) to extract bitumen from oil sands in a multistage cleaning process similar to Hooshiar's process (Hooshiar *et al*., 2012). They found cyclohexane was the best solvent with 94.4% recovery and 1.4 wt% fine solids in the recovered bitumen. Continuing their work, Nikakhtari *et al*. (2014) worked with low, medium, and high fines content oil sands. They found that extracting bitumen from oil sands with cyclohexane, the solids content in the recovered bitumen was 2 to 11 wt% on a solvent-free basis and the global bitumen recovery was above 92% for the three oil sands. Pal *et al*. (2015) followed the research of Hooshiar *et al*. (2012) and Nikakhtari *et al*. (2013) using the same extraction procedure with a blend of cycloalkane and paraffinic solvents. The bitumen recovery was above 95%.

Solvent based extraction processes have not been yet been commercialized, largely due to poor solvent recovery from the oil sands (Nikakhtari *et al.*, 2013; Osacky *et al.*, 2013) and a fine solids content in the bitumen product that exceeds pipeline specifications (Pal *et al*., 2015). These processes also have the inherent flammability and explosion hazards of working with organic solvents.

This thesis focuses on the separation of fine solids. As noted above, the key to the paraffinic froth treatment process is that the precipitated asphaltenes flocculate and collect the solids and water in the diluted bitumen. Asphaltenes, water, and solids form flocs larger than individual components and settle faster. (Long *et al.*, 2002; Romanova *et al.*, 2004; Zahabi *et al.*, 2010; Zawala *et al.*, 2012). The same principle can be applied to a non-aqueous extraction process. In either case, the settling rate of the flocculated material is critical to the process.

2.5 Particle Settling

2.5.1 Fundamentals of Settling

The mechanics of particles in motion inside liquids involves three kinds of forces: gravitational, buoyant, and drag forces. When one particle is settling through a fluid in one dimension, the velocity reaches a maximum (terminal velocity) when the drag and buoyant forces exactly balance the gravitational force. For spherical particles inside high viscosity liquids with no shear forces and a low Reynolds number, the expression for terminal velocity or settling rate is given by Stokes' law (Allen, 2003):

$$u = \frac{g(\rho_s - \rho_m)d^2}{18\mu_m} \tag{2-5}$$

where u is the settling rate, ρ_s is the solid density, ρ_m is the mixture density, μ is the viscosity, d is the solid diameter, and g is the gravitational acceleration.

Stokes' law does not apply directly to solvent/bitumen mixtures with flocculated asphaltene particles. Factors such as floc porosity and permeability, and particle concentration affect the settling rate. The polydispersity of the floc sizes must also be taken into accounted. Each factor is discussed below.

Floc Porosity

In order to calculate settling rates for flocculated material, the diameter and effective density of the floc are required. The effective density is related to the porosity of the floc. A convenient choice for diameter is the maximum diameter. In this case, the spherical volume occupied by the floc is simply:

$$V_{floc} = \frac{\pi}{6} d^3_{floc} \qquad\qquad (2\text{-}6)$$

where V_{floc} and d_{floc} are the spherical volume and maximum diameter of the floc. The spherical volume is the volume traced by the floc if it were rotated over all angles, Figure 2.2.
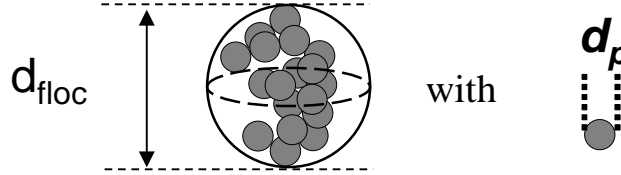
Figure 2.2. A schematic of a floc illustrating the maximum diameter and spherical volume.

The actual volume of the particles in the floc, V_{act}, is given by:

$$V_{act} = n_f \frac{\pi}{6} d^3_p \qquad\qquad (2\text{-}7)$$

Here, it assumed that the primary particles are spherical and identical. The porosity of a floc so defined is then given by:

$$\phi_{floc} = 1 - \frac{V_{act}}{V_{floc}} = 1 - n_f \left(\frac{d_p}{d_{floc}} \right)^3 \qquad\qquad (2\text{-}8)$$

The effective density of the flocs is given by:

$$\rho_{eff} = (1 - \phi)\rho_p + \phi\rho_m \qquad\qquad (2\text{-}9)$$

Equations (2-8) and (2-9) are combined to obtain the following expression for the effective density of a floc:

$$\rho_{eff} = \rho_m + \left(\frac{d_{floc}}{d_p} \right)^{Df-3} (\rho_p - \rho_m) \qquad\qquad (2\text{-}10)$$

The effective density, ρ_{eff}, is equivalent to the solid density, ρ_s, in Equation 2.5 when the solid is defined as the floc. Equation (2.10) is then substituted into Stokes' law (Equation 2.5) to obtain the settling rate of a floc as follows (Li and Logan, 2001; Woodfield and Bickert, 2001):

$$u_0 = \frac{g(\rho_s - \rho_m)d^2_{floc}}{18\mu_m} \left(\frac{d_{floc}}{d_p} \right)^{Df-3} \qquad\qquad (2\text{-}11)$$

22

Floc Permeability

To account for the effect of fluid flow through a porous settling particle, a drag coefficient (Ω) is usually added to Stokes' law as follows (Li and Logan, 2001; Long *et al.*, 2004; Rahmani *et al.*, 2005b):

$$u_p = \frac{u_0}{\Omega} \tag{2-12}$$

where u_p is the modified settling rate and Ω is a drag coefficient that accounts for the effect of drag force through the porous particle. Brinkman (1947a, 1947b) related the drag coefficient to the porosity of the floc as follows:

$$\Omega = \frac{2\beta^2 \left(1 - \frac{\tanh \beta}{\beta}\right)}{2\beta^2 + 3\left(1 - \frac{\tanh \beta}{\beta}\right)} \tag{2-13}$$

where $\beta = \frac{d_{floc}}{2\sqrt{\kappa}}$ and κ is the permeability:

$$\kappa = \frac{d_p^2}{72}\left[3 + \frac{4}{1 - \phi_{floc}} - 3\sqrt{\frac{8}{1 - \phi_{floc}} - 3}\right] \tag{2-14}$$

where d_p is the diameter of primary particle and $(1-\phi_{floc})$ is the solid fraction calculated using Equation (2-8). This approach has been applied to high porosity aggregates (Tang and Raper, 2002) such as asphaltenes flocs (Long *et al.*, 2004; Rahmani *et al.*, 2005b).

The permeability is expected to be insignificant for flocs with porosities below 0.8 (Long *et al.*, 2004) or β values above 10.9 (Rahmani *et al.*, 2005b). For distributions of fractal flocs, the permeability may be insignificant for small flocs but become significant for large flocs because the porosity increases with floc size (Li and Logan, 2001; Elimenech *et al.*, 1998).

Particle Concentration – Hindered Settling

In dilute particle suspensions, the particles settle independently and do not interact with each other. When the particle concentration increases, the particles are close together and their interactions

affect the settling rate. The wake of a big particle falling in a vertical line next to a smaller particle can drag the smaller particle along creating a satellite effect. Another effect in closed systems is the upward displacement of liquid as the particles settle. This fluid movement can slow down or even transport smaller particles upwards and reduces the global settling rate. The net effect is termed hindered settling and results in a lower settling rate in more concentrated suspensions (Allen, 2003; Elimenech *et al.*, 1998).

For mono-disperse spherical particles settling at Reynold's number below 500, the usual form of the hindered settling equation is:

$$u_h = u_p F(\alpha_f)$$
(2-15)

$F(\alpha_f)$ is a function of the volume fraction of the fluid, α_f. Masliyah (1979) suggested two forms of the function $F(\alpha_f)$: the Richardson and Zaki equation (Richardson and Zaki, 1954),

$$F(\alpha_f) = \alpha_f^n$$
(2-16)

or the Barnea and Mizrahi equation (Barnea and Mizrahi, 1973),

$$F(\alpha_f) = \frac{\alpha_f}{\left(1 + (1 - \alpha_f)^{1/3}\right) \exp\left[\dfrac{5(1 - \alpha_f)}{3\alpha_f}\right]}$$
(2-17)

Note, when $\alpha_f \to 1$, $F(\alpha_f) \to 1$ and Equation (2-15) becomes Stokes' equation. The Richardson and Zaki equation has been used in a number of asphaltene settling studies (Long *et al.*, 2004; Saadatmand, 2008; Valinasab, 2006; Zahabi *et al.*, 2010). The values for the exponent *n* reported in these studies are provided in Table 2.3.

Table 2.3. Values for exponent *n* of Richardson and Zaki equation used in previous studies. C5C6 is a 50/50 by mass mixture of *n*-pentane and *n*-hexane, and *n*-C7 is *n*-heptane.

Reference	Mixture	n
Long *et al.*, 2004	Bitumen froth/C5C6	4.27
Long *et al.*, 2004	Bitumen froth/*n*-C7	7.02-11.43
Valinasab, 2006	Bitumen froth/*n*-C7	11.43
Saadatmand, 2008	Bitumen froth/*n*-C7	4.35
Zahabi *et al.*, 2010	Model oil/*n*-C7	4.27

Floc Size Polydispersity

Many flocculated systems have a distribution of floc sizes, as shown in Figure 2.3 for a mixture of *n*-heptane and bitumen. Typically the number or volume mean diameter of the distributions are reported. The number mean diameter, d_n, is given by:

$$d_n = \frac{\sum f_i d_i}{\sum f_i}$$

(2-18)

and the volume mean diameter, d_v, is given by:

$$d_v = \frac{\sum f_i d_i^4}{\sum f_i d_i^3}$$

(2-19)

where d_i is the diameter and f_i is the number frequency of particles in the ith interval of the distribution.

Misleading results are obtained if settling rates are calculated based on the mean diameters. According to Stokes' law, large particles will settle more rapidly and small particles more slowly. Hence, polydisperse systems tend to develop a gradient of particle sizes and the rate at which the top interface moves and particle-free supernatant appears may be governed by the smallest particles. In this case, it may be necessary to model the settling of each particle (or representative interval of particle size) individually and update the location of each particle and the overall concentration at each position in the column of fluid over time.
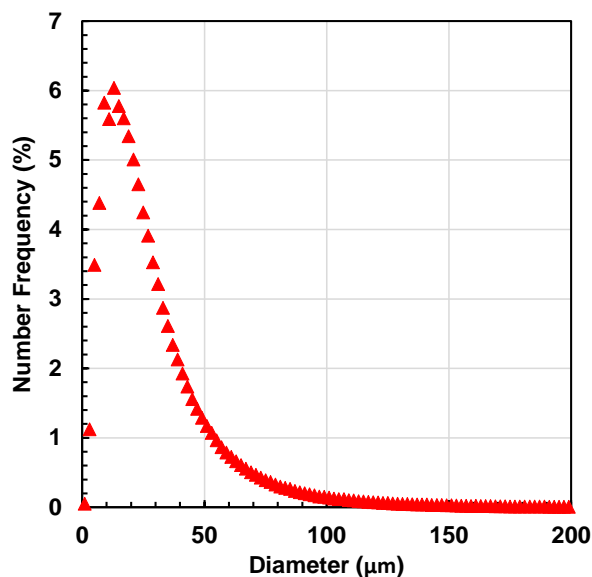
Figure 2.3. Floc size distribution of asphaltenes in a mixture of *n*-heptane and bitumen, 62.5 wt% *n*-heptane and 21°C.

2.5.2 Settling of Flocculated Asphaltenes

Previous studies have considered the flocculated material from paraffinic froth treatment processes and asphaltene flocs formed in model oils. Flocs from froth treatment processes are composed of emulsified water, dispersed solids and precipitated asphaltenes. While the settling rates of these flocs will differ from flocs consisting only of asphaltenes, the experimental methods and trends with solvent content, solvent type, temperature and solid content are relevant.

<u>Effect of Solvent Content</u>

Long *et al.* (2002) demonstrated that precipitating asphaltenes dramatically accelerates the settling of water and solids from diluted bitumen froth. They compared visually determined settling rates when the bitumen was diluted with toluene or *n*-hexane at conditions with and without asphaltene precipitation at 40°C. For solvent/bitumen (S/B) ratios between 0.7 and 2.0 (no precipitation), there was no settling; both mixtures had stable water and well dispersed fine solids in the oil phase. For *n*-hexane diluted bitumen at S/B ratios of 1.5, 1.8 and 2.0 (above the onset of precipitation), flocs of water, fine solids and precipitated asphaltene formed and settled. The settling rate increased from 0.12 to 0.37 cm/min, as the S/B ratio increased from 1.5 to 2.0, as expected with

the lower density and viscosity of the medium and increased amount of precipitation. Similar results were obtained by Zahabi *et al*. (2010) for the settling rate of asphaltene flocs precipitated from mixtures of *n*-pentane and a model oil prepared with 5 wt% pitch material, 0.5 to 4 wt% silica, and toluene.

Long *et al.* (2002) and Zahabi *et al.* (2010) also found that the asphaltene/water/solid flocs from the diluted froth exhibited zone settling represented in Figure 2.4. Soon after precipitation, all of the flocs were uniformly distributed in the liquid. As the flocs settled, three zones formed: the clear supernatant (CS), a transition zone (TZ), and a sediment zone (SZ). The clear supernatant had the lowest floc concentration and was positioned above the transition zone. The transition zone had a constant floc concentration which was higher than that of the clear supernatant. Tracking the position of this interface versus time gave the average settling rate of flocs. The sediment zone was the bottommost zone and had the highest floc concentration due to floc accumulation. After all of the flocs settled, the sediment zone compacted over time. Long *et al.* (2002, 2004), Zahabi *et al.* (2010) and Kosior *et al.* (2015) plotted the position of the interface between the clear supernatant and the transition zone versus time, as shown in Figure 2.5. They calculated the mean floc settling rate as the slope of the line from point A to point B where the floc settled at a constant "free settling" rate.

Effect of Solvent Type

Long *et al*. (2004) and Kosior *et al.* (2015) observed that the lighter the solvent used to dilute bitumen froth, the faster the settling rate of asphaltene flocs. Long *et al*. (2004) measured the settling rate of asphaltene flocs from bitumen froth diluted with either a mixture of *n*-pentane/*n*-hexane 50/50 wt% (C5C6) or pure *n*-heptane. At constant mixing and settling temperature of 30 °C, flocs settling rates were 0.5 cm/min at C5C6 S/B=2 and 2.5 cm/min at *n*-heptane S/B=3. Although *n*-heptane precipitates less asphaltene at S/B=3 than C5C6 at S/B= 2, and the density and viscosity of the solution are higher, the settling rate with *n*-heptane was slower because flocs were smaller and had looser structures. Therefore, the lighter the solvent, the faster the settling rate. Similarly, Kosior *et al.* (2015) diluted bitumen froth with *n*-pentane and *n*-hexane at 30°C

and S/B= 1.6 and 2.4, respectively, to maintain a similar amount of asphaltene precipitation. The settling rates were 3.0 and 1.0 cm/min for *n*-pentane and *n*-hexane solvents, respectively.
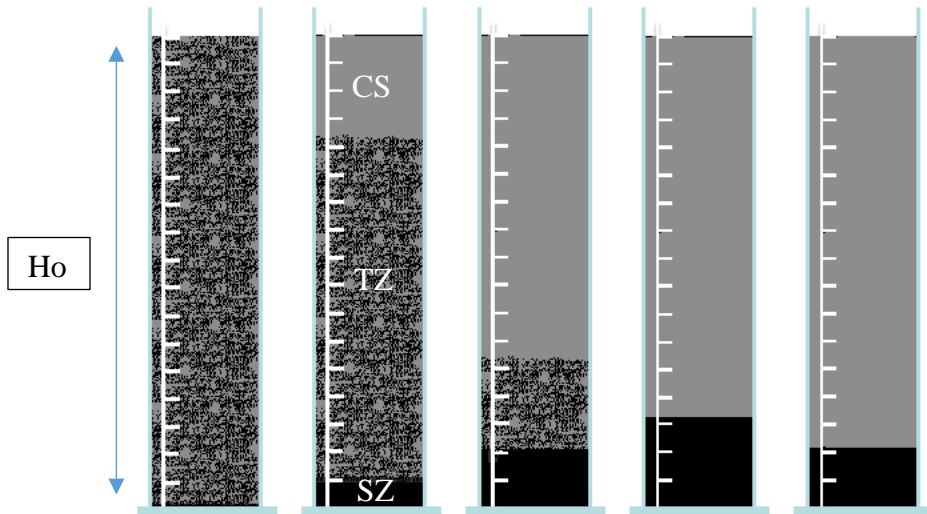
Figure 2.4. Different zones in the settling process of flocs.
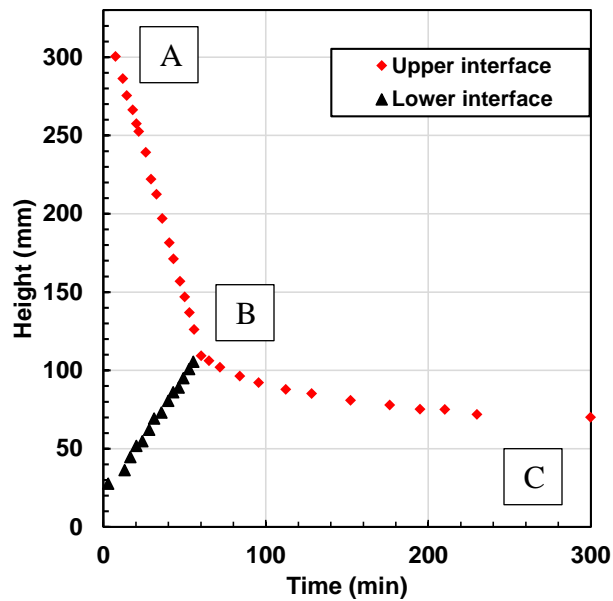
Figure 2.5. Settling plot of the *n*-hexane/bitumen froth, S/B=2, 40 °C. (Long *et al*., 2002)

28

Effect of Temperature

The settling rate of asphaltene flocs precipitated with several different solvents increased as temperature increased (Kosior *et al*, 2016; Long *et al*., 2004). Long *et al*. (2004) found that the settling rate of bitumen froth diluted with C5C6 at S/B=2, increased from 2.4 to 9.7 cm/min when the mixing temperature increased from 30 to 100°C. With *n*-heptane, the settling rate increased from 0.4 to 2.0 cm/min as the temperature increased from 30 to 80°C. Kosior *et al.* (2015) diluted bitumen froth with *n*-pentane, *iso*-pentane and *n*-hexane, at temperatures ranging from 30 to 90 °C. The floc settling rate for the three solvents increased linearly with the temperature in a semi-log plot.

Effect of Solid Content

Zahabi *et al*. (2010) investigated the effect of silica particle content on the settling rate of asphaltene flocs. They visually measured the settling rate of asphaltene flocs precipitated from mixtures of *n*-pentane and a model oil prepared with 5 wt% pitch material, 0.5 to 4 wt% silica, and toluene. The settling rate increased from 0.16 to 0.29 cm/min when the silica content increased from 0 to 4 wt% corresponding to an increase in the floc density.

Effect of Mixing Speed

Zawala *et al.* (2012) investigated the effect of mixing energy on the settling rate of flocs from diluted bitumen froth with *n*-pentane at S/B=1.8. *In situ* and isolated floc settling rates were measured. *In situ* experiments were performed inside the autoclave cell and the settling rate was measured through a glass window. Isolated floc experiments were performed in a glass column, where only one to a few asphaltene aggregates were added. In both cases, the settling rates were measured tracking individual flocs. When the mixing energy between bitumen froth and solvent increased from 0.1 to 20 kJ/kg, the mean *in situ* settling rate increased from 4 to 68 cm/min. The settling rate increased because at a higher mixing energy the flocs contained more mineral solids, increasing the density of the floc. For isolated flocs, the settling was faster for larger particles although the data were scattered. For flocs of the same diameter, the settling rate was faster for flocs obtained at a higher mixing rate, suggesting that the flocs produced at higher shear rates were more compact (higher fractal dimension). Zawala *et al.* (2012) also observed an increase in

asphaltene floc density in the presence of silica particles when they increased the mixing speed of preparation, because the mixing increased the inorganic solids content in the flocs.

Rahmani *et al*. (2005b) studied the effect of mixing speed in the settling rate of individual flocs from a model oil. The model oil was prepared by mixing asphaltenes in solutions of 17 wt% toluene and 83 wt% heptane to obtain asphaltene concentration of 62.5 mg/L. *n*-Heptane was added to precipitate asphaltenes at 36 and 75 rpm. A sample of ~3mL was transferred into a settling column filled with a solvent of the same solubility parameter as the original medium in order to measure the settling rate. The settling rate of the flocs ranged between 0.1 and 0.6 cm/min. Therefore, there was not a considerable change in the settling rate produced by a change in the mixing speed. The flocs settling velocities did not increase as the floc diameter increased; the authors speculated that the larger flocs had more irregular shapes and lower floc effective density than the smaller flocs reducing their settling rate. Note that the flocs in Rahmani's study were more fractal-like than the compact structures observed by Zawala *et al.* (2012).

Limitations of Measurement Methods

The visual method used to measure the mean settling rate of asphaltenes (Kosior *et al.*, 2016; Long *et al.*, 2002, 2004; Zahabi *et al.*, 2010) or settling rate of individual particles (Rahmani *et al.*, 2005a, 2005b; Zawala *et al.*, 2012) has difficulties when the interface between clear zone and transition zone is not visible, because diluted bitumen becomes opaque or the floc concentration is low. In an effort to overcome these issues in diluted bitumen froth, Kosior *et al.* (2016) used an ultrasound method to measure the settling rate of asphaltene flocs. They validated that the position of the upper interface through time measured with the ultrasonic method matched visual method data for free settling. Another way to overcome these issues is using the gravimetric method, which is presented in Chapter 3.

Chapter Three: Experimental Methods

This chapter presents the experimental methods used to determine the bitumen sample properties, asphaltene yield curves, toluene insoluble content, onset point of asphaltene precipitation, asphaltene floc size distributions, and settling rates.

3.1 Chemicals and Materials

Two Western Canadian bitumen samples from SAGD processes were used in this work, WC-B-A3 and WC-B-B2. The first sample was supplied by Japan Canada Oil Sands and it was dewatered in the field. The second sample came from Shell Canada Ltd and it was dewatered by the Alberta Research Council. The water contents were measured by Karl Fischer titration (Baydak, 2016) and are reported in Table 3.1. Note, the water content of the Shell sample is relatively high because the residual emulsified water had settled during storage and the sample taken for this work came from the bottom half of the pail. Toluene (99.5% purity) and *n*-pentane (>98% purity) from BDH and *n*-heptane (technical) from Anachemia were purchased from VWR International LLC.

Table 3.1. Bitumen samples properties

Bitumen Sample	Water Content wt%	Density at 21°C kg/m³	Viscosity at 21°C mPa.s
WC-B-A3	2.4	1008.8[a]	153,000[b]
WC-B-B2	5.0	1013.9[c]	89,200[c]

[a] This thesis
[b] Marquez, 2016
[c] Ramos-Pallares *et al*., 2016 (bitumen was named WC-B-B1)

Three types of solid particles were used to validate the FBRM and micrographic method. A Coulter® CC latex bead size standard with a nominal diameter of 43 μm and a mode in the range of 40 to 45 μm was obtained from Beckman Coulter[TM]. EcoChrom[TM] Silica 32-63 with a median diameter between 45-55 μm, as reported by MP Biomedicals, was purchased from Fisher Scientific. PVC spheres dispersed in water at a solids content of 8.33 wt% and an average number mean diameter of 101.7 μm were provided by Mettler Toledo.

3.2 Bitumen Property Measurements

Densities were measured at 21°C using an Anton Paar DMA 4500M density meter. The instrument precision was ±0.01 kg/m³. The repeatability of the measurements was ±0.05 kg/m³. The density of the WC-B-B2 bitumen was measured directly in another project by Ramos-Pallares *et al.* (2016). The density for WC-B-A3 could not be measured directly due to its high viscosity. Instead, solutions of the sample in *n*-heptane were prepared at 20, 30, and 40 wt% *n*-heptane and the bitumen density was calculated from the following density mixing rule (Saryazdi *et al.*, 2013):

$$\rho_{mix} = \left[\frac{w_1}{\rho_1} + \frac{w_2}{\rho_2} - w_1 w_2 \left(\frac{1}{\rho_1} + \frac{1}{\rho_2} \right) \beta_{12} \right]^{-1} \tag{3-1}$$

where subscripts 1 and 2 denote *n*-heptane and bitumen, respectively, ρ_{mix} is the density of the mixture, *w* is the mass fraction, and β_{12} is the binary interaction parameter defined as:

$$\beta_{ij} = -0.092 \left| 0.435 - 2 \left(\frac{|v_1 - v_2|}{v_1 + v_2} \right) \right| + 0.022 \tag{3-2}$$

where v_1 and v_2 are the specific volume (in m³/kg) of *n*-heptane and bitumen, respectively. Equation (3-1) was fitted by least squares to the density data of the mixtures of *n*-heptane and bitumen to obtain the bitumen density.

Viscosities were measured in another project in Dr. Yarranton's research group by Ramos-Pallares (2016) and Marquez (2016) using an Anton Paar Model MCR-52 cone-and-plate rheometer equipped with a temperature controller. Several combinations of shear rate and shear stress were measured at each of three temperatures between 30 and 100°C. At each temperature, the viscosity was determined from the slope of the stress versus shear rate. Linear Newtonian behavior was observed in all cases. The viscosity data were fitted with the modified Walther equation (Yarranton *et al.*, 2012):

$$\log(\log(\mu + 1)) = A - B \log(T) \tag{3-3}$$

where μ is the dynamic viscosity of the bitumen at atmospheric pressure, *T* is temperature, and *A* and *B* are fitted parameters specific for each fluid. The viscosity at 25 °C was calculated by extrapolating the fitted equation. The repeatability of the bitumen viscosities was ±5%.

3.3 Asphaltene Yields

Asphaltene yield is defined as the mass of asphaltenes precipitated by a poor solvent, such as an *n*-alkane, divided by the mass of bitumen. Asphaltene yield curves are determined based on a yields measured for a series of mixtures of solvent and bitumen each at a different solvent content. Figure 3.1 is an example yield curve from Akbarzadeh *et al*. (2005).
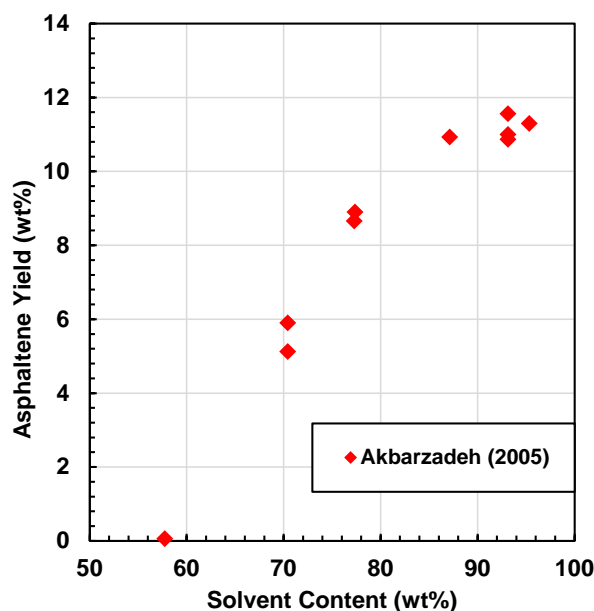
Figure 3.1. Asphaltene yield curve for Athabasca bitumen diluted with *n*-heptane at 23 °C. Data from Akbarzadeh *et al.* (2005).

To measure an asphaltene yield, a mixture of bitumen and solvent was prepared in a 30 mL vial at a solvent content above the onset of asphaltene precipitation, approximately 58 wt% *n*-heptane, Figure 3.1. A known mass of bitumen was added to a vial and then the specified mass of solvent was added in two stages. First, solvent was added from a pipette at a rate of approximately 1.2 g/minute while manually stirring, always with a total solvent content below the onset of precipitation. Second, as soon as the viscosity was low enough, a magnetic stirrer was placed in the vial and the remaining solvent was added over 12 seconds while stirring. This mixture was sonicated in an ultrasonic bath for 50 minutes at room temperature and left for the desired settling time: 1.5 hours.

Next, the mixture was centrifuged using a Hettich Model EBA 12 centrifuge for 5 min at 5000 rpm (2711 RCF) to create a compact precipitate at the bottom of the vial. The supernatant was carefully removed using a pipette to avoid solid losses. The precipitate was washed using 20 mL of solvent, sonicated for 60 minutes, centrifuged at the conditions mentioned above, and the supernatant was again removed. This washing procedure was performed twice. The precipitate was dried for 24 hours in a fume hood and then dried for 4 days at 60°C and 70 kPa of vacuum (approximately 20 kPa absolute pressure). After 4 days, the final precipitate mass was measured.

The precipitate contains asphaltenes and any toluene insoluble material present in the bitumen; hence, the precipitate yield is the yield of asphaltenes and toluene insolubles. Once the toluene insoluble content was determined (see Section 3.4), the asphaltene yield was calculated. The asphaltene yields were repeatable to ±0.25 wt%, based on a 90% confident interval.

3.4 Toluene Insolubles

Toluene insolubles are defined as mineral material precipitated along with the asphaltenes and can include sand, clay, ash, and adsorbed organics (Hooshiar *et al.*, 2012; Mitchell and Speight, 1972; Zhao *et al.*, 2001). Bitumen was mixed with 20 mL of toluene in a 30 mL vial in two steps. First, toluene was added from a pipette at 1.2 g/minutes while the mixture was stirred manually. Second, as soon as the viscosity was low enough, a magnetic stirrer was placed in the vial and the remaining solvent was added over 3-5 minutes while stirring. The mixture was sonicated for 50 minutes at room temperature and left to settle for 24 hours. Then, the mixture was centrifuged using a Hettich Model EBA 12 centrifuge for 5 minutes at 5000 rpm (2711 RCF). The supernatant was carefully removed using a pipette to avoid loss of precipitate. The precipitate was washed with 20 mL of toluene, sonicated for 60 min, and centrifuged again. The toluene wash was performed at least twice until the supernatant was clear and colorless. Then the sediment was dried for 24 hours in a fume hood and 4 days at 60 °C and 70 kPa of vacuum. After 4 days, the dried precipitate and vial were weighed to obtain the toluene insoluble content of the bitumen. The toluene insoluble content was repeatable to ±0.06 wt% based on a 90% confidence interval.

3.5 Onset of Asphaltene Precipitation

The onset of asphaltene precipitation is defined as the lowest precipitant (*n*-alkane in this case) content at which asphaltenes precipitate from the bitumen. To determine the onset, *n*-heptane (or *n*-pentane) was added to the bitumen and a yield curve was measured as described in Section 3.3, with a focus on data near the expected onset composition. A precipitation time of 1.5 hours was selected since the settling experiments (Section 3.8) lasted between 10 minutes and 3 hours. The asphaltene yield was extrapolated to zero using a linear regression to find the onset, as shown in Figure 3.2. Based on the scatter and uncertainty of the yield measurements, the precision of the extrapolated onsets is ±0.6 wt%. The repeatability of the yield was ±0.5 wt% based on a 90% confidence interval, lower than the uncertainty of the extrapolation. Therefore, the larger uncertainty was used when reporting the onsets; in this example, the onset is 56.3±0.6 wt% *n*-heptane.
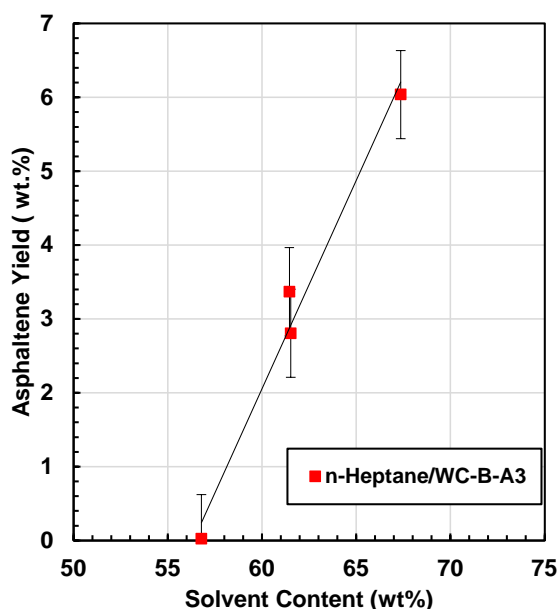
Figure 3.2. Gravimetric determination of the onset of asphaltene precipitation from *n*-heptane diluted bitumen at 1.5 hours.

3.6 Preparation of Mixtures with Flocculated Asphaltenes

Mixtures of solvent (*n*-heptane or *n*-pentane) and bitumen with flocculated asphaltenes were prepared for floc size distribution measurements and for settling experiments. The bitumen and the solvent were mixed in two stages, pre-dilution and precipitation, as shown in Figure 3.3. These stages are similar to the two extraction stages in the non-aqueous extraction process (Adeyinka and Speirs, 2010; Hooshiar *et al.*, 2012; Nikakhtari *et al.*, 2013). In the pre-dilution stage, sufficient solvent was added to create a homogenous mixture without precipitating asphaltenes. The dilution reduced the viscosity of the fluid, allowing for rapid mixing in the precipitation stage. In the precipitation stage, sufficient solvent was added to reach the target solvent content and precipitate asphaltenes. A detailed procedure is provided below. The floc size distribution of the precipitated asphaltenes was measured using two techniques: a micrographic method described in 3.7.1 and the Focused Beam Reflectance Measurement (FBRM) method described in Section 3.7.2.
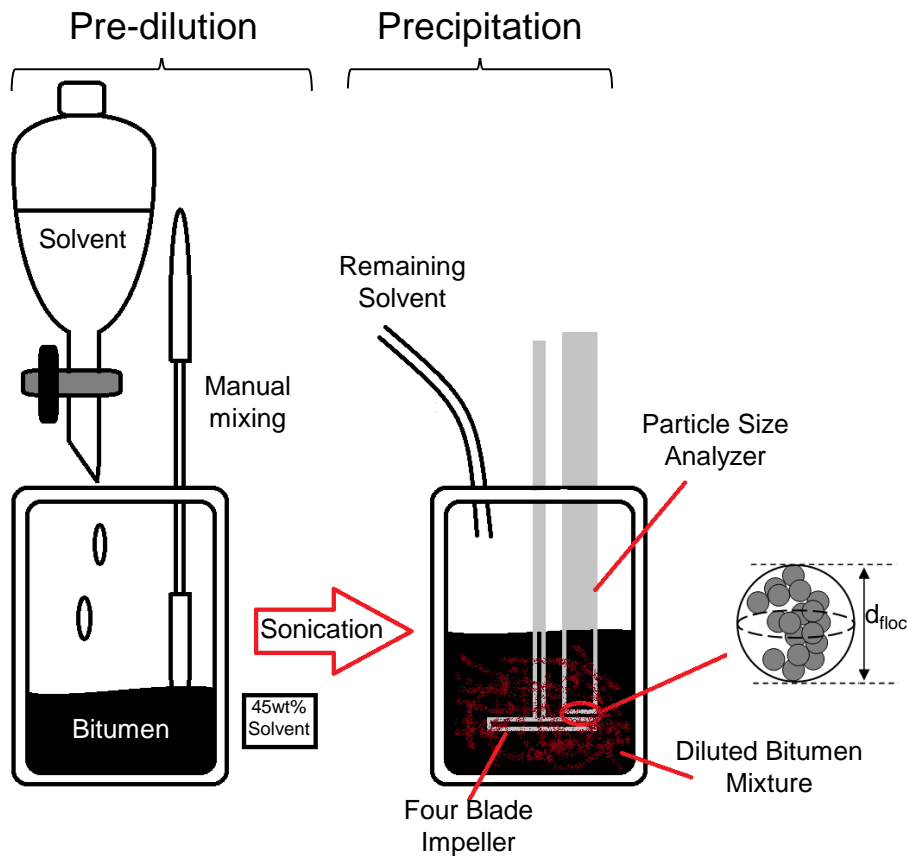
Figure 3.3. Experimental set up for flocculation experiments.

To start a flocculation experiment, a known mass of bitumen was placed in a beaker with an internal diameter of 7.4 cm and a height of 12.6 cm. Next, a specified mass of solvent was added from a separatory funnel in two steps to pre-dilute the bitumen at a solvent content below the onset of precipitation (approximately 45 wt%). In the first step, the solvent was added dropwise at a rate of approximately 1 mL/min, while the solution in the beaker was stirred manually. The second step of solvent addition commenced when the viscosity of the solution was low enough to use a magnetic stirrer. The stopcock of the separatory funnel was opened to increase the solvent flow rate to approximately 2 mL/min. The mixture was sonicated in an ultrasonic bath for 50 minutes. If solvent evaporation occurred, more solvent was added to maintain a constant mass. It was confirmed visually and in independent tests with the particle size analyzer that no asphaltene precipitation occurred at this stage.

Note that the pre-dilution procedure was designed with two mixing steps to address an issue identified in a previous study (Shafiee, 2014) where a detection limit was encountered at an *n*-heptane content of 75 wt%. Below this *n*-heptane content, the FBRM method failed to detect the flocs above the noise level. The problem was caused by poor mixing and was eliminated with the modified procedure.

After the pre-dilution stage, the FBRM probe and a 4-blade impeller with a 5 cm diameter were placed in the beaker containing the pre-diluted bitumen. The mixer was turned on at the specified speed and the specified mass of solvent to precipitate the asphaltenes was added to achieve the final solvent content. The solvent was added in less than 12 seconds using a separatory funnel. Then, the particle size analyzer was turned on to start the measurement. Samples for micrographic measurements were collected with a pipette as required.

Note that the mixing speeds were restricted to a range of 195 to 330 rpm. Below 195 rpm, the flocculated asphaltenes started to settle. At speeds greater than 330 rpm, large vortexes formed and air entrainment was observed (Shafiee, 2014). All experiments in this thesis were conducted at 195 rpm. The Reynolds numbers at 195 rpm for the two bitumen samples considered in this

study are presented as a function of the *n*-heptane content in Figure 3.4. The Reynolds number (Re) for an impeller in a cylindrical geometry is defined as follows:

$$\text{Re} = \frac{\rho_m N D_{imp}}{\mu_m}$$
(3-4)

where ρ_m is the density of the mixture, kg/m³, N is the rotational speed, 1/s, D_{imp} is the diameter of the impeller, and μ_m is the viscosity of the mixture, Pa.s. For this geometry, a Reynolds number greater than 10,000 indicates turbulent flow and a Reynolds number less than unity indicates laminar flow. If the Reynolds number is between 1 and 10,000 the system is in transition flow which, for batch mixing, means turbulent flow close to the impeller and laminar flow in the periphery regions (Coulson *et al.*, 1999). The experiments in this study are in the transition flow regime except at solvent contents above 90 wt% where the flow becomes fully turbulent. The difference in Reynolds number for the mixtures prepared with the two samples are due to differences in the viscosity and density of the bitumen.
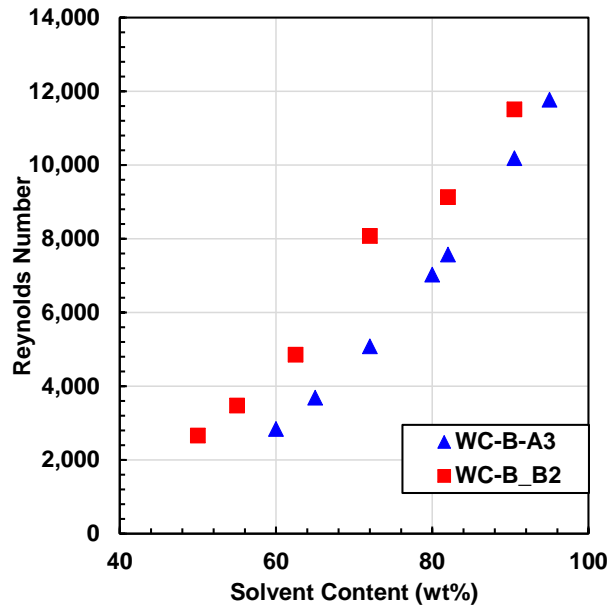
Figure 3.4. Reynolds numbers for *n*-heptane/bitumen mixtures at different solvent content.

38

3.7 Particle Size Distribution Measurements

Two methods were performed to measure the floc size distributions: micrography and Focused Beam Reflectance Measurement (FBRM). The reported particle size distribution for irregular particles depends upon the method of measurement and calculation (Allen, 2003). The experimental method, calculation method, and a comparison of each method are discussed below. As will be shown, each method was better suited for a different range of solvent contents.

Note that while the distributions were required for the settling calculations performed in this thesis, the average diameter of the distribution was often used for comparing data trends. Two ways to express the average diameter of the particles were used: the number mean diameter and the volume mean diameter. The number mean diameter (d_n) was used for experiments related to settling processes, Equation (2-18), and the volume mean diameter (d_v), Equation (2-19), was used for the sake of comparison with external references.

3.7.1 Micrographic Method

A Carl Zeiss Axiovert S100 optical microscope equipped with an Axiocam video camera was used to capture floc images. To obtain an image, a sample was collected using a pipette from the flocculation beaker described in Section 3.6 after 50 minutes of flocculation time. Two droplets of the sample were placed on a microscope glass slide with coverslip and several images were taken. Preliminary tests with multiple samples indicated that two samples with a total of 150 floc measurements were sufficient to obtain a repeatable distribution.

The floc diameters were measured using Axiovision SE64 software. The maximum diameter of each floc was marked manually with a cursor and then a distribution was calculated from the marked diameters. At least 150 flocs were measured to create a floc size distribution. For mixtures of *n*-heptane and bitumen, the size distributions were broad and therefore flocs were counted at two magnifications: flocs smaller than 45 μm were measured from 16 images at 40x magnification and flocs larger than 45 μm were measured from one image at 10x magnification. The total area examined at each magnification was the same: 16 images at 40x is equivalent to one image at 10x. Since the areas were matched, the distributions at 10x and 40x magnifications were simply added

together to obtain an average distribution. For mixtures of *n*-pentane and bitumen, there were few flocs smaller than 45 μm and therefore all of the flocs were measured only at 10x magnification. Note, the maximum diameter of the floc was measured because it is equivalent to the diameter of the encased sphere defined in Section 2.5.1. The number and volume mean diameter were determined for each distribution.

Validation

The method was first tested on Coulter® CC monodisperse spherical latex beads with a nominal diameter of 43 μm and a mode in the range of 40 to 45 μm. Figure 3.5 shows the cumulative number frequency distribution of the beads measured with the microscopic method. The measured number mean diameter and mode for the distribution are the same, 45.2 ±0.9 μm, and are within 1 μm of the reported mean diameter. No particles were observed below 40 μm but a small number of particles were detected between 50 and 60 μm. Overall, the microscopic method provides an accurate measurement for nearly uniform spherical particles.
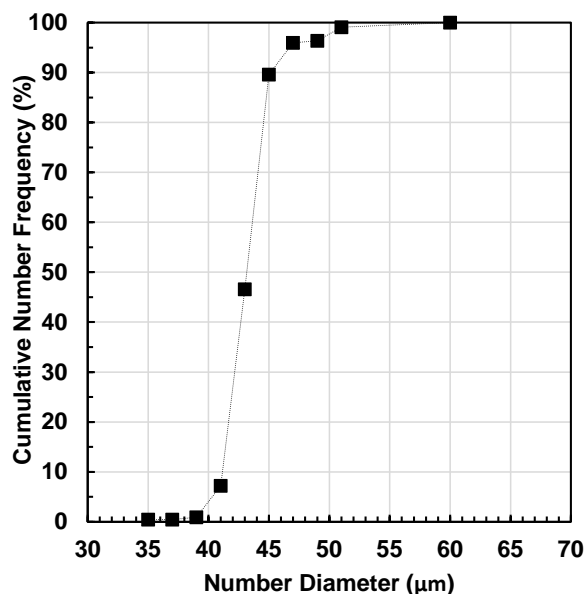
Figure 3.5. Cumulative number size distribution measured with the micrographic method for Coulter® CC latex beads standard with a nominal diameter of 43 μm.

The microscopic method was next tested on EcoChrom^{TM} Silica 32-63. These particles are irregular, Figure 3.6, and the cumulative number frequency distributions for the minimum and maximum diameter from the microscopic method are shown in Figure 3.7. The average diameter of each particle was calculated as the average of the minimum and maximum diameters and the calculated average size distribution is also shown in Figure 3.7. The minimum, average, and maximum number mean diameters were 48.4, 62.5 and 76.3±1.3 μm, respectively. The reported mean diameter for this silica sample is between 45-55 μm, but the provider did not specify the method of measurement. The minimum number mean diameter is within the reported mean diameter range but the calculated average is approximately 10 μm higher. This example illustrates the challenges in measuring and reporting the size distributions of irregular particles. The microscopic method gives results that are consistent with the reported values but cannot be completely validated without knowing the measurement method used by the supplier.
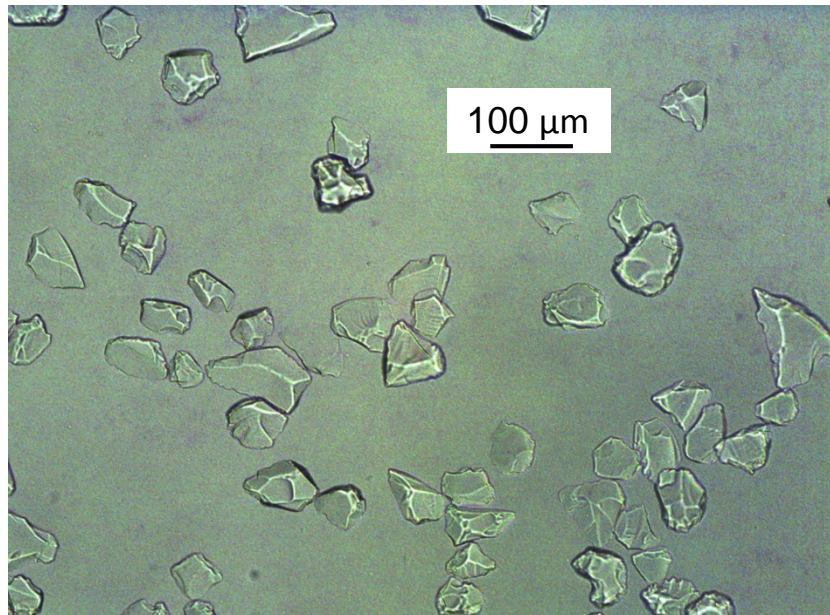
Figure 3.6. Micrograph of EcoChrom^{TM} MP Silica 32-63 at 10x magnification.

Applicability to Flocculated Asphaltenes

Optical micrography is the only method were individual particles are directly observed and measured. However, it requires sampling, is time consuming, and is not applicable at all conditions. It can be used only at conditions where the concentration of the solids is small enough to be able to identify independent particles. If the solid concentration is high, particles overlap and it is often not possible to identify the edge of each independent particle. For instance, in Figure 3.8a, it is possible to observe the edge of independent particles and the diameter of each particle can be easily measured. However, in Figure 3.8b, the particles are overlapping and the apparent diameter will not represent the actual value. The actual diameter of the particles also affects the quality of the measurement because bigger particles are easier to measure than small ones and small particles are more easily obscured by the larger particles.
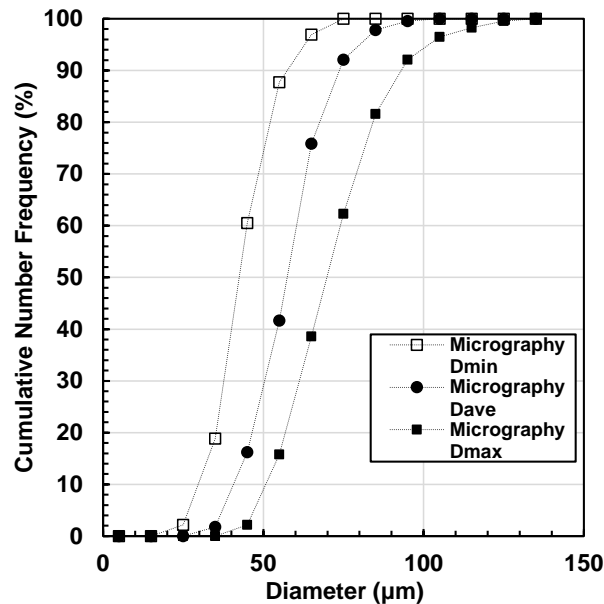
Figure 3.7. Cumulative particle size distribution measured with microscopic method for EcoChrom^{TM} Silica 32-63.
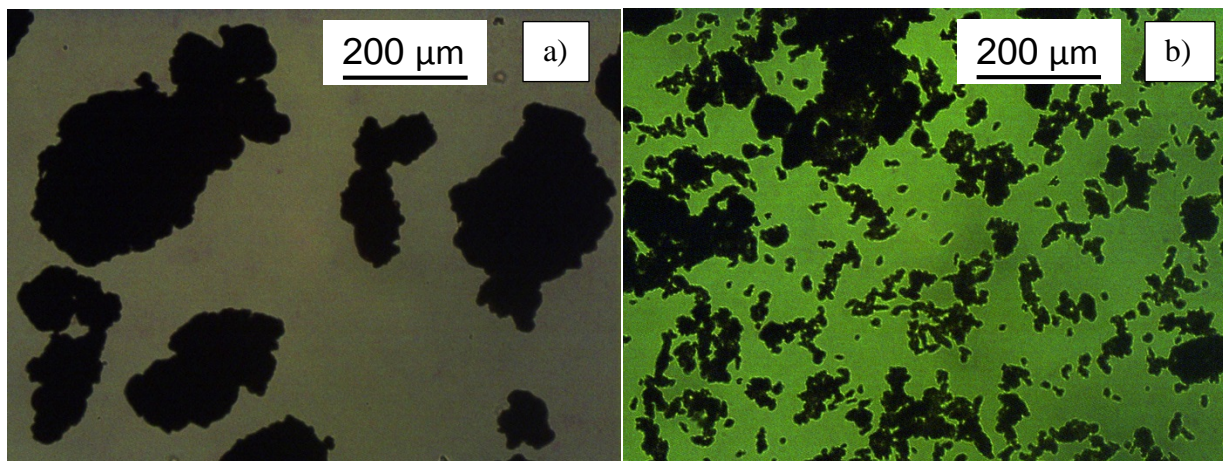
Figure 3.8. 10x micrograph for flocculation system: a) asphaltene flocs from WC-B-A3 bitumen diluted with *n*-pentane at 70 wt%; b) asphaltene flocs from WC-B-A3 bitumen diluted with *n*-heptane at 72 wt%.

Another issue is that flocculated solids can change their shape, structure, or diameter when removed from their original mixture. The micrographs must be acquired rapidly enough to observe a representative sample. For most of the asphaltene flocs, the structures changed gradually after the flocs settled on the surface of the slide, and the images had to be taken while some of the flocs remained in motion, usually within 40 seconds of sampling. When 40 seconds was insufficient to obtain all of the required images, a new droplet sample(s) was taken to collect the remaining images.

The conditions at which valid distributions could be collected depended on the solvent. The flocculation experiment conditions at which the microscopic method could be used for asphaltene flocs are presented in Section 3.7.3.

3.7.2 Focused Beam Reflectance Measurement Method

Although the micrographic method is accurate when representative images can be obtained, it is slow and cumbersome to perform and does not apply over all of the conditions to be considered in this study. An alternative is the Focused Beam Reflectance Method (FBRM).

The Focused Beam Reflectance Measurement (FBRM) technique was performed with a Lasentec Model D600 Particle Size Analyzer. This technology measures the *in-situ* chord length distribution of flocs, where chord length is defined as a straight line between any two points on the edge of an individual particle (Lasentec, 2002). To measure this line, a laser beam (wavelength 780 nm) is focused to a point where a mechanical device rotates (4500 rpm) the beam in a circular path. When the beam intersects a particle, the scattered light is reflected to the probe. A photodetector in the probe generates a pulse that represents the two points at the edge of the particle, Figure 3.9. The chord length is determined from the pulse width and the laser velocity (2 m/s), (Clain *et al*., 2015; Xu, 2000). A primary chord length distribution is constructed from the chord length measurements of many particles. The size range is divided into Cartesian or logarithmic intervals termed *bins* and the number count for each bin is reported. The number count is the number of particles intersected by the laser in its circular path over 1 second. It is not a true measure of the solid concentration but can be used as a qualitative indicator. Number or volume weighted frequency distributions are calculated from the bin counts.
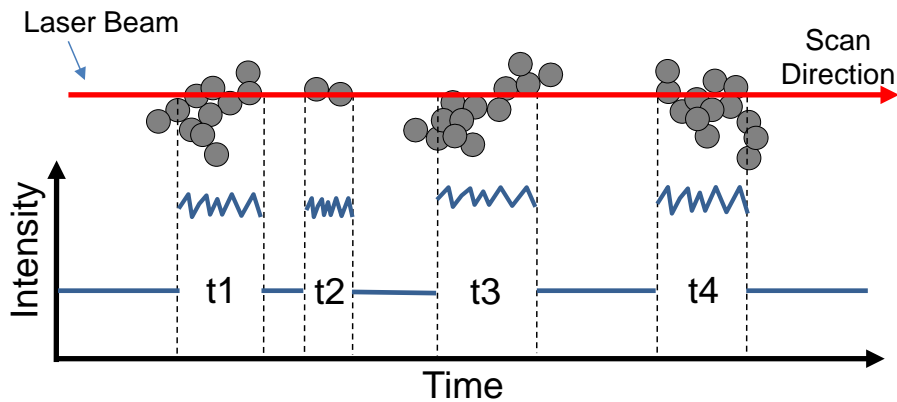
Figure 3.9. Light scattering method used to measure flocs chord length.

There are three hardware settings in the particle size analyzer to consider: nucleation, measuring time, and fine/coarse measurement. The nucleation setup was not relevant for this study. The measuring time defines the number of particle counts; the longer the time, the more particles are measured, and the greater statistical accuracy. In this study, a measurement period of 30 seconds was selected to obtain sufficient counts in each time interval and avoid spikes in the distribution,

but still keep track of changes in the distribution over time. The fine setting detects smaller particles and provides higher resolution to the lower end of the particle size distribution. It is best suited to non-aggregating particles. The coarse setting is designed for aggregated particles. Therefore, the coarse setup was used for the flocculated asphaltene systems considered in this study.

The data collected during a flocculation experiment are a series of floc size distributions and number counts. The distributions were approximately lognormal at all conditions at which valid measurements were obtained, Figure 3.10. For convenience, only the number and volume mean diameter and the number count over time are reported for the flocculation experiments, Figure 3.11.
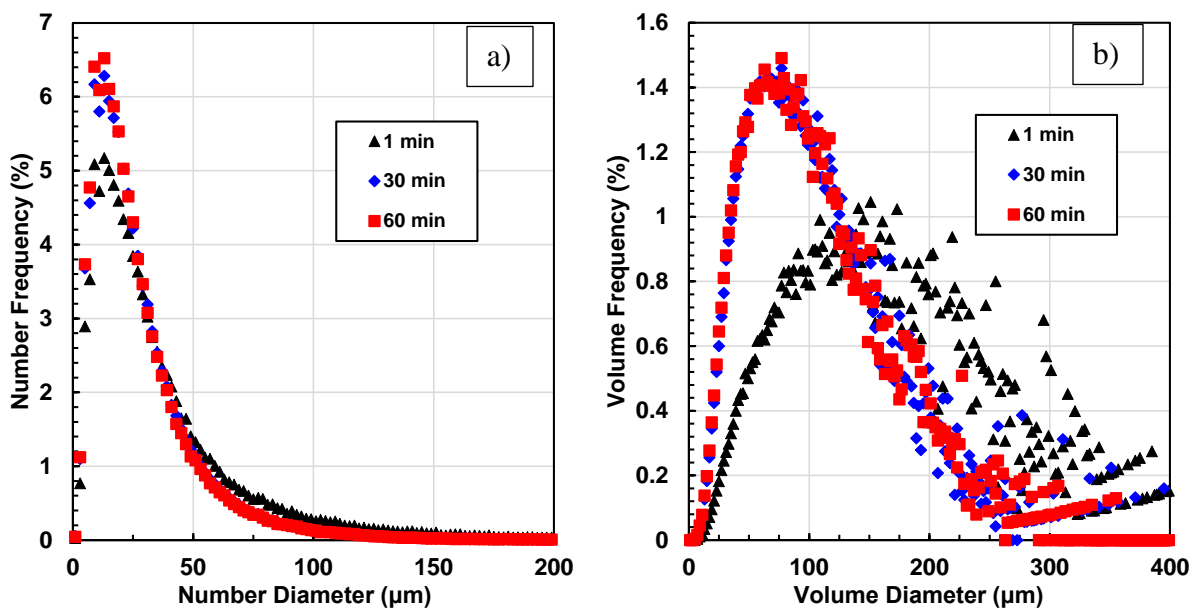
Figure 3.10. Size distributions over time for *n*-heptane/WC-B-B2 at 62.5 wt% solvent, 195 rpm and 21°C: a) number frequency size distribution; b) volume frequency size distribution.
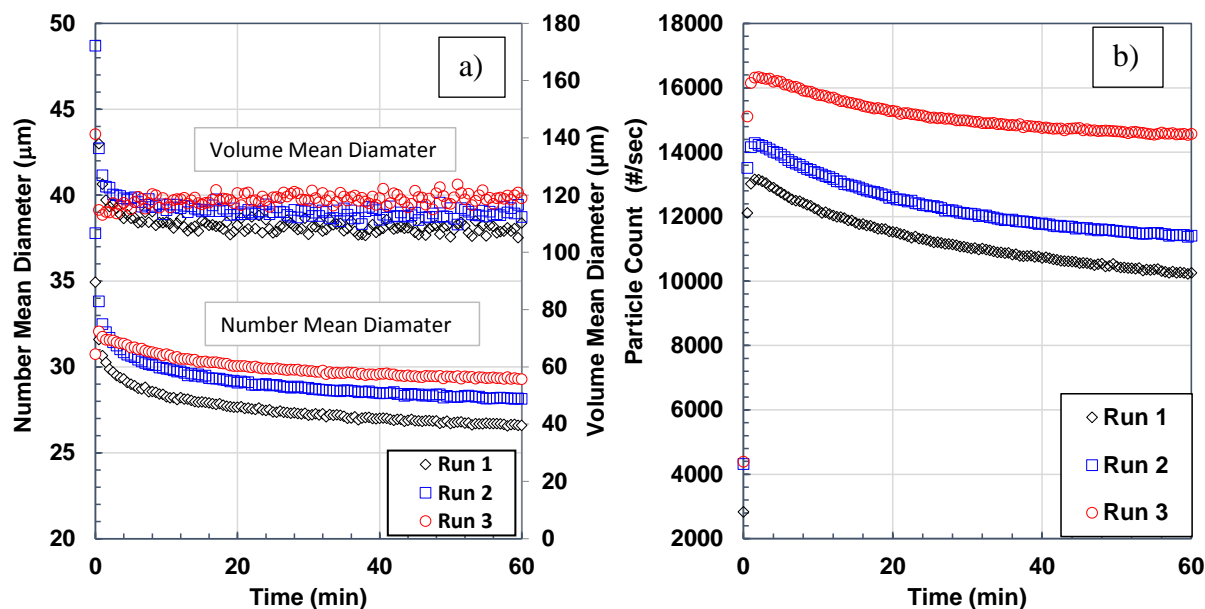
Figure 3.11. Repeatability measurement for *n*-heptane/WC-B-B2 at 62.5 wt% solvent, 195 rpm and 21°C: a) number and volume mean diameters; b) particle count.

<u>Repeatability and Reproducibility</u>

To test the repeatability of the measurements for flocculated asphaltenes, the flocculation experiments for *n*-heptane/WC-B-B2 mixtures at 195 rpm and 21°C were performed three times. The repeats at 62.5 wt% *n*-heptane are shown in Figure 3.11 as an example. After 60 minutes, the number mean diameter for the three experiments was 28.0 ±2.3 µm (8.1%), the volume mean diameter was 113.9 ±7.6 µm (6.7%), and the particle count was 12,100 ±600 (5.1%) based on a 90% confidence interval. The confidence intervals reported are an average of the confidence intervals calculated at different solvent contents.

The reproducibility of chord length was tested with the PVC spheres from Mettler Toledo. The size distribution was approximately lognormal and therefore linear bins were selected to maintain the same resolution throughout the distribution. In both cases, the distributions were analyzed without calibration (no weighting). The comparison between the reference data from Mettler Toledo and the measured data are presented in the Figure 3.12. The measured number mean diameter for the distribution was 94±10 µm compared with the reported value of 101.7±10 µm, based on a 90% confidence interval. The measurements are not significantly different.

46

<u>Calibration</u>

The chord size distribution does not represent the real size distribution even for spherical particles, because the chord length is a random distance between two points on the edge of the particle; hence, this method will produce a distribution of sizes even for perfect mono-disperse solids (Boxall *et al.*, 2010; Schümann *et al.*, 2015). In this study, the particles are irregular flocs which increases the probability of obtaining a particle size distribution further from the real values.

The measured primary chord length distributions are calibrated to better match the actual particle diameter distributions. The calibration gives a different weighting factor to different sized particles. For example, providing greater weight to large particles compensates for the fact that in general chord lengths are shorter than the actual diameter. The calibration provides a number frequency for each bin as follows:

$$f_{N,i} = w_i \frac{n_i}{n_T} \tag{3-5}$$

where $f_{N,i}$ is the calibrated number frequency for bin i, n_i, is the number of primary chord measurements within bin i, n_T, is the total number of primary chord measurements and w_i is the weighting factor given by:

$$w_i = \frac{d_i^{\gamma}}{\sum_{j=1}^{N} d_j^{\gamma}} N \tag{3-6}$$

where d_i is the bin midpoint, γ is the calibration exponent, and N is the total number of channels. The exponent could be -1, 0, 1, 2 or 3, according to the nature of the solids in the system. If $\gamma=0$, the diameter distribution is the same as the primary chord distribution.
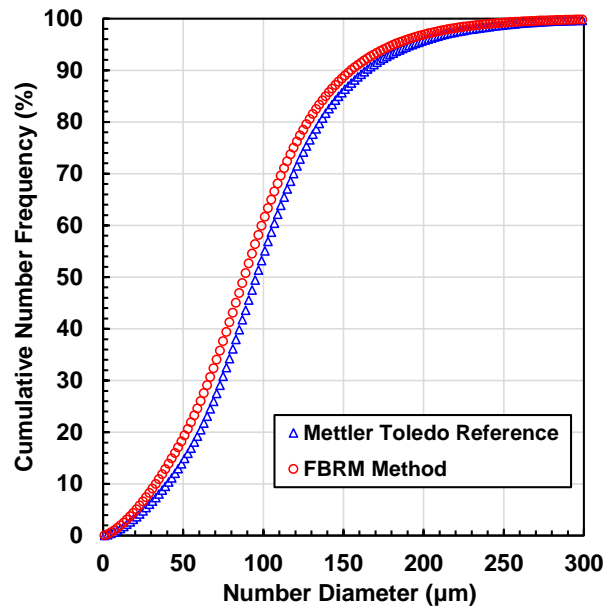
Figure 3.12. Comparison of cumulative particle size distribution of PVC spheres measured with FBRM with reference data from Mettler Toledo.

To illustrate the calibration procedure, the FBRM method was applied to several known particle size distributions. First, the FBRM was tested with the same standard 43 μm spherical latex beads used to test the micrographic method, Figure 3.13. The hardware settings for these measurements were a measuring time of 30 seconds and the fine configuration. The measurements were calibrated with an exponent of 0. The particle mean diameter from the calibrated FBRM was 51.8±0.4 μm based on a 90% confidence interval after 20 repeats. The average diameter is within 8 μm of the standard; however, the particle distribution from the FBRM is significantly broader than the micrographic distribution. The apparent particles sizes below 40 μm arise from chord measurements across sections of the spherical particle other than its complete diameter. The diameters above 70 μm may be generated from overlapping particles. The two sources of error appear to cancel each other when calculating the mean diameter.
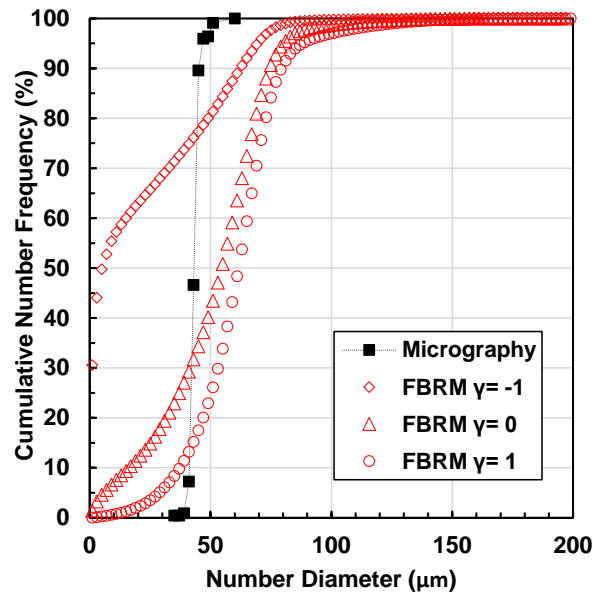
Figure 3.13. Comparison of the cumulative particle size distributions measured with the FBRM and microscopic methods for a Beckman Coulter^{TM} latex bead standard with a nominal diameter of 43 μm.

The FBRM method was next tested on EcoChrom^{TM} Silica 32-63. The hardware settings for these measurements were a measuring time of 30 seconds and the coarse configuration. The measurements were calibrated with exponent γ=3. The distributions from the FBRM and microscopic methods are compared in Figure 3.14. Even with the cubic weighting factor, the number mean diameter from the FBRM distribution, 44.3±4.2 μm, was significantly less than the number mean diameter of the distribution ,76.3±1.3 μm, from the microscopic method. The FBRM method appears to skew to lower values for irregular particles, probably because there are more chances to measure shorter chord lengths.
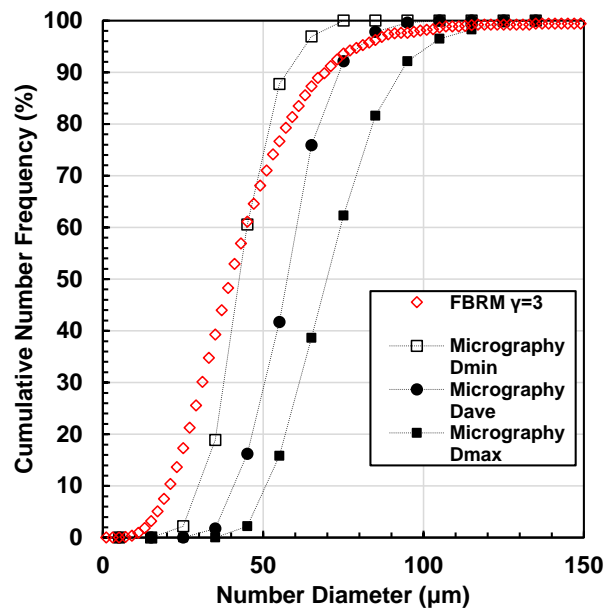
Figure 3.14. Comparison of the cumulative particle size distributions measured with the microscopic and FBRM methods for EcoChrom^{TM} Silica 32-63.

Finally, the FBRM calibration method was applied to the Mettler Toledo standard PVC spheres. It was assumed that the microscopic method provided an accurate absolute measurement of the size distribution. The minimum and maximum size distributions of the PVC spheres were measured using the microscopic method. The average diameter of each particle is calculated as the average of the minimum and maximum diameter, Figure 3.15. The number mean diameter of the distribution was 144±7 μm. The uncalibrated (γ=0) and calibrated (γ=2) FBRM distributions are compared with the microscopic method in Figure 3.15. The FBRM distributions are broader than the microscopic method. The uncalibrated distribution is also skewed to lower values because all chords samples were sampled. The uncalibrated FBRM data does not report higher diameters than the micrographic method and therefore does not appear to count overlapping flocs as single units. The number mean diameters of the calibrated distribution is 150±13 μm, within 8 μm of the microscopic method distribution.
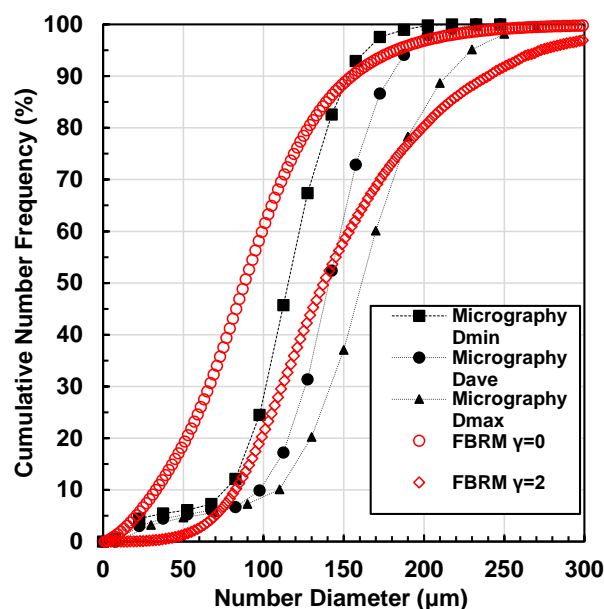
Figure 3.15. Calibration of cumulative particle size distribution of PVC spheres measured with FBRM to distribution from micrographic method.

As the above examples illustrate, the calibration depends on the shape of the particles and their size distribution and therefore there is no universal calibration (Boxall *et al.*, 2010; Clain *et al.*, 2015; Greaves *et al.*, 2008; Heath *et al.*, 2002; Li *et al.,* 2005; Schümann *et al.*, 2015). The general consensus is that each system requires its own calibration between methods. The approach taken in this thesis for flocculated asphaltenes is discussed in the Section 3.7.3.

Applicability to Flocculated Asphaltenes

The Lasentec Particle Size Analyzer measures the chord length over a specified time (here 30 seconds) and saves the data in 1324 primary channels between 0 and 1024 µm. Low particle counts lead to low particles per channel and higher variation in the volume and number particle size distributions. For instance, if the particle count is 2500 counts per second, the number of counts per channel in 30 seconds would be 56.65. The less counts per channel, the lower the statistical stability.

If the particle count is too low, the particle size distributions become erratic, include peaks at random diameters, and no longer have a lognormal shape. Figure 3.16a and 3.16b present particle

size distributions and number counts for bitumen diluted with *n*-heptane at solvent contents of 45, 50, and 55 wt%. At 45 wt% solvent content, the mixture is below the onset of asphaltene precipitation and there are no asphaltene flocs. The particle count of 21 #/sec is very low and the size distribution is random; the apparent signal is simply noise. At 50 wt% solvent content, there is some asphaltene precipitation but the particle count is only 18 #/sec. Although the apparent size distribution appears less random, the particle count is not above the noise level. The signal to noise ratio is too high to obtain valid data. At 55 wt% solvent content, the particle count is 3600 #/sec, the particle size distribution is smooth, and has a lognormal shape. This distribution meets the criteria for a valid measurement. The exact flocculation experiment conditions at which valid distributions can be obtained for flocculated asphaltenes are discussed later.
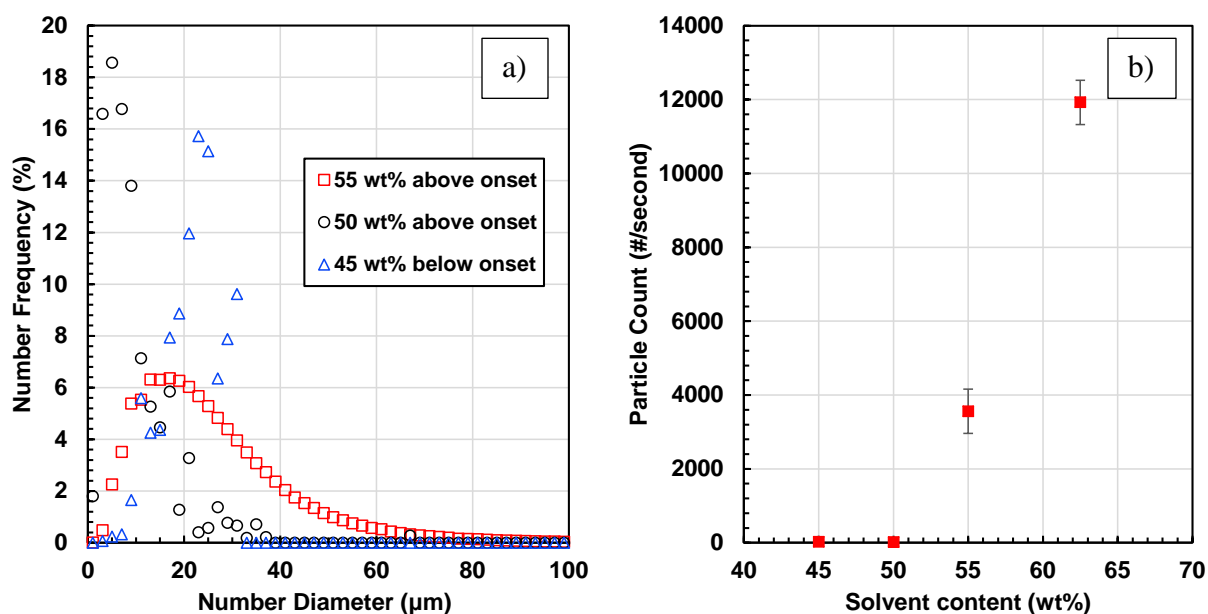
Figure 3.16. a) Frequency Distribution and b) Particle Count, for WC-B-B2 bitumen diluted with n-heptane at 45, 50 and 55 wt% solvent content.

3.7.3 Application of the Particle Size Distribution Methods to Flocculated Asphaltenes

There are two issues to address for the application of the microscopic and FBRM particle size distribution measurements: 1) the conditions at which each method is valid; 2) the calibration of the FBRM method. To address these issues, the floc size distributions from three diluted bitumen systems were measured: *n*-pentane/WC-B-A3, *n*-heptane/WC-B-A3 and *n*-heptane/WC-B-B2.

52

Applicability of Methods

Note, calibrated distributions are required to assess the applicability of the FBRM method but the applicable range is required to appropriately set the calibration. As will be shown later, the best calibration exponent is 0 or -1. Therefore, the applicability of the method is evaluated using both calibration exponents.

First consider mixtures of n-pentane and WC-B-A3 bitumen. The mean diameters from each method are compared at n-pentane contents of 60, 70, 85 and 95 wt% in Figure 3.17a. The number mean diameters from the FBRM method with calibration exponent $\gamma=-1$ and $\gamma=0$ are well below the microscopic method at n-pentane contents below 95 wt%. For these mixtures, clear micrographs with little overlap of the particles were obtained, Figure 3.18, and therefore the micrographic data were considered to be reliable. The size distributions from the FBRM became erratic at n-pentane contents below 95 wt%, Figure 3.19. It appears that either the flocs were not reaching the FBRM probe or only a part of each floc was detected by the probe. In either case, the method is unreliable at n-pentane contents below 95 wt%. Figure 3.20 shows that above 95 wt% n-pentane content, the particle count is above 8000 #/sec. With a high count and smooth size distribution, the FBRM at 95 wt% is expected to be reliable. The data were then screened to remove all of the unreliable data and for the best calibration exponent (discussed later); the screened data are presented in Figure 3.17b.
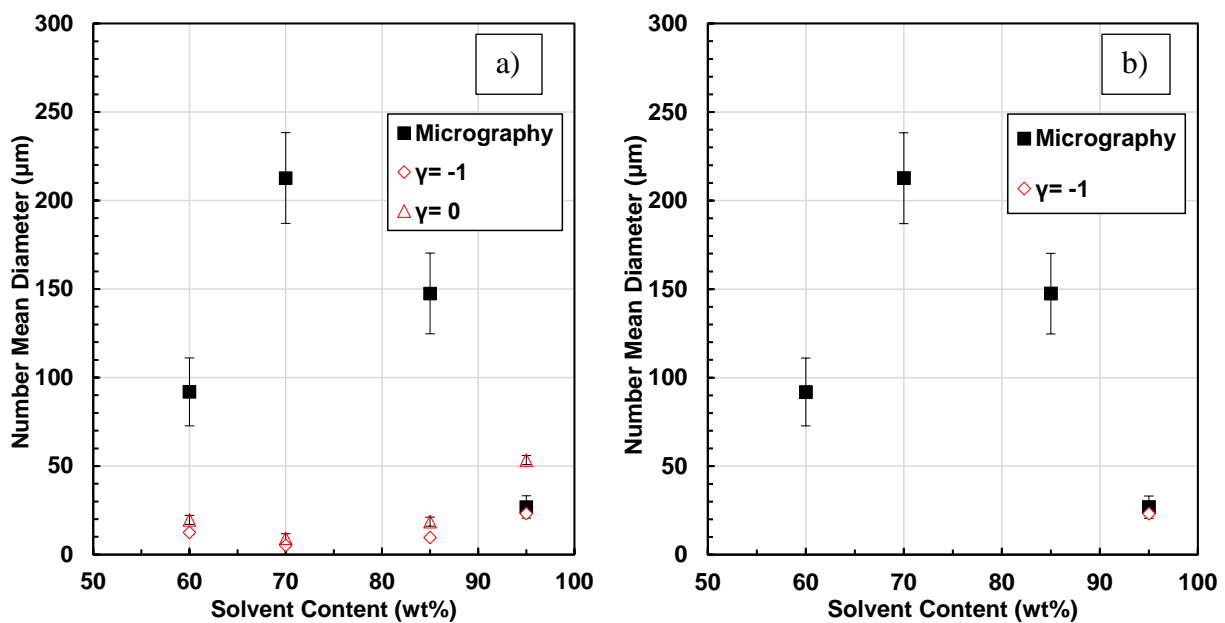
Figure 3.17. Comparison of FBRM and microscopic method number mean diameter for mixtures of *n*-pentane and WC-B-A3 bitumen at 21°C: a) all data; b) screened data.
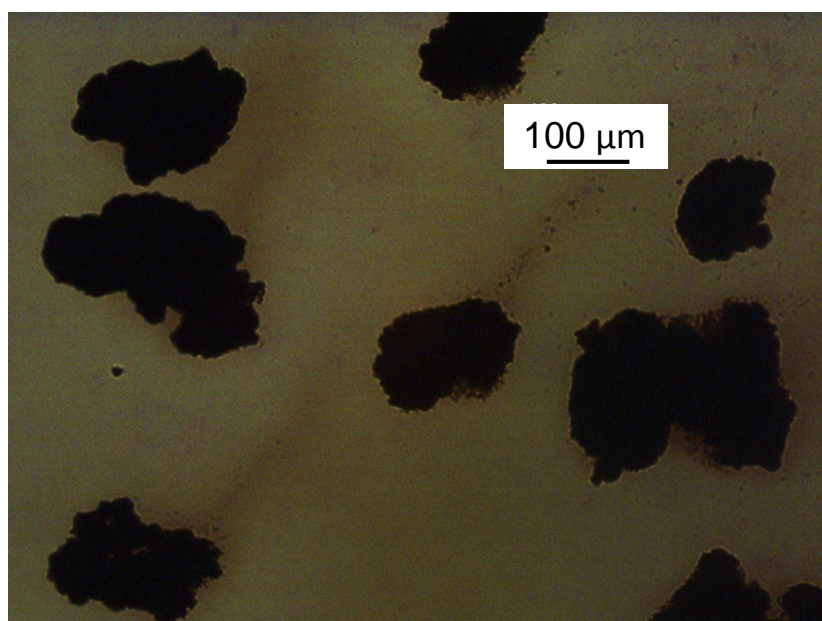
Figure 3.18. Micrograph asphaltene floc from *n*-pentane/WC-B-A3 at 70 wt% solvent.
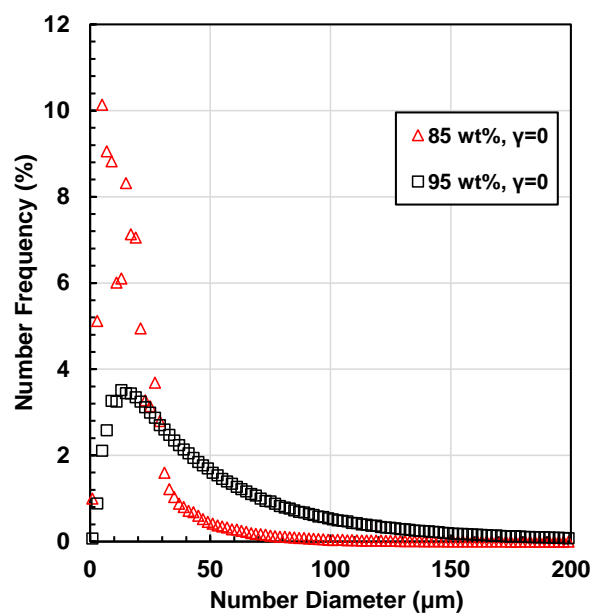
Figure 3.19. FBRM number diameter distributions for mixtures of 85 and 95 wt% *n*-pentane in WC-B-A3 bitumen at 21°C.
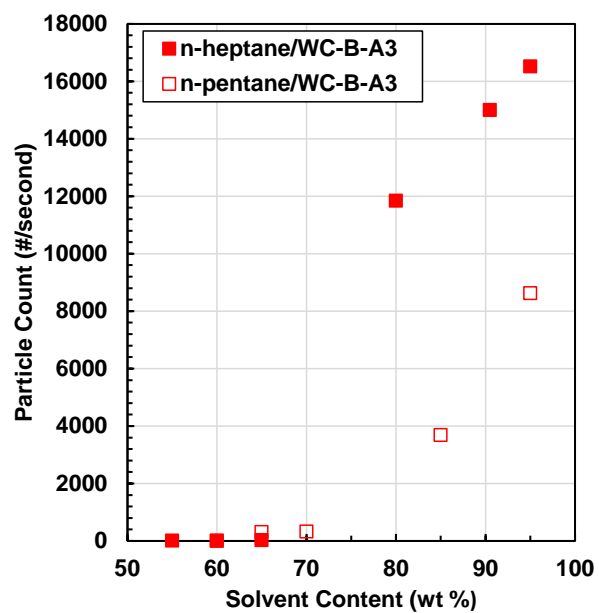
Figure 3.20. Particle count versus solvent content for mixtures of *n*-pentane or *n*-heptane with WC-B-A3 bitumen at 21°C.

Next, consider mixtures of *n*-heptane and WC-B-A3 bitumen. The number mean diameters from each method are compared at *n*-heptane contents of 60, 65, 72, 80, 90.5 and 95 wt% in Figure 3.21a. The micrographic measurements at 60 to 72 wt% *n*-heptane content were considered reliable because independent particles could be clearly identified and measured, Figure 3.22a. Above 80 wt% *n*-heptane, the flocs overlapped on the slide after a very short time and it was not possible to identify independent flocs and obtain a reliable measurement, Figure 3.22b. The size distributions from the FBRM became erratic at *n*-heptane contents below 80 wt%, Figure 3.23. Hence, the FBRM method is unreliable at *n*-heptane contents below 80 wt%. Figure 3.20 shows that the number count required for the reliable measurements was at least 8,400 and possibly as high as 12,000. When the unreliable data are screened out and the calibration exponent set to zero (discussed later), a more consistent picture of the effect of *n*-heptane content on the number distribution emerges, Figure 3.21b.
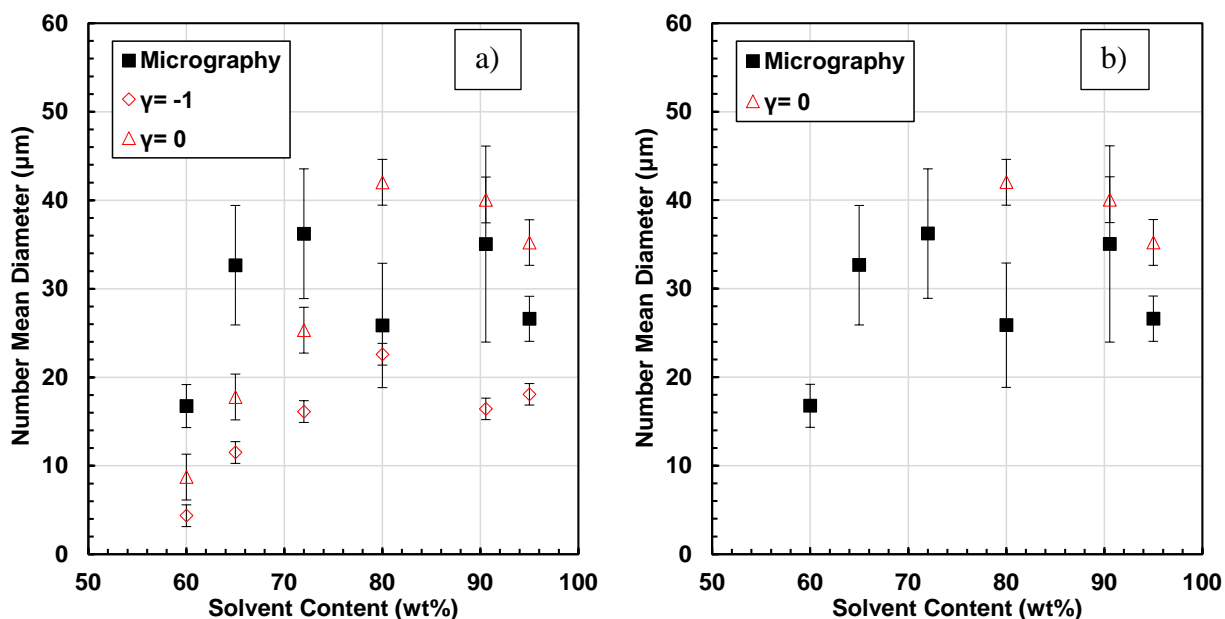
Figure 3.21. Comparison of FBRM and microscopic method number diameter for mixtures of *n*-heptane and WC-B-A3 bitumen at 21°C: a) all data; b) data after screening.
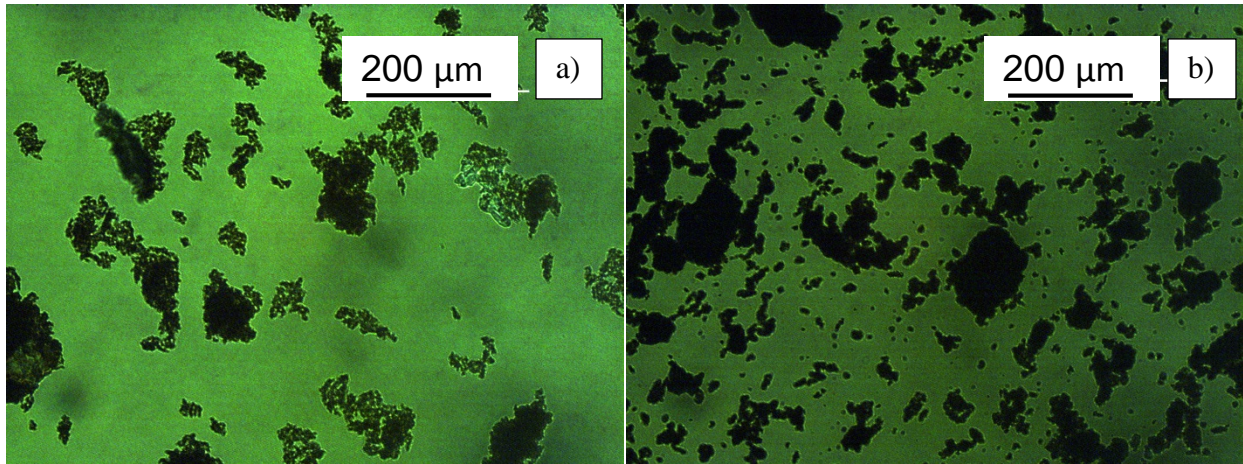
Figure 3.22. Asphaltene flocs micrographs for mixtures of *n*-heptane and WC-B-A3 bitumen at 21°C and *n*-heptane contents of: a) 65 wt% ; b) 80 wt%.
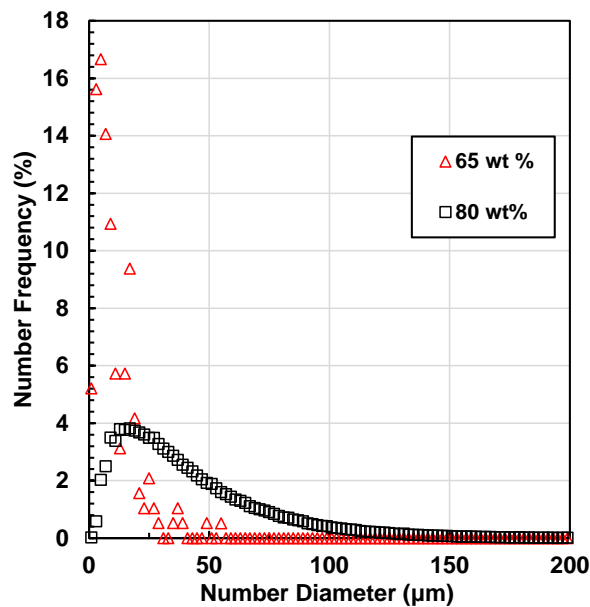
Figure 3.23. FBRM number diameter distributions for mixtures of 65 and 80 wt% *n*-heptane in WC-B-A3 bitumen at 21°C.

Finally, consider mixtures of *n*-heptane in WC-B-B2 bitumen. The number mean diameters from FBRM data processed with calibration exponents of 0 and -1 are presented in Figure 3.24a. The micrographic method was not performed for this system because the need for this method was only recognized later in the study and there was not enough of this bitumen sample left at that time to

57

perform more experiments. As discussed in Section 3.7.2, the FBRM method was valid for *n*-heptane contents at and above 55 wt% for these mixtures; the particle size distributions were smooth and had a lognormal shape, Figure 3.16a. Figure 3.24b shows that, for this system, particle counts of 3,600 counts/second (at 55 wt% *n*-heptane) were sufficient for reliable measurements.
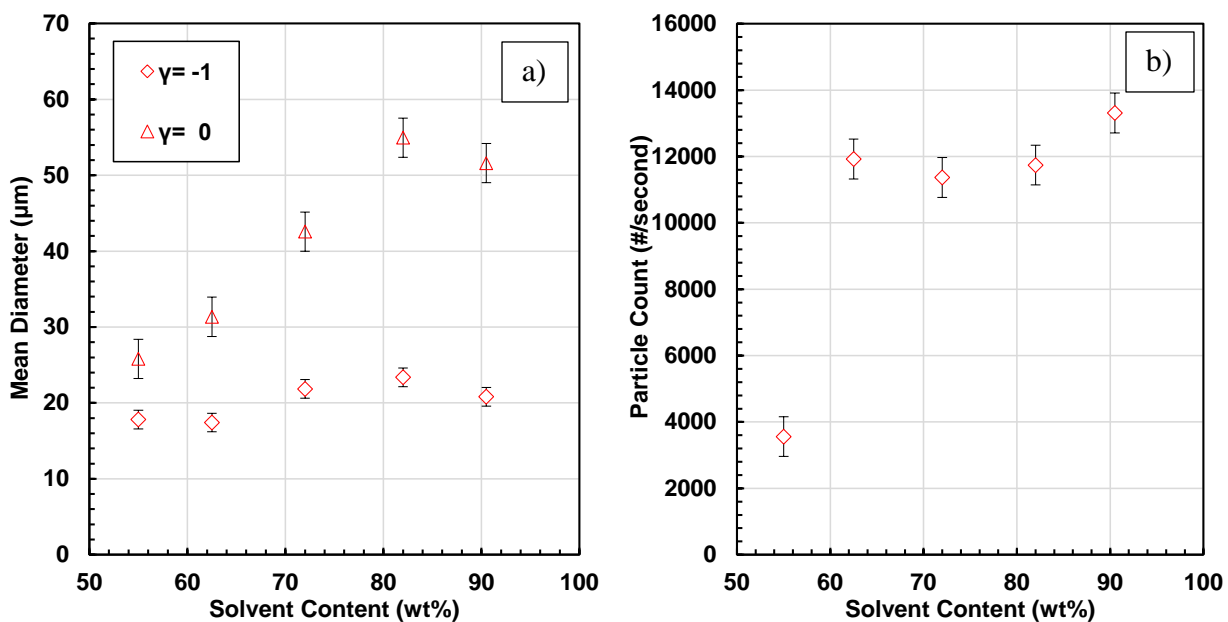
Figure 3.24. Particle count versus solvent content for mixtures of *n*-heptane with WC-B-B2 bitumen at 21°C.

Based on the data for all three systems, a number count threshold of 4000 ±1500 was defined as the criteria for a valid FBRM measurement of asphaltene floc size distributions. No general criterion was found for the micrographic method and valid ranges were determined for each system individually. Table 3.2 shows the conditions and solvent concentration where each method is applicable.

Table 3.2. Applicable conditions for the FBRM and micrographic methods.

Mixture	Method	Solvent Content (wt %)
n-pentane/WC-B-A3	Micrographic	55.0 – 95.0
n-heptane/WC-B-A3	Micrographic	60.0 - 72.0
n-pentane/WC-B-A3	FBRM	≥95
n-heptane/WC-B-A3	FBRM	72.0 - 95.0
n-heptane/WC-B-B2	FBRM	55.0 - 90.5

FBRM Calibration

To determine the best calibration weighting factor for the FBRM, only the data where both the microscopic and FBRM data were valid were considered. Since the settling rate calculation method used later in this thesis is based on the maximum diameter of the floc, the FBRM was calibrated to the maximum diameter distributions measured with the microscopic method.

First consider *n*-pentane diluted bitumen. Figure 3.25 compares the cumulative diameter distributions from the FRBM method (calibrated with $\gamma= -1$ and $\gamma= 0$) with the distribution from the micrographic method at 95 wt% *n*-pentane in WC-B-A3. The FBRM distribution with the calibration exponent $\gamma= -1$ is very similar to the micrographic method distribution and is the best choice for *n*-pentane diluted bitumen. The number mean diameters from the calibrated FBRM distribution and from the micrographic method are statistically the same: 23.2±5.0 µm from FBRM compared with 26.9±5.0 µm from the micrographic method.

Now consider WC-B-A3 bitumen diluted with *n*-heptane. Figure 3.26 compares the cumulative diameter distributions from the FRBM method (calibrated with $\gamma = -1$ and $\gamma = 0$) with the distribution from the micrographic method at 95 wt% *n*-heptane in WC-B-A3. The distribution from micrography is in between of both calibrations with smaller flocs closer to the $\gamma = 0$ calibration and large flocs closer to the $\gamma = -1$ calibration. The number mean diameters of the calibrated FBRM are 35.2±3.5 µm and 18.1±3.5 µm, respectively, and they bracket the number

mean diameter from the microscopic method 26.6±2.6 μm. Hence, the data from this one comparison is not sufficient to choose the best calibration exponent.
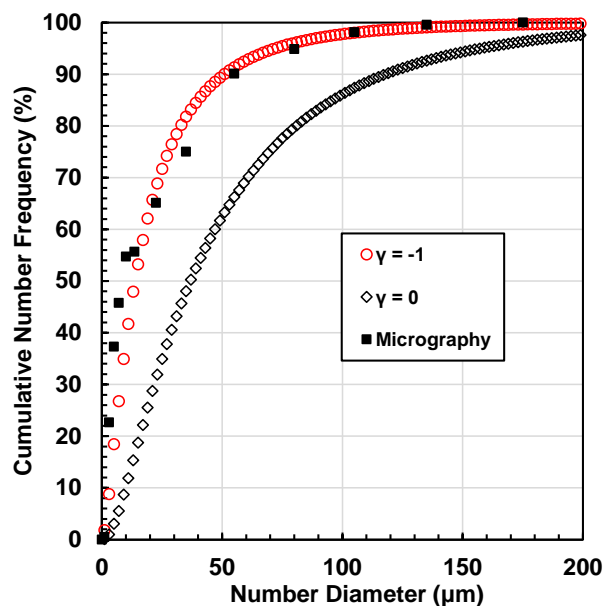
Figure 3.25. Cumulative particle distribution of asphaltene flocs from mixtures of *n*-pentane and WC-B-A3 bitumen at 95 wt% and 21°C, measured with the FBRM and microscopic methods.

Figure 3.21a compares the number mean diameters for the screened data from FBRM with the microscopic data at all solvent contents. For $\gamma = -1$, the number mean diameters from the FBRM are smaller than those from the micrographic method and do not follow the same trend. For $\gamma = 0$, the FBRM mean diameters are slightly larger than the micrographic method mean diameters but follows the same trend. As will be shown later, the shape of this trend is consistent with the settling rate results. Hence, a calibration exponent of $\gamma = 0$ is the best choice for this system.

Although microscopic method distributions were not available for the *n*-heptane diluted WC-B-B2 bitumen, the trends in the calculated number mean diameters were compared with settling data to help identify the best choice for the calibration exponent. For mixtures of *n*-heptane in WC-B-B2 bitumen, a calibration exponent of $\gamma = -1$ leads to constant diameters along the solvent content composition range, Figure 3.24a. An exponent of 0 leads to diameters that increase with *n*-heptane

content reaching a maximum at approximately 80 wt% *n*-heptane. As will be shown later, the settling rates also increase with *n*-heptane content and reach a maximum at 80 wt% *n*-heptane. Hence, a calibration exponent of 0 is more consistent with the settling data and is recommended for *n*-heptane diluted bitumen.
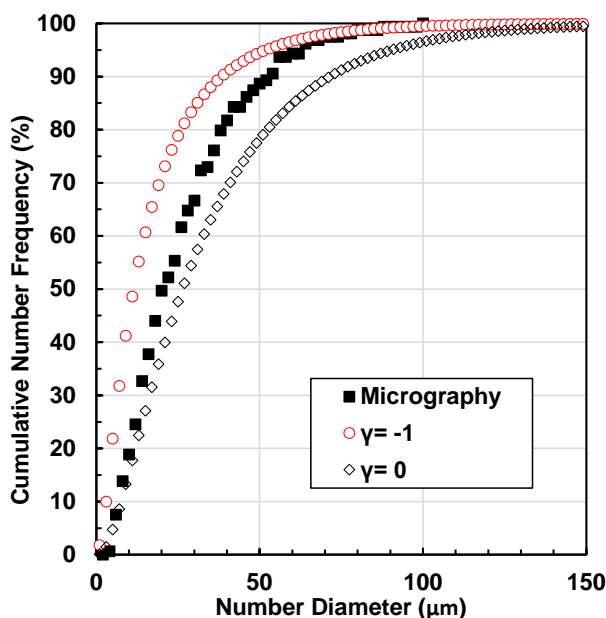
Figure 3.26. Cumulative particle distribution of asphaltene flocs from mixtures of *n*-heptane and WC-B-A3 bitumen at 95 wt% and 21°C, measured with the FBRM and microscopic methods.

3.8 Settling Experiments

Two methods were performed to measure the settling rate of the flocs: the visual method and the sampling method. The visual method was performed when the asphaltene floc concentration was high and the solution was transparent enough to track the interface over time. The sampling method was used for lower asphaltene floc concentrations and opaque solutions where the interface was not visible. The conditions where each experiment was used for either *n*-pentane or *n*-heptane mixtures will be discussed in Section 5.5.

3.8.1 Visual Method

The mixture from the flocculation experiment (Section 3.6) was poured into a 200 mL graduated cylinder with an inside diameter of 3.5 cm. Flocs started to settle immediately and the interface position was visually tracked over time. A flashlight with an incandescent light was focused on the interface with a magnifying glass to improve the visibility of the flocs. The data were plotted as a settling curve; that is, the interface height versus time. To measure the repeatability of this method, the settling rate for flocs in a mixture of n-heptane and WC-B-B2 bitumen at 62.5 wt% solvent content was measured 6 times. The repeatability of the settling rate was ±0.02 cm/min (5.5%) based on a 90% confidence interval.

The above approach was used for the n-heptane diluted bitumen mixtures but, for the n-pentane diluted mixtures, the upper interface was not visible and could not be tracked. Instead, the settling rate was measured by tracking the lower (sediment) interface. The lower interface height increased from zero up to a maximum value where the sediment started to compact. To estimate the settling rate two assumptions were made: the initial height of the flocs was the total height of the liquid and the maximum height of the bottom interface was the point where the upper and bottom interfaces intersected. The settling rate was calculated as the slope between these points. This method was compared and validated with the visual method and ultrasound techniques by Kosior *et al*. (2016) measuring settling flocs from bitumen froth.

3.8.2 Sampling Method

As with the visual method, the mixture from the flocculation experiment (Section 3.6) was poured into a 200 mL graduated cylinder with an inside diameter of 3.5 cm. The mixture was left to settle for a specified time between 10 minutes and 2 hours. After the desired time, a 50 mL glass syringe with a stainless steel needle (length = 30 cm, diameter = 1 mm) was used to remove layers of fluid in sequence from top to bottom. Ten layers of approximately 20 mL each were collected, as shown in Figure 3.27.

Figure 3.27 also shows the procedure for determining the asphaltene and toluene insoluble content of each layer. Each layer was transferred into a 30 mL glass vial to measure its volume and mass.

All samples were centrifuged at 4000 rpm for 5 minutes to separate asphaltenes and toluene insolubles from the supernatant. The supernatant was removed from the vial using a pipette. The residual solids in the vial were washed twice with solvent following the washing procedure described in Section 3.3. After four days of drying, the solid mass was measured to obtain the asphaltene and toluene-insoluble content of each layer. The dried solids were washed with toluene to measure the toluene-insoluble content in each layer following the procedure described in Section 3.4. The final toluene-insoluble content was measured after drying for 4 days. This method could only be applied if the settling time was greater than 10 minutes because at least 4 minutes were required to recover all the samples.
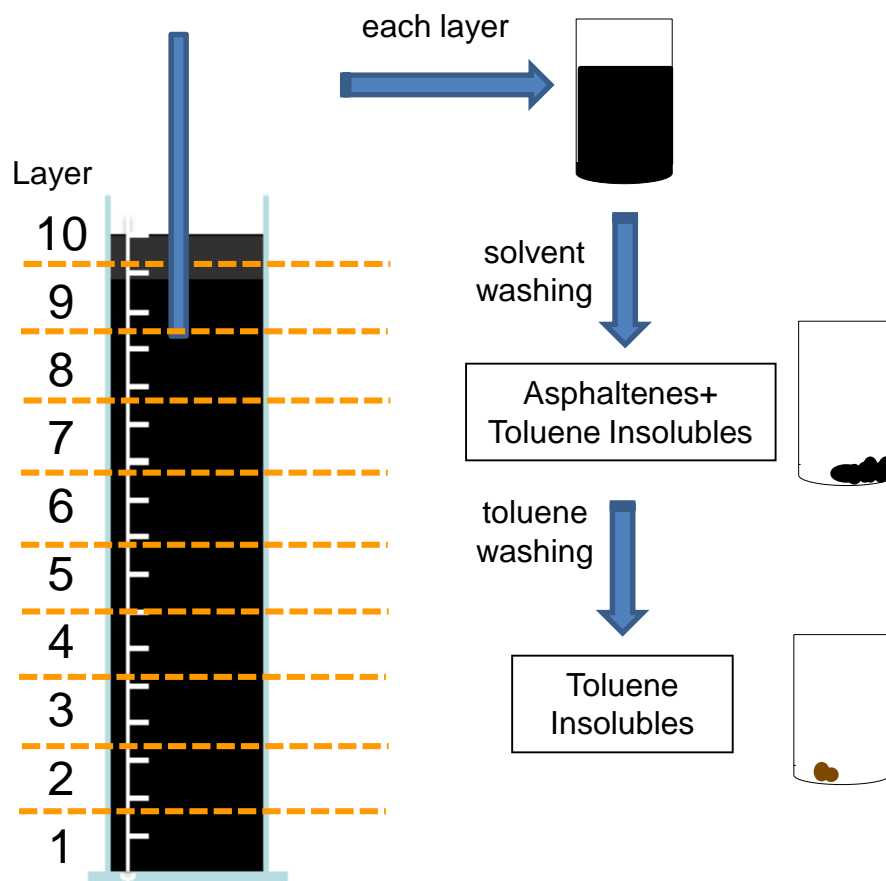
Figure 3.27. Sampling method for the measurement of asphaltene precipitated and toluene-insolubles.

The location of the interface at any given time was determined from the asphaltene and toluene insoluble solid volume fraction profiles as shown for the asphaltenes in Figure 3.28. As will be discussed later, the interface location was the same for the asphaltenes and the toluene insolubles. Above the interface, the solid content is nearly constant and significantly lower than immediately below the interface. The interface is selected as the midpoint between the lowest layer of constant low solids content and the uppermost layer where the solids content increases, Figure 3.28. Since the layer thickness is 2.1 cm, the uncertainty for the position of the interface is ±1 cm.
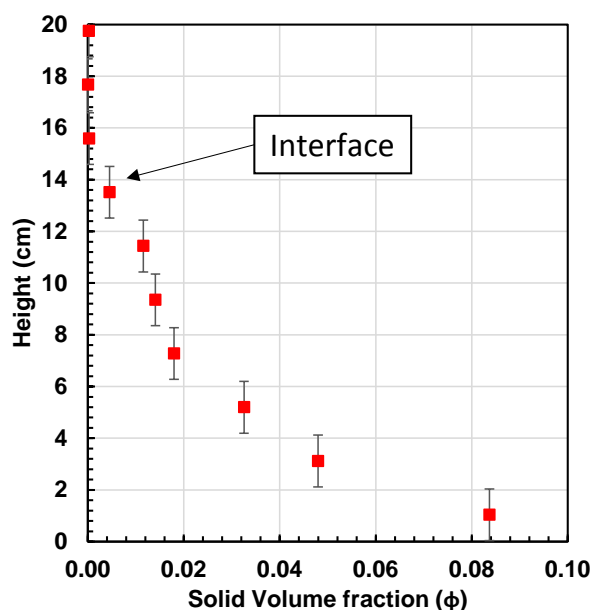
Figure 3.28. Volume fraction profile for flocculated asphaltenes from mixtures of *n*-heptane and WC-B-B2 at 62.5 wt% solvent content, 21°C, and atmospheric pressure.

There are other three sources of uncertainty with the sampling method:

1. The samples are not all collected at the same time; there is up to a 4 minute difference between collecting the first and last samples. The data are all reported at the midpoint time giving a ±2 minute error.

2. There is some error in the mass measurements. A repeat was performed at 20 and 45 minutes for the mixture of 62.5 wt% *n*-heptane in WC-B-B2 bitumen at 21°C. The repeatability for the solid volume fraction was ±0.002.

3. There are some errors in recovering the asphaltenes. The asphaltene mass recovered after each experiment was approximately ±25% different than the expected mass from the yield curve for each bitumen sample. Positive errors can occur when the asphaltenes are washed with pure solvent. Since some supernatant is trapped inside the asphaltenes, extra asphaltenes could precipitate from this trapped supernatant when the solvent is added. Negative errors occur when some asphaltenes stick to the surface of the graduated cylinder and remain there.

3.8.3 Consistency of the Settling Rate Methods

To compare the settling methods, the settling rate of asphaltenes flocs from a mixture of 62.5 wt% *n*-heptane and 37.5 wt% WC-B-B2 bitumen at 21°C was measured with both methods, as shown in Figure 3.29. The location of the interface is systematically lower for the sampling method. However, the slope is identical within the error of the measurements: 0.36 ± 0.10 cm/min for the sampling method and 0.37 ± 0.02 cm/min for the visual method.
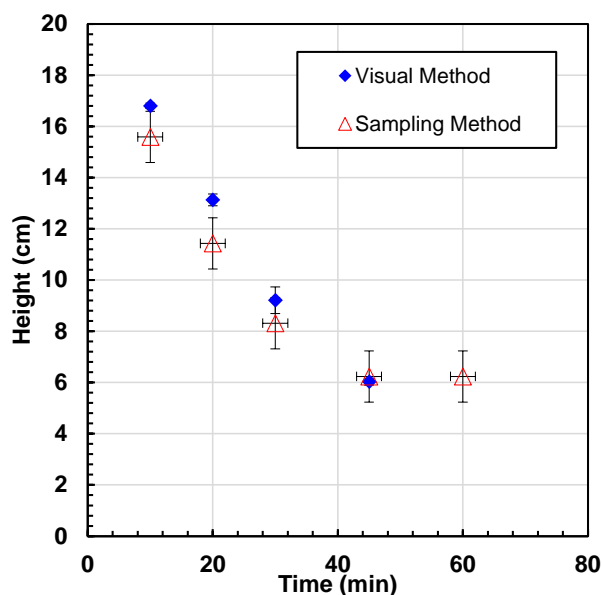
Figure 3.29. Comparison of settling plots from visual and sampling methods for a mixture of *n*-heptane and WC-B-B2 bitumen at 62.5 wt% solvent content, 21°C, and atmospheric pressure.

3.8.4 Sediment Volume Method

The sediment volume method was developed by Duran (2016) to determine the fractal dimension of asphaltene flocs based on the volume they occupy when settled, as shown in Figure 3.30. Initially, flocs settle freely at a constant rate and the interface moves downward linearly when plotted versus time, as shown in Figure 3.31. A sediment accumulates but is difficult to detect in an opaque fluid. However, when all of the solids have settled, the interface coincides with the height of the sediment. The sediment volume decreases slowly after this point as it compacts. Hence, there is a change in slope when all of the solids have settled. The initial "uncompacted" sediment volume was determined from the change in slope in the settling curve. The final "compacted" volume was measured at 24 h in all cases.
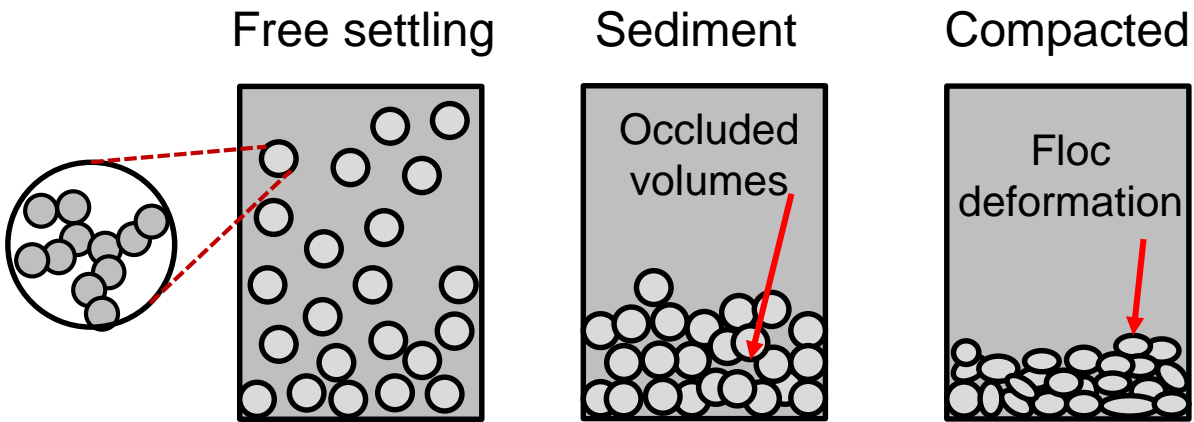
Figure 3.30. Settling process for fractal flocs from settling, sediment and compaction.

The sediment volume is related to the fractal dimension of the flocs as follows:

$$V_{sed} = \frac{m_A \sum_{i=1}^{Nf} f_i \left(\dfrac{d_i}{d_p} \right)^3}{\rho_A \sum_{i=1}^{Nf} f_i \left(\dfrac{d_i}{d_p} \right)^{Df}} \tag{3-7}$$

where V_{sed} is the "uncompacted" sediment volume, m_A is the mass asphaltenes, ρ_A is the density of the asphaltenes, f_i is the number frequency of each diameter in interval i, d_i is the floc diameter

size distribution, d_p is the diameter of the primary particle, and D_f is the fractal dimension. The only unknown is the fractal dimension and it was adjusted to match the measured sediment volume.
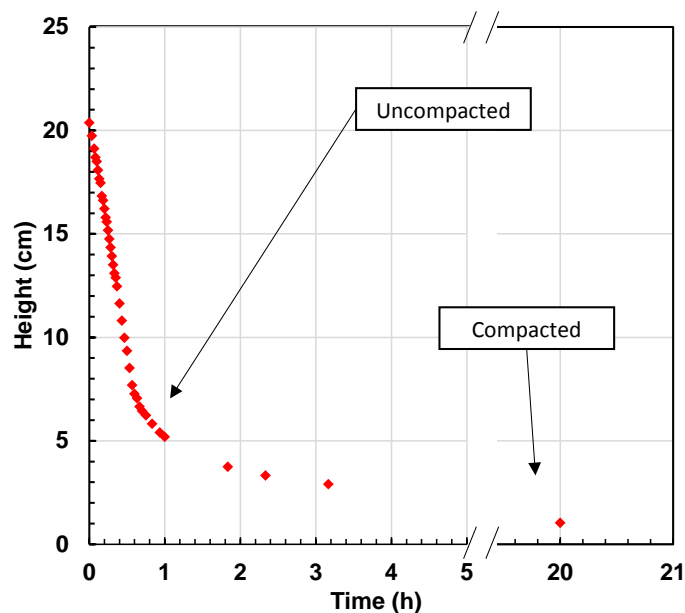
Figure 3.31. Settling plot of flocs from a mixture of *n*-heptane and WC-B-B2 bitumen at 62.5 wt% *n*-heptane, 21°C and atmospheric pressure.

The fractal dimension can be determined from the initial uncompacted sediment volume or the final compacted sediment volume. At the initial condition, the flocs are less likely to have deformed but there may be a significant volume of occluded solvent trapped between the flocs. There is less occluded volume at the final condition but the flocs may have been deformed. Therefore, fractal dimensions are determined for both volumes to establish a range for the fractal dimension. In addition, a lower limit for the fractal dimension can be determined by assuming that the flocs occupy the entire volume of the mixture.

Chapter Four: Settling Model

This chapter presents a numerical model of the settling of a polydisperse size distribution of asphaltene flocs through a column of fluid. The model was adapted from the original version developed by Valinasab (2006) and Saadatmand (2008). To develop this model, it was assumed that:

- the total mass of the asphaltene particles is constant; that is, no asphaltene precipitation occurs during the settling experiment.
- all of the asphaltene particles are 1 μm spheres
- the floc size distribution is constant; that is, no flocculation or shattering occurs during the settling experiment.
- the asphaltene flocs are fractal structures.
- the fractal dimension is the same for all flocs.
- the sediment has a constant porosity; that is, no compaction occurs during the settling experiment
- the particle concentration does not affect the viscosity of the liquid and can be accounted for with a hindering factor.

The model represents the column of fluid as a one dimensional series of layers, Figure 4.1. Briefly, the layers are populated with an initial size distribution of flocs. A finite number of flocs is used and each floc represents a concentration of flocs of the same size. The effective density of each floc is determined from its volume and fractal dimension. At each time step, the movement of each floc is calculated using a hindered settling rate equation and its position is updated. At the end of the time step, the particle concentration of each layer is updated and the procedure is repeated. When the floc concentration exceeds a threshold value, the layer is considered to be filled (to be a sediment) and no more particles are permitted to settle into that layer. A schematic of the model algorithm is provided in Figure 4.2.

The inputs to the model are the fluid density and viscosity, the mass of precipitated asphaltenes, the asphaltene particle density, the floc number diameter distribution, the fractal dimension of the

flocs, and the porosity of the sediment layer. The model is to be used to determine the fractal dimension that provides the best fits to settling data (an iterative procedure) or to predict settling rates from a known fractal dimension (a single pass procedure). In both cases the output of the model is a concentration profile of the flocs along the column at each time step. The settling rate is determined from the change in the interface height of the output profile over a series of time steps. The model was programed in MATLAB®. The model is described in more detail below.
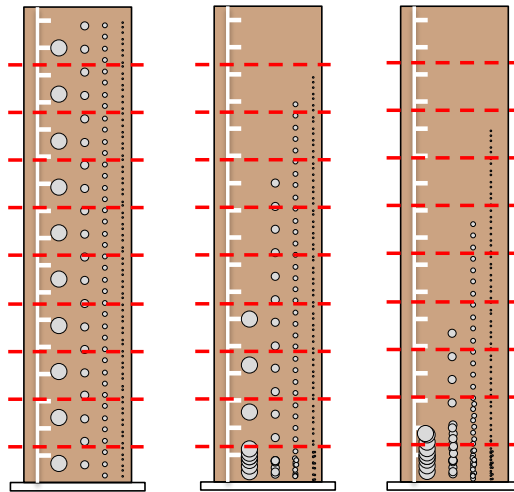
Figure 4.1. Allocation of flocs with different diameters along the cylinder at different settling times.
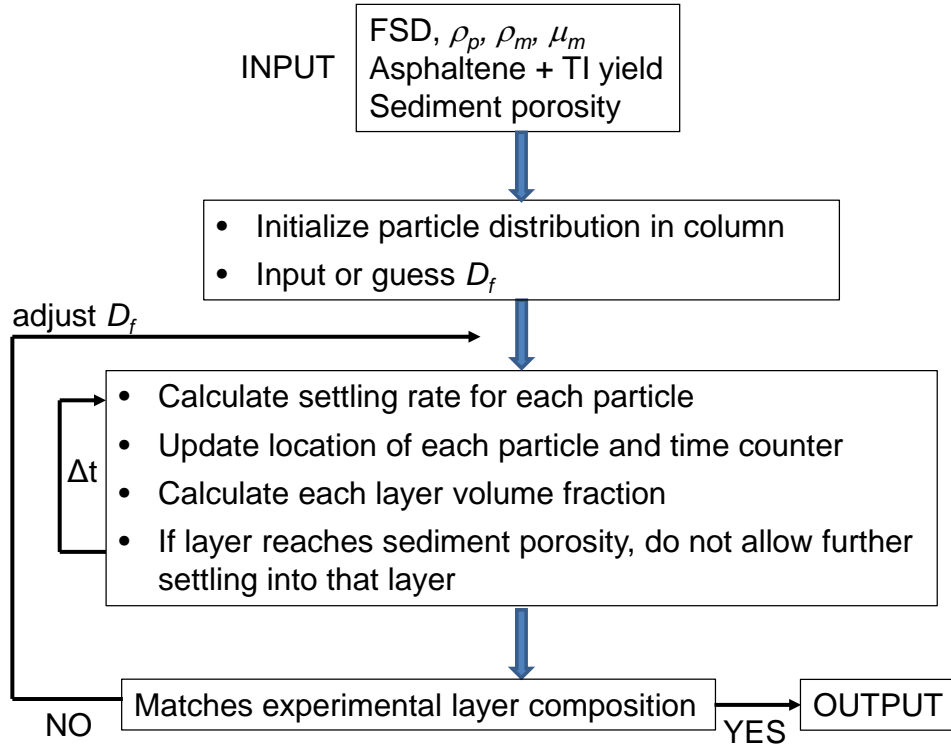
Figure 4.2. Algorithm for the calculation of the fractal dimension.

4.1 Representation of Flocs

The asphaltene flocs are described with a number distribution of maximum diameters where the maximum diameter is the measured diameter in the experiments performed in this thesis. Each asphaltene floc is represented as a mass of asphaltene particles inside a spherical volume described by the maximum diameter of the floc as shown in Figure 4.3. The asphaltene particles are assumed to be monodisperse spherical particles. The mass of such a floc is related to the fractal dimension as follows:

$$m_i = n_f \frac{\pi}{6} d_p^3 \rho_A = \frac{\pi}{6} \left(\frac{d_{floci}}{d_p} \right)^{Df} d_p^3 \rho_A \tag{4.1}$$

where m_i is the mass of the particles inside floc i, n_f is the number of primary particles in the floc, d_p is the diameter of primary particles, d_{floci} is the maximum diameter of the floc, ρ_A is the density of asphaltenes, and D_f is the fractal dimension. The volume of the floc is given by:

$$V_i = \frac{\pi}{6} d_{floci}^3 \qquad (4.2)$$

and the density of the floc is then given by:

$$\rho_i = \frac{m_i}{v_i} = \left(\frac{d_{floci}}{d_p}\right)^{Df-3} \rho_A \qquad (4.3)$$
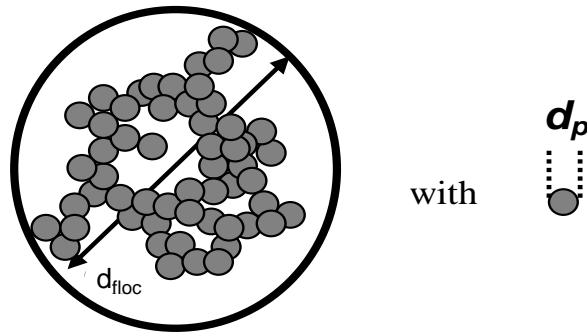
Figure 4.3 Representation of an asphaltene floc: d_p is the diameter of an individual asphaltene particle, d_{floc} is the maximum diameter of the floc.

4.2 Initialization

To reduce the computational requirements, the size distribution of the flocs is represented with 10^5 flocs. Each floc represents a concentration of flocs of that size at that location. The input floc size distributions were divided into bins of equal size interval. The minimum diameter was 1 µm, the maximum diameter was 499 µm, and the increment was 2µm.

The fluid column is divided evenly into ten layers. Flocs of each size are allocated along the graduated cylinder equidistantly. This distance is calculated by dividing the total height of the mixture by the number of particles with a certain diameter.

4.3 Layer Solid Volume Fraction and Free Fluid Fraction Calculations

Solid Volume Fraction

The solid volume fraction in each layer is required to compare with experimental data and is given by:

$$\varepsilon_j = \frac{m_j}{\rho_A A L} \tag{4.4}$$

where ε is the volume fraction of the particles (not flocs), m is the mass of particles, A is the cross-sectional area, L is the thickness, and subscript j is the layer counter.

The mass of particles in each layer is calculated from the number count of each floc as follows:

$$m_j = \sum_i n_{ij} m_{ij} = \sum_i n_{ij} \frac{\pi}{6} \left(\frac{d_{floci}}{d_p} \right)^{Df} d_p^3 \rho_A \tag{4.5}$$

where m_j is the mass of particles in layer j and n_{ij} is the number of flocs with size i in layer j. Note, the expression for the mass of each floc that appears in the final term was obtained from Eq. 4.1.

The number of *modeled* flocs of each size in each layer is counted at the end of each time step but must be converted into the *actual* number of flocs. The actual number of each floc is scaled to the modeled number based on the ratio of the actual total number of flocs to the number of flocs in the model as follows:

$$n_{ij} = \frac{n_{ij}^{mod} N_f}{10,000} \tag{4.6}$$

where n_{ij} and n_{ij}^{mod} are the actual and modeled number of flocs of size i in layer j, and N_f is the total number of flocs in the experiment. The total number of flocs is determined from the total mass of asphaltenes divided by the average mass of asphaltenes in each floc as follows:

$$N_f = \frac{m_A}{\sum f_i m_i} = \frac{m_A}{\frac{\pi}{6} d_p^{3-Df} \rho_A \sum f_i d_{floci}^{Df}} \tag{4.7}$$

where m_A is the mass of precipitated asphaltenes and f_i is the number frequency of floc i.

Free Fluid Fraction

The free fluid volume fraction in each layer is required for the hindered settling calculation. The fluid fraction is the fluid surrounding the flocs excluding entrained fluid (any fluid within the

sphere inscribed within the maximum diameter of each floc). The volume of the flocs in each layer is determined from the number count as follows:

$$V_{f,j} = \sum_i n_{ij} V_{ij} = \sum_i n_{ij} \frac{\pi}{6} d_{floci}^3 \qquad (4.8)$$

where $V_{f,j}$ is the volume occupied by the flocs in layer j. Hence the free fluid volume fraction in each layer is given by:

$$\alpha_j = \frac{V_j - V_{f,j}}{V_j} = 1 - \sum_i \frac{n_{ij}}{V_j} \frac{\pi}{6} d_{floci}^3 \qquad (4.9)$$

where α_f is the free fluid volume fraction in layer j.

4.4 Settling Rate Calculations

The next step is to model the movement of the flocs through time. The distance each floc moves for each time step is calculated as follows:

$$\Delta h_i = u_i \Delta t \qquad (4.10)$$

where Δh_i is the change in height, u_i is the settling rate of floc i, and Δt is the time step (usually 1 second). A time step of 0.1 minutes was found to provide numerical error below the error of the measurements, as will be discussed later. The new position of each particle at time $t+\Delta t$ is then:

$$h_{t+\Delta t} = h_t - \Delta h \qquad (4.11)$$

The settling rate of each particle is calculated from Stokes' Law applied to porous flocs, Equation 2-11. The permeability of the floc (Eq. 2-12) and the hindering effect from the Richardson and Zaki approach (Eq. 2-16) are included to obtain the following settling rate expression:

$$u_h = \frac{g(\rho_A - \rho_l)d_p^2}{18\mu_m \Omega} \left(\frac{d_{floci}}{d_p} \right)^{Df-3} \alpha_f^n \qquad (4.12)$$

where ρ_l is the density of the liquid mixture, μ_l is the mixture viscosity, α_f is the volume fraction of the fluid, and n is the Richardson and Zaki hindering exponent. In this thesis, the hindering exponent, n, was set to 4.65 as recommended by Richardson and Zaki for low Reynolds numbers and applied by Saadatmand (2008) to froth settling. Further discussion about the sensitivity to the

73

hindering exponent will be presented in Chapter 5. As noted in Chapter 2, the permeability factor is given by (Long *et al.*, 2004; Rahmani *et al.*, 2005):

$$\Omega = \frac{2\beta^2\left(1 - \dfrac{\tanh\beta}{\beta}\right)}{2\beta^2 + 3\left(1 - \dfrac{\tanh\beta}{\beta}\right)} \tag{4.13}$$

where $\beta = \dfrac{d_{floc}}{2\sqrt{\kappa}}$ and κ is the permeability given by:

$$\kappa = \frac{d_p^2}{72}\left[3 + \frac{4}{1-\phi} - 3\sqrt{\frac{8}{1-\phi} - 3}\right] \tag{4.14}$$

where d_p is the diameter of primary particle and (1-ϕ) is the solid fraction calculated using Equation 2.8.

4.5 Particle Tracking and Sedimentation

Flocs are not allowed to settle below the bottom of the column or into a sediment layer. If, at the end of a time step, the calculated position of the floc is negative (below the bottom of the column) it is reset to zero. If the location is within a defined sediment layer, it is reset to the bottom of the layer above the sediment.

A layer is defined to be a sediment if its solid volume fraction exceeded a defined threshold. After each time step, the solid volume fraction of each layer is determined and compared with the threshold. If the threshold is exceeded, all of the particles in the sediment layer are fixed in their current position and no longer allowed to settle. The threshold was set to the measured sediment porosity in each case.

4.6 Fitting Model to Data

The model stops when it reaches the input settling time. At any pre-specified time and at the end of the run, the solid fractions in each layer are reported. Hence, the output is a series of concentration profiles over the length of the column. The model was fit to experimentally

measured concentration profiles or interface heights over time. In this thesis, the fractal dimension was varied to match the experimental data.

Fitting Concentration Profiles

The model was fitted to the concentration profiles in the free settling region; that is, not including the sediment. In this study, the top seven layers of the model were considered for data fitting. The fractal dimension was iterated to minimize the square difference between the experimental and calculated solid volume fractions using the following optimization function:

$$OF = 1{,}000{,}000 \sum \left(\varepsilon_{\exp, j} - \varepsilon_{\text{mod}\,el, j} \right)^2 \tag{4-15}$$

where OF is the optimization function and the subscripts *exp* and *model* stand for the experimental data point and the model output for layer j, respectively. Note, the error was multiplied by one million to obtain OF values in the order of unity. The optimization function was minimized using the fminbnd function in MATLAB®. This function was used to adjust the variable, D_f, in a constrained range from 2.0 to 3.0 in all mixtures. The OF function was evaluated along the given range and it has a concave trend and in all cases exhibited a global minimum with no local minima as shown in Figure 4.4.
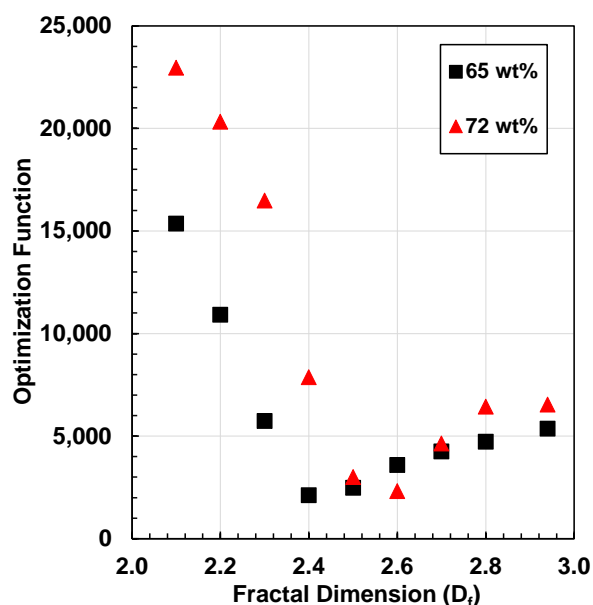
Figure 4.4. Optimization function evaluated for the mixture h-heptane/WC-B-A3 at 65 and 72 wt% solvent content.

Fitting Interface Location

For experiments where the visual method was performed, the solid fractions were not available. Instead, the position of the upper interface at different times was recorded. Hence, the location of the interface in the model was required for data fitting. The interface was located as a distinct change in the volume fraction profile of the asphaltenes calculated from the model. For example, Figure 4.4 presents the solid volume fraction calculated with the settling model for the *n*-heptane/WC-B-B2 mixture. In order to match experimental data, the model results were analyzed in terms of layers. Recall that the height of each layer was 2.1 cm except layer 1 with a height of 1.05 cm. In this example, the interface was identified in layer 7 (between 11.4 and 13.5 cm) after 20 minutes and in layer 6 (between 9.4 and 11.4 cm) after 30 minutes of settling. The same procedure was applied for all the solvent/bitumen mixtures at different solvent content and settling times.
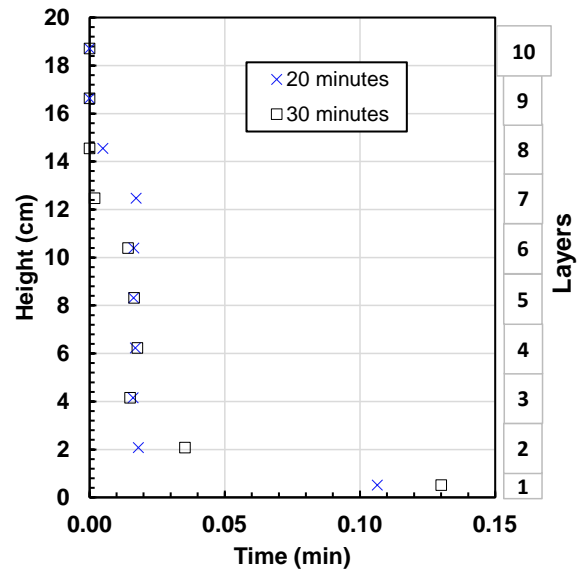
Figure 4.5. Solid volume fraction profile of asphaltene flocs from *n*-heptane/WC-B-B2 mixture at 62.5 wt% solvent content, calculated after 20 and 30 minutes settling with Df=2.65.

Chapter Five: Results and Discussion

The objective of this thesis was to measure and model the settling and removal of fine solids with asphaltenes precipitated from bitumen diluted with a paraffinic solvent. This chapter presents the required data including the amount and size distribution of the flocculated asphaltenes, the fractal dimension of the flocs, the density and viscosity of the diluted bitumen, and the settling rates. First, the onset (solvent content at which asphaltenes start to precipitate) and yield of the precipitated asphaltenes are presented. The data and methods used to determine the density and viscosity of the diluted bitumen are explained. The particle size distributions and fractal dimensions of the flocs formed from the precipitated asphaltenes and co-flocculated toluene insoluble material (such as sand and clay) are shown at different solvent contents. The settling rate of the asphaltene flocs and toluene insolubles are presented as a function of solvent content. Finally, the data are modeled and the model is tuned to fit the settling data by adjusting the fractal dimension of the flocs. The fitted fractal dimensions are compared with the fractal dimensions from the sediment volume method to validate the model.

Two bitumen samples were considered in this thesis: WC-B-A3 and WC-B-B2. As noted in Chapter 3, both samples were obtained from SAGD processes prior to any chemical addition. The *n*-pentane insoluble asphaltene content and the toluene insoluble (TI) content of each oil is reported in Table 5.1. The paraffinic solvents considered in this thesis were *n*-pentane and *n*-heptane. Data were collected for the following mixtures: *n*-pentane/WC-B-A3, *n*-heptane/WC-B-A3, and *n*-heptane/WC-B-B2.

Table 5.1. Toluene insoluble content of bitumen samples.

Bitumen Sample	Asphaltene Content wt%	TI Content wt%
WC-B-A3	12.0	0.02
WC-B-B2	14.5	0.16

5.1 Yield and Onset of Asphaltene Precipitation

The onset of asphaltene precipitation (the solvent content at which precipitation occurs) was required to design the flocculation and settling experiments. The asphaltene yield at a given solvent content was required to determine the mass of precipitated asphaltenes in the flocculation and settling experiments. This mass is a required input for the settling model.

Figure 5.1 shows the yield of asphaltene precipitation for the *n*-pentane/WC-B-A3 and *n*-heptane /WC-B-A3 mixtures measured after 1.5 hours at different solvent contents. As expected from Akbarzadeh *et al.*, (2005) and Wiehe *et al.*, (2005), the asphaltene yield increased monotonically as the solvent content increased, and the asphaltene yield is higher with *n*-pentane than with *n*-heptane. The asphaltene content of the WC-B-B2 bitumen, Figure 5.2, compares the yield curve for the *n*-heptane/WC-B-B2 and *n*-heptane/WC-B-A3 mixtures. The ultimate yield is proportional to the asphaltene content and is higher for the WC-B-B2 bitumen than the WC-B-A3 bitumen.
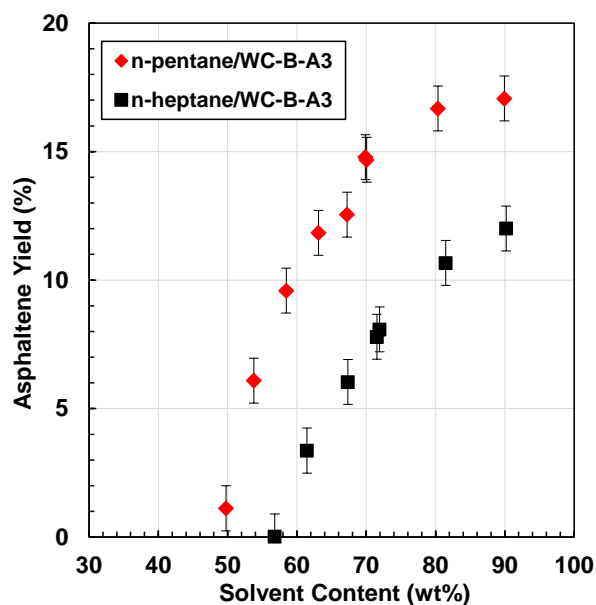
Figure 5.1. Asphaltene yield from WC-B-A3 bitumen diluted with *n*-pentane and *n*-heptane at 21°C and 1.5 hours after contact with the solvent.
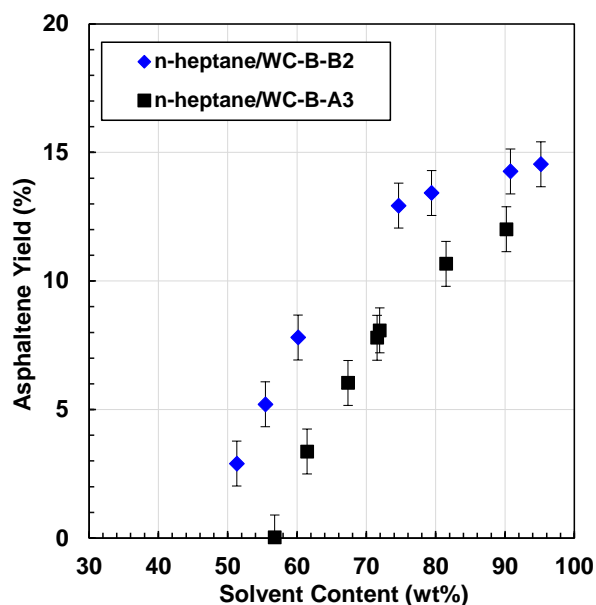
Figure 5.2. Asphaltene yield from WC-B-B2 bitumen diluted with *n*-heptane at 21°C and 1.5 hours after contact with the solvent.

The onsets of asphaltene precipitation were calculated from the yield curves in Figures 5.1 and 5.2 using the extrapolation method described in Section 3.5, and are reported in Table 5.2. The greater the solubility of the asphaltenes, the higher the onset. Hence, the onset in *n*-heptane is higher than the onset in *n*-pentane. The onset for WC-B-A3 bitumen is higher than the onset for WC-B-B2 bitumen indicating that the WC-B-A3 bitumen is a better solvent for asphaltenes than the WC-B-B2 bitumen.

Table 5.2. Onset of asphaltene precipitation for different solvent/bitumen mixtures. The onset solvent contents have an uncertainty of ±0.6 wt%.

Mixture	Onset, wt%
n-pentane/WC-B-A3	47.6
n-heptane/WC-B-A3	56.3
n-heptane/WC-B-B2	46.1

5.2 Density and Viscosity of Diluted Bitumen

The density and viscosity of the continuous phase (the supernatant in the settling experiments) of the diluted bitumen after asphaltene precipitation are required to calculate the settling rates. The

density of the supernatant was measured from samples taken from the settling experiments after a settling time of 24 hours. The densities for the three mixtures are reported in Figure 5.3. The density of supernatant from both WC-B-A3 and WC-B-B2 diluted with *n*-heptane was similar at solvent contents above 50 wt% because the density of both bitumen samples is similar and the solvent content is relatively high. The density of the supernatant from the mixture *n*-pentane/WC-B-A3 was lower because the density of the *n*-pentane is lower than the density of the *n*-heptane. These results are in agreement with densities measured by Saryazdi *et al*. (2013) and Nourozieh *et al*. (2014).
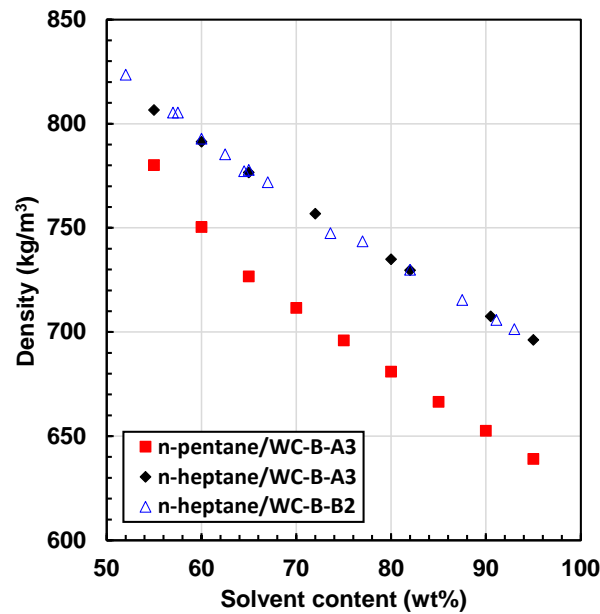
Figure 5.3. Measured density of supernatant from *n*-pentane/WC-B-A3, *n*-heptane/WC-B-A3 and *n*-heptane/WC-B-B2 mixtures at different solvent contents.

The viscosity of the supernatant was calculated using the Expanded Fluid model (Yarranton and Satyro, 2009) given by:

$$\mu - \mu_0 = 0.165\left(\exp(c_{2,mix}\beta_{mix}) - 1\right) \tag{5-1}$$

where μ is the viscosity of the fluid in mPa.s formulated as a departure from the diluted gas viscosity μ_0, $c_{2,mix}$ is a parameter specific to each mixture and β_{mix} is the correlation parameter between the density and the viscosity. The mixture parameters $c_{2,mix}$ and β_{mix} were calculated using the mixing rules recommended by Ramos-Pallares *et al*. (2016). The solvent parameters were

obtained from Yarranton and Satyro (2009). The parameters for the bitumen were obtained by fitting viscosity data. The binary interaction parameter required for the mixing rules was determined from a correlation to the specific gravities of the solvent and the bitumen (Ramos-Pallares *et al*., 2016). Details are provided in Appendix A.

Figure 5.4 presents the viscosity of the three mixtures at different solvent contents. As expected, the viscosity decreases exponentially as the solvent content increases. Although the viscosity of the WC-B-A3 was higher than the WC-B-B2, the viscosities of the diluted bitumens are similar because they are approaching the solvent viscosity and some of the asphaltenes have been precipitated out of the bitumen. The viscosity of the bitumen diluted with *n*-pentane is lower than the viscosity when diluted with *n*-heptane because *n*-pentane has a lower viscosity than *n*-heptane. The calculated viscosity is in agreement with viscosities measured by Shafiee (2014) ranging from 0.50 to 0.68 for diluted bitumen with *n*-heptane above 87.5 wt% solvent content. Note, the measured densities were used as the model input and small errors in the density caused some deviations from a smooth viscosity trends versus solvent content.
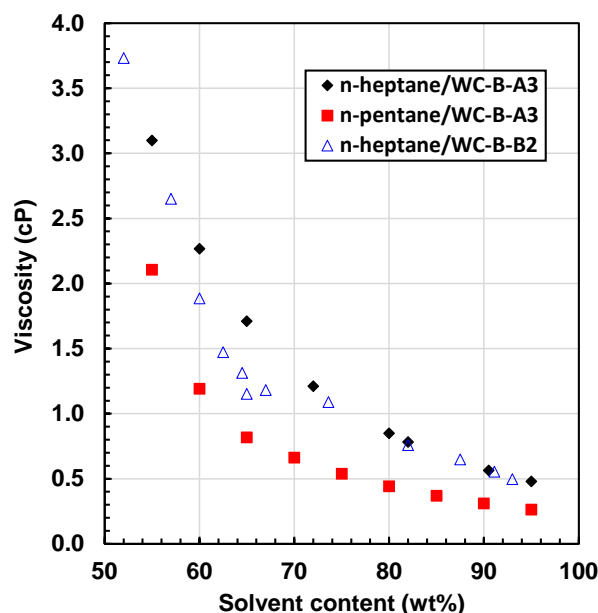
Figure 5.4. Calculated viscosity of supernatant from *n*-pentane/WC-B-A3, *n*-heptane/WC-B-A3 and *n*-heptane/WC-B-B2 mixtures at different solvent contents. The deviations for the latter mixture are caused by small errors in the measured density used as an input to the model.

5.3 Asphaltene Floc Size Distributions

The asphaltene floc size distributions are a key factor in the settling rates. Note that asphaltene flocculation is being examined in detail in a separate project and, in this thesis, the distributions are only considered as required to interpret and model the settling data. The floc size distributions were measured for the *n*-pentane/WC-B-A3, *n*-heptane/WC-B-A3 and *n*-heptane/WC-B-B2 mixtures at solvent contents above the onset of asphaltene precipitation. Typical floc size distributions are presented below and then the floc size distributions for the three mixtures are presented.

5.3.1 Asphaltene Flocs

Asphaltene flocs from diluted bitumen are generally highly polydisperse in size with irregular structures which can be loose (low fractal dimension) to compact (high fractal dimension) depending on the conditions at which they formed. Figure 5.5 is a series of micrographs illustrating the effect of increasing solvent content on the flocs formed in *n*-heptane/WC-B-B2 mixtures. The asphaltene flocs increased in size as the *n*-heptane content increased from 57.5 to 80.0 wt% and then remained constant at higher dilutions. There was a wide distribution of floc sizes at all compositions. The flocs were compact at low *n*-heptane content but became more loosely structured as the *n*-heptane content increased.

Figure 5.6 compares micrographs of asphaltene flocs precipitated from WC-B-A3 bitumen diluted to a 70 wt% *n*-pentane content at 21°C with those precipitated from the same bitumen diluted to a 72 wt% with *n*-heptane content. The flocs formed in *n*-pentane tend to be larger, more compact, and less polydisperse.

Duran *et al.* (2017) have shown that the flocs are in fact fused structures that form within seconds via simultaneous nucleation, growth, and flocculation. The final structure are glassy and non-sticky; they can be shattered at sufficient shear rate but will not re-flocculate at lower shear rates. Therefore, the floc size distributions measured in the micrographs and with the FBRM method are expected to be representative of the flocs in the settling experiments.
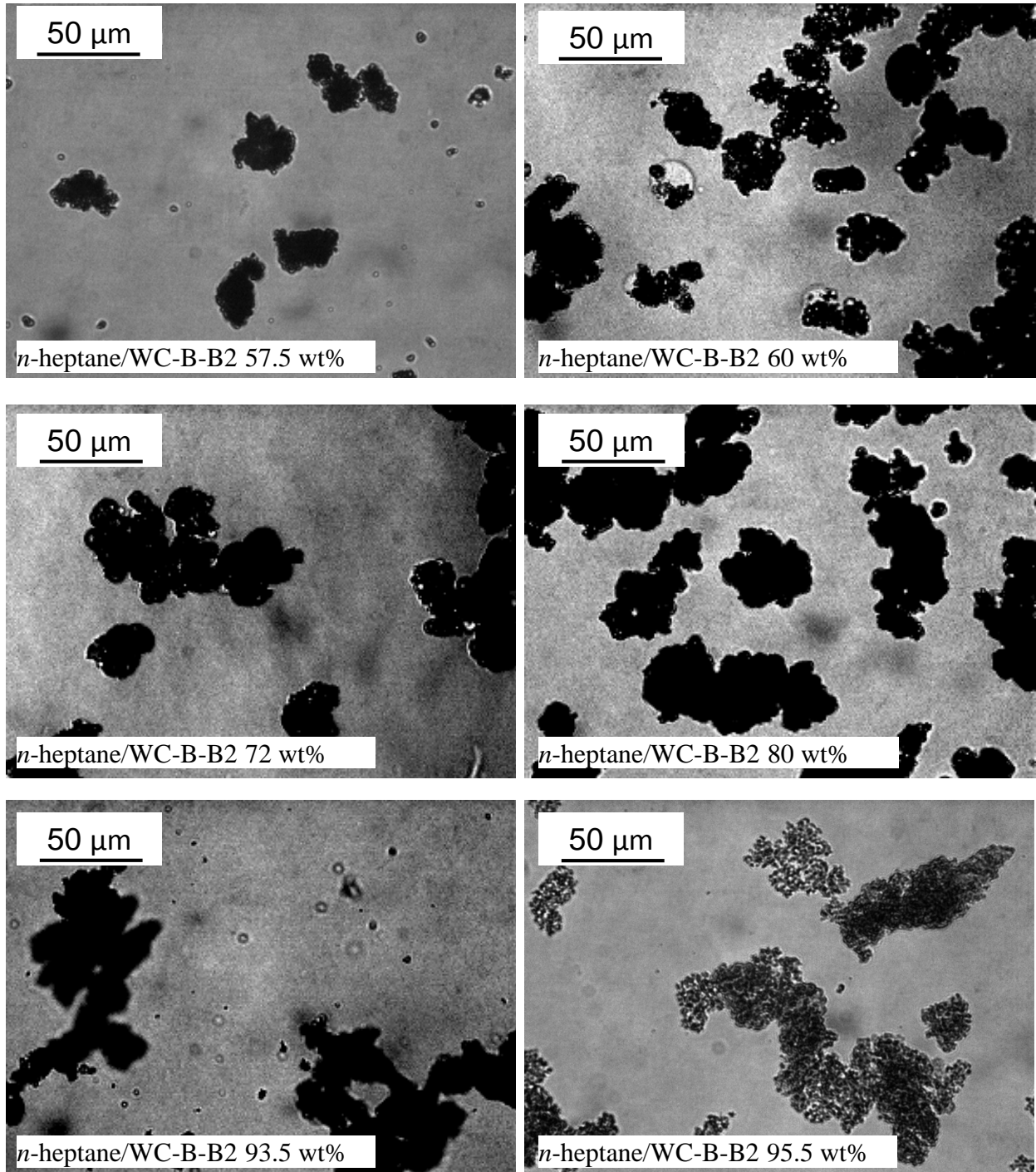
Figure 5.5. Micrographs of asphaltene flocs from *n*-heptane/WC-B-B2 bitumen at 21°C and *n*-heptane contents from 57.5 to 95 wt%. (Duran, 2016)
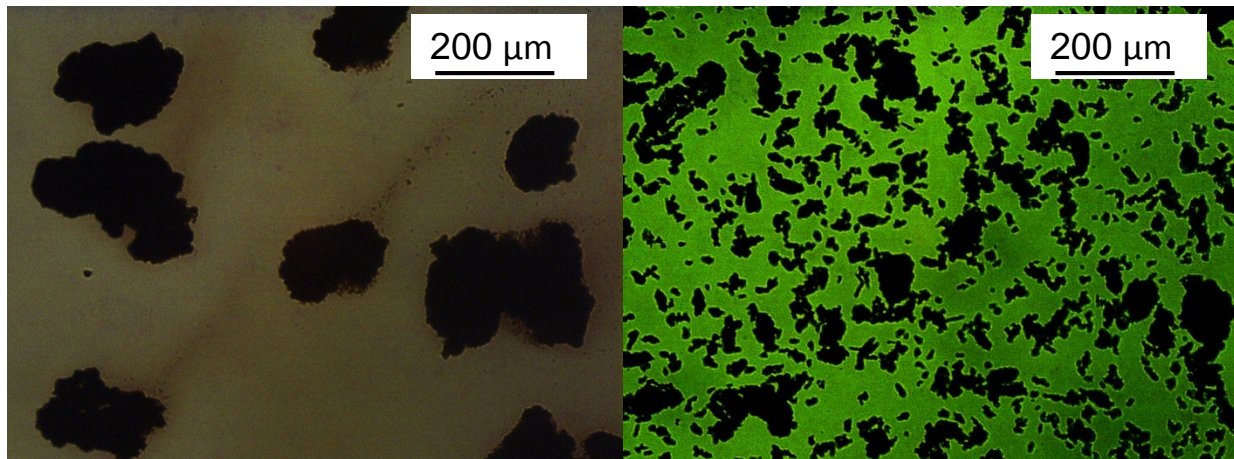
Figure 5.6. Micrographs of asphaltene flocs from WC-B-A3 bitumen/solvent mixtures: a) 70 wt% *n*-pentane; b) 72 wt% *n*-heptane.

5.3.2 Shape of Asphaltene Floc Size Distribution

Figure 5.7a presents two examples of number frequency distributions for asphaltene flocs from the *n*-heptane/WC-B-A3 mixture at two solvent contents, 72 wt% and 80 wt%. Both number frequencies have an approximately lognormal distribution. All the floc number size distributions from the *n*-pentane/WC-B-A3, *n*-heptane/WC-B-A3 and *n*-heptane/WC-B-B2 mixtures had similar shapes (see Appendix B). Hence, the approximately lognormal shape of the floc size distribution is independent of the sample, solvent type, and solvent content. These number frequency distributions are in agreement with the distributions reported in the literature (Calles *et al*., 2008; Daneshvar, 2005; Ferworn *et al*., 1993; Rastegari *et al*., 2004; Shafiee, 2014).
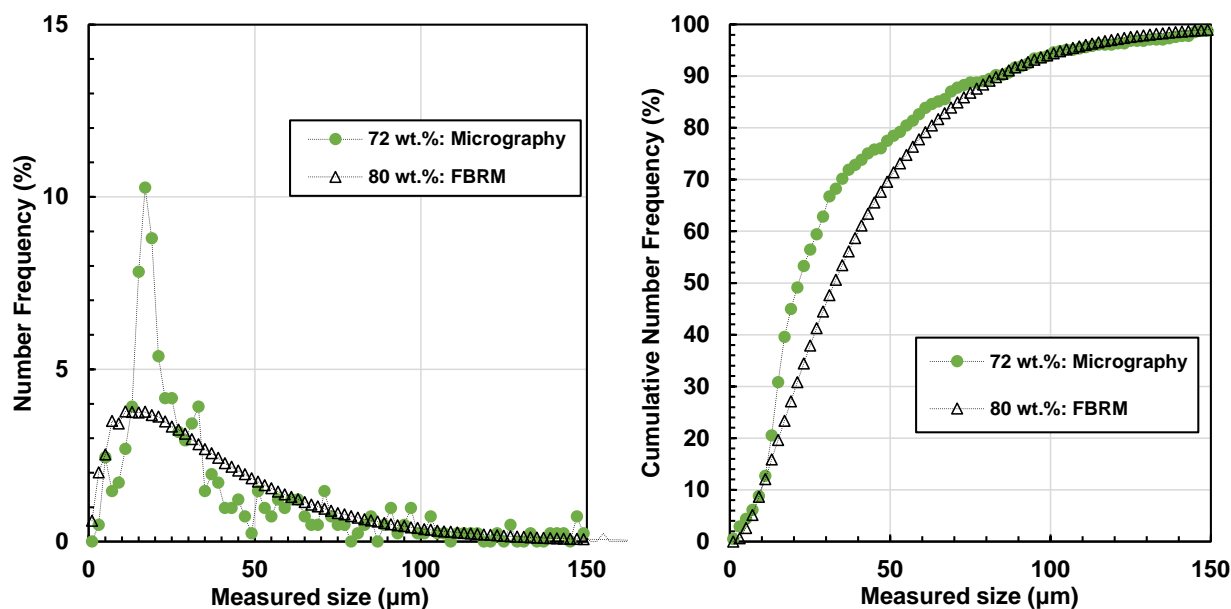
Figure 5.7. Number frequency (a) and cumulative number frequency (b) distributions of asphaltene flocs from *n*-heptane/WC-B-A3 mixtures after 1.5 hours at 21°C and at 72 wt% and 80 wt% solvent content.

The distributions at 72 and 80 wt% *n*-pentane were measured with the micrographic and FBRM methods, respectively. Since the micrographic method is based on a lower floc count than the FBRM, the number frequency distributions from this method are not as smooth and continuous as the number frequency distributions from the FBRM method. Therefore, cumulative number frequency distributions will be used to compare results. The cumulative number frequency distributions in Figure 5.7b correspond to the number frequency distributions in Figure 5.7a. As noted in Chapter 3, the FBRM was calibrated to be in overall agreement with the microscopic method but, as shown in Figure 5.7b, some differences remain in individual cases. These differences are generally small compared with the effects of solvent type and content as will be seen below.

In the following discussion, the following parameters are considered when representing the distributions:

1) the number mean diameter, d_n, given by:

$$d_n = \frac{\sum f_i d_i}{\sum f_i} \tag{5-2}$$

2) the area mean diameter, d_A, given by:

$$d_V = \frac{\sum f_i d_i^2}{\sum f_i d_i} \tag{5-3}$$

3) the volume mean diameter, d_V, given by:

$$d_V = \frac{\sum f_i d_i^4}{\sum f_i d_i^3} \tag{5-4}$$

4) the log number mean diameter, d_{LN}, given by:

$$d_{LN} = e^{\mu_{\ln d} + \sigma_{\ln d}^2 / 2} \tag{5-5}$$

5) the standard deviation, σ_d, given by:

$$\sigma_d = \sqrt{e^{2\mu_{\ln d} + \sigma_{\ln d}^2} \left(e^{\sigma_{\ln d}^2} - 1 \right)} \tag{5-6}$$

where f_i is the number frequency of interval i, and μ and σ with subscript "lnd" are the mean and standard deviation of the logarithmic distribution. The log mean diameter and the standard deviation give the statistically correct interpretation of the mean and breadth of the distribution. The settling model was tested with the number mean, log mean, area mean, and volume mean diameter. As will be discussed later, the number mean diameter was selected because it is simple and best matched the settling rates with the measured fractal dimensions. The volume mean diameter is used to compare with data from the literature.

5.3.3 Floc Size Distributions

_n_-Pentane/WC-B-A3 Mixtures

Figure 5.8 shows the cumulative number frequency distribution of the asphaltene flocs from the _n_-pentane/WC-B-A3 mixtures at different solvent contents. The number mean diameter and the standard deviation of the distributions are provided in Table 5.3. The breadth of the distribution and the mean diameters increased as the _n_-heptane content increased to 70 wt% and then decreased at higher dilutions. As expected in a flocculating system, the trend in the mean diameter corresponds approximately to the concentration of precipitated asphaltenes which peaks at an _n_-

pentane content of 65 wt%, Figure 5.9. In other words, the lower the inter-particle distance, the greater the flocculation.

In general, the volume mean diameters of the *n*-pentane asphaltene flocs are consistent with the literature data. Daneshvar (2005) measured the volume mean diameters (d_V) of asphaltene flocs as 300 μm at 95 wt% *n*-pentane content in diluted bitumen. Calles *et al.* (2008) reported lower values with number mean diameters between 18 and 78 μm for *n*-pentane contents ranging between 75 and 96 wt%.
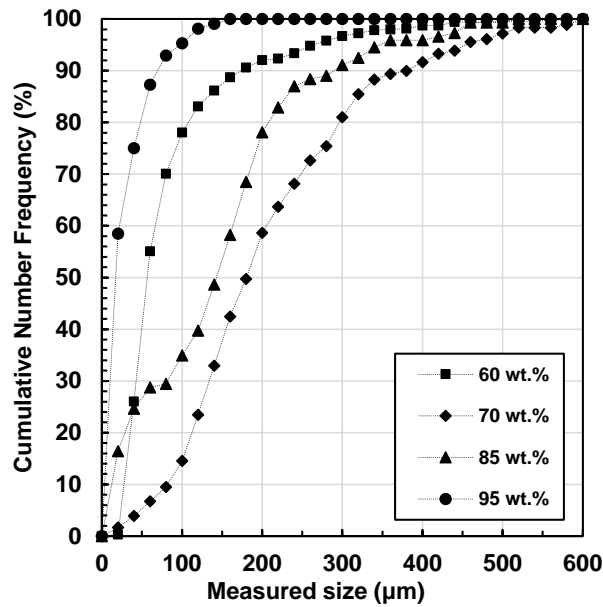
Figure 5.8. Cumulative floc size distribution measured with the micrographic method for *n*-pentane/WC-B-A3 mixtures after 1.5 hours at 21°C and at *n*-pentane contents from 60 to 95 wt%.

Table 5.3. Number mean diameter, volume mean diameter, log number mean diameter, lower and upper limits of standard deviation for asphaltene floc size distributions from n-pentane/WC-B-A3 mixtures after 1.5 hours at 21°C and at n-pentane contents from 60 to 95 wt%.

n-Pentane Content wt%	d_n µm	d_V µm	d_{LN} µm	σ_d µm
60	85	365	80	60
70	205	395	215	165
85	145	334	180	325
95	30	105	25	45
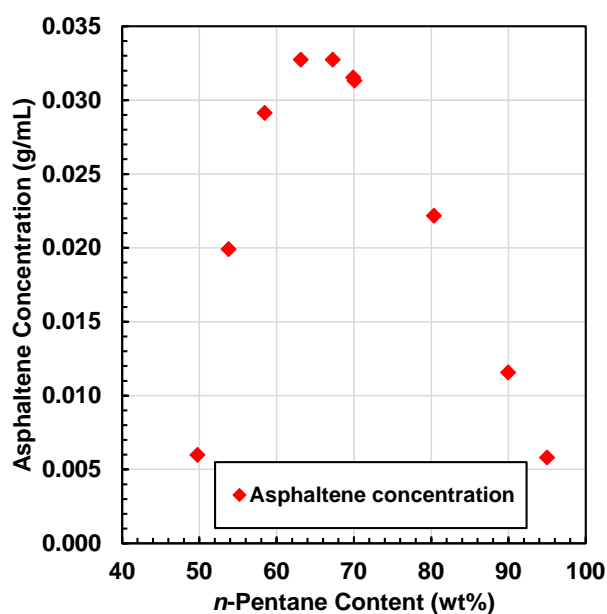
Figure 5.9. Precipitated asphaltene concentration from n-pentane/WC-B-A3 mixture after 1.5 hours at 21°C from 50 to 95 wt%.

<u>n-Heptane/WC-B-A3 Mixtures</u>

Figure 5.10 presents the cumulative number frequency distribution of the asphaltene flocs from the n-heptane/WC-B-A3 mixtures at different solvent contents. The number mean diameter and the standard deviation of the distributions are provided in Table 5.4. The number mean diameter of the distributions increased from 60 to 65 wt% n-heptane content but did not change significantly at higher dilutions. The breadth of the distribution increased up to 90.5 wt% n-heptane. The maximum in the mean diameters again corresponds approximately to the maximum concentration of precipitated asphaltenes which peaks at an n-heptane content of 72 wt%, Figure 5.11. However,

the mean diameter did not decrease at higher dilutions when the asphaltene concentration decreased. It is possible that as the medium becomes less compatible with the asphaltenes, the driving force for flocculation increases and overcomes the effect of reduced asphaltene particle concentration.

It is not known why the sustained mean diameters are observed in the *n*-heptane diluted bitumen but not in the *n*-pentane diluted bitumen. Note that such inconsistencies also appear in the literature. Ferworn *et al.* (1993), Rastegari (2004), and Daneshvar (2005) reported an increase in the volume mean diameter of flocculated asphaltenes as the *n*-heptane content increases with a plateau above 92 wt% solvent content. However, Calles *et al.* (2008) reported that the diameter increased monotonically as the solvent content increased and Shafiee (2014) found a maximum volume mean diameter around 92 wt% solvent content.
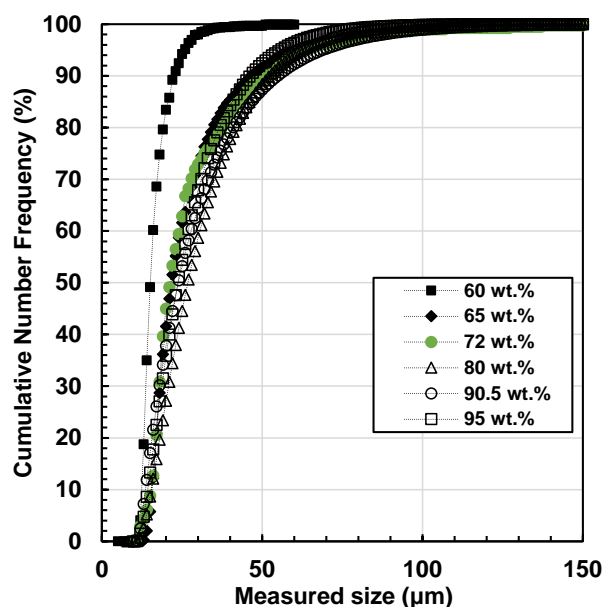
Figure 5.10. Cumulative floc size distribution of *n*-heptane/WC-B-A3 mixtures after 1.5 hours at 21°C and at *n*-heptane contents from 60 to 95 wt%. Closed and open symbols indicate data collected with the microscopic and FBRM methods, respectively.

Table 5.4. Number mean diameter, volume mean diameter, log number mean diameter, lower and upper limits of standard deviation for asphaltene floc size distributions from *n*-heptane/WC-B-A3 mixture at different solvent content.

n-Heptane Content wt%	d_n μm	d_V μm	d_{LN} μm	σ_d μm
60.0	17	51	13	9
65.0	33	163	33	31
72.0	36	175	38	34
80.0	42	117	43	47
90.5	39	158	43	67
95.0	35	105	36	44
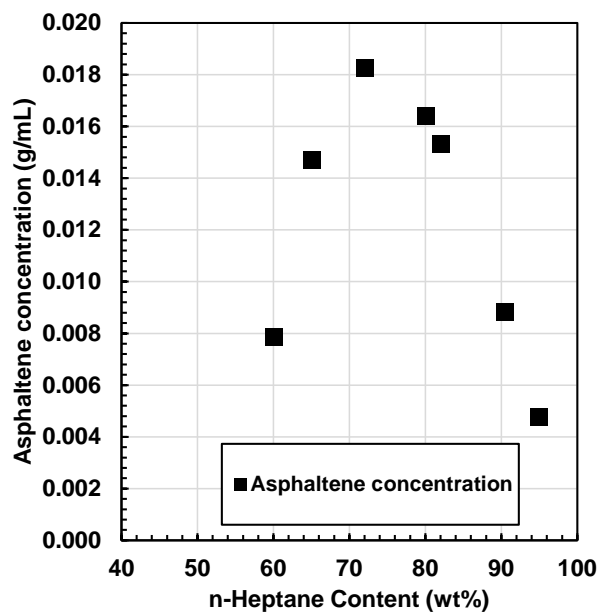
Figure 5.11. Precipitated asphaltene concentration from *n*-heptane/WC-B-A3 mixture after 1.5 hours at 21°C from 60 to 95 wt%.

Figure 5.12 shows that the number mean diameter of the flocs from the *n*-heptane/WC-B-A3 mixtures are significantly smaller than flocs from the *n*-pentane/WC-B-A3 mixtures. Asphaltenes are more soluble in *n*-heptane than in *n*-pentane (Wiehe *et al.*, 2005). It appears that when the asphaltenes come out of solution in a more soluble medium, there is less driving force for aggregation and smaller structures are formed.
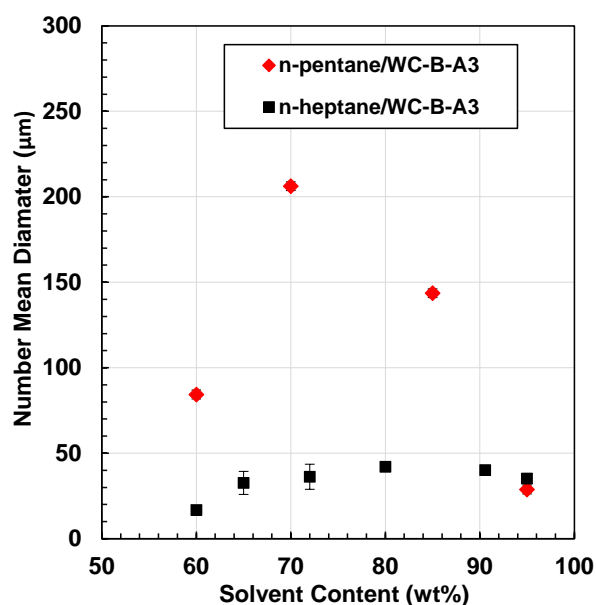
Figure 5.12. Number mean diameter for asphaltene flocs from *n*-pentane/WC-B-A3 and *n*-heptane/WC-B-A3.

n-Heptane/WC-B-B2 Mixtures

Figure 5.13 presents the cumulative number frequency distribution of the asphaltene flocs from the *n*-heptane/WC-B-B2 mixtures at different solvent contents. The number mean diameter and the standard deviation of the distributions are provided in Table 5.5. Figure 5.14 shows that the flocs in the *n*-heptane/WC-B-B2 mixture follow the same trend versus *n*-heptane content as the flocs in the *n*-heptane/WC-B-A3 mixture but are larger at any given condition. The larger floc size may arise from the poorer solubility of the asphaltenes in the WC-B-B2 bitumen versus the WC-B-A3 bitumen, as noted in Section 5.1.

In general, the volume mean diameters of the *n*-heptane asphaltene flocs are consistent with the literature data. Ferworn *et al.* (1993) measured volume mean diameters between 196 and 286 μm at *n*-heptane solvent content ranging 77 to 96 wt%. Daneshvar (2005) measured volume mean diameters of 85, 145 and 105 μm at *n*-heptane contents of 83, 91 and 97 wt%, respectively. Similarly, Shafiee (2014) measured volume mean diameters of 165, 130 and 110 μm at 88, 93 and 95 wt% *n*-heptane content.
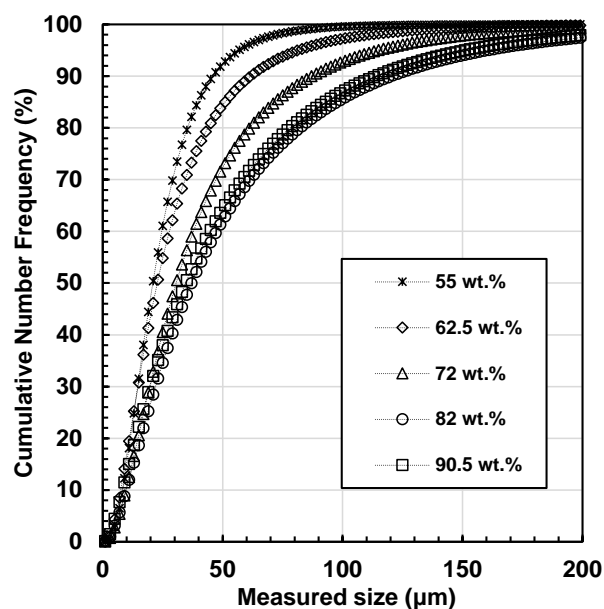
Figure 5.13. Cumulative floc size distribution of *n*-heptane/WC-B-B2 mixtures after 1 hour at 21°C and at *n*-heptane contents from 55 to 90.5 wt%. All data were collected with the FBRM method.

Table 5.5. Number mean diameter, volume mean diameter, log number mean diameter, lower and upper limits of standard deviation for asphaltene floc size distributions from *n*-heptane/WC-B-B2 mixture at different solvent contents.

n-Heptane Content wt%	d_n μm	d_V μm	d_{LN} μm	σ_d μm
55.0	26	70	26	18
62.5	31	133	32	29
72.0	43	160	43	43
82.0	55	217	57	67
90.5	52	211	54	67
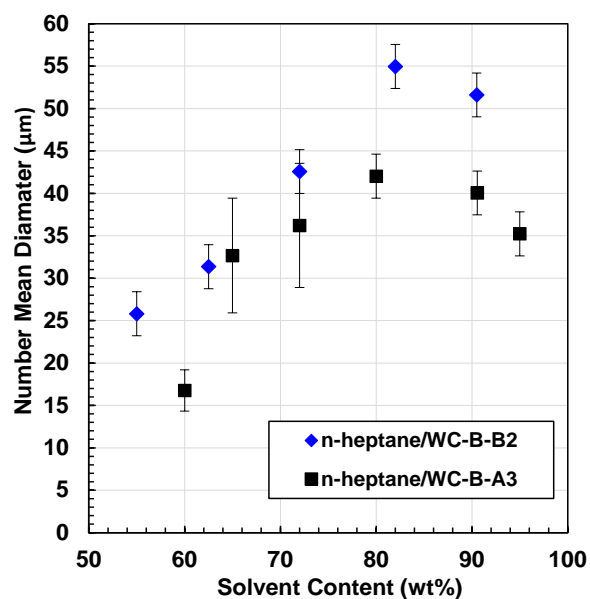
Figure 5.14. Number mean diameter for asphaltene flocs from *n*-heptane/WC-B-B2 and *n*-heptane/WC-B-A3.

5.4 Fractal Dimension of Asphaltene Flocs

The fractal dimension is used to account for the porosity of the floc and therefore influences the settling rate. The higher the fractal dimension, the lower the porosity, and the greater the settling rate. The fractal dimension (D_f) was calculated for the *n*-pentane/WC-B-A3, *n*-heptane /WC-B-A3, and *n*-heptane/WC-B-B2 mixtures using the sediment volume method. Since the amount of occluded material in the sediment and the deformation of the flocs was not known, the fractal dimension was calculated from both the uncompacted and compacted sediment volumes using Equation (3-6).

5.4.1 Effect of Solvent Type and Content on Fractal Dimension of Asphaltene Flocs

Figure 5.15 presents the fractal dimension of asphaltene flocs from the *n*-pentane/WC-B-A3 and *n*-heptane/WC-B-A3 mixtures at different solvent contents. All of the calculated fractal dimensions ranged from 1 to 3 as expected for 3 dimensional objects (Mandelbrot, 1983). Also as expected, the fractal dimension from the uncompacted volume was smaller than from the compacted volume because the same mass of flocs were occupying a larger space. The fractal dimensions increased with increasing solvent content to a maximum and then decreased at high

dilutions. The maxima were broader than observed with the floc sizes but occurred at a similar solvent content (70 to 80 wt%). The fractal dimension appears to correlate with the asphaltene particle concentration. It is possible that the collision rate was higher while the asphaltenes precipitated (and fused together) leading to large and more compact flocs.

The fractal dimension for the flocs in the *n*-pentane/WC-B-A3 mixtures were higher than those of the *n*-heptane/WC-B-A3 mixtures at the same solvent content. In other words, *n*-pentane flocs are more compact and less porous than *n*-heptane flocs. This interpretation was confirmed with micrographs of asphaltene flocs at three different solvent contents, 60, 70 and 95 wt%, Figure 5.16. In general, the asphaltene flocs in *n*-pentane diluted bitumen (images on left) were more compact and rounded than the flocs in *n*-heptane diluted bitumen (images on right). More rounded and compact flocs will have a higher fractal dimension than the more loosely structured flocs. The flocs may be more compact in *n*-pentane because it is a poorer solvent for asphaltenes than *n*-heptane and therefore the asphaltene particles would be more strongly attracted to each other while the flocs formed.
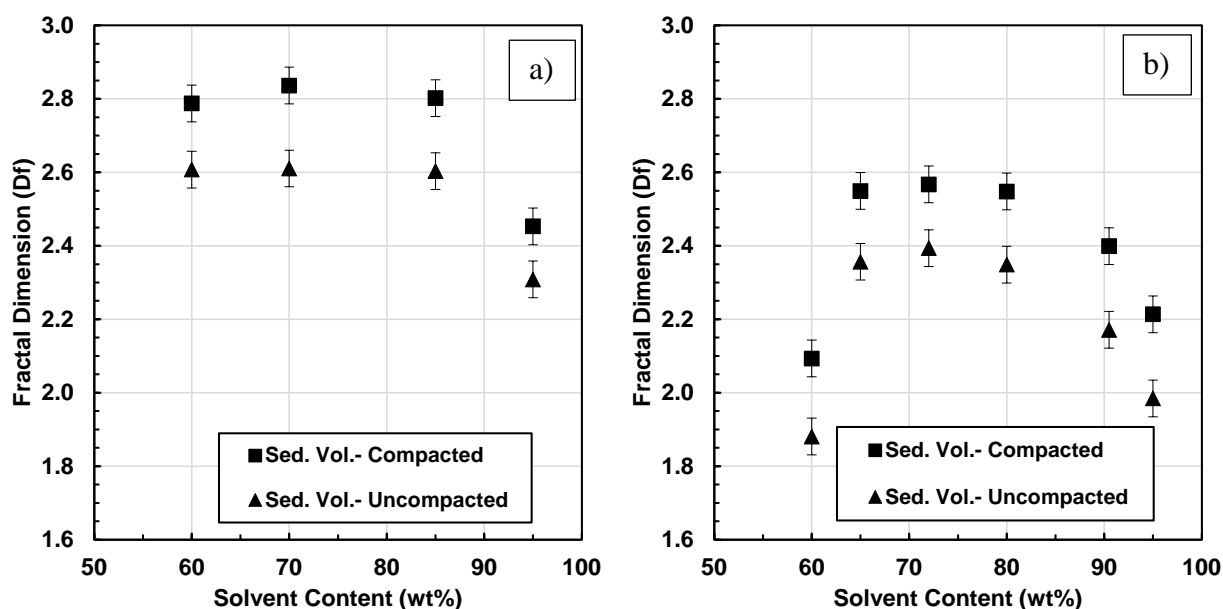
Figure 5.15. Fractal dimension of asphaltene flocs in WC-B-A3 bitumen at 21°C diluted with: a) *n*-pentane and b) *n*-heptane.

95
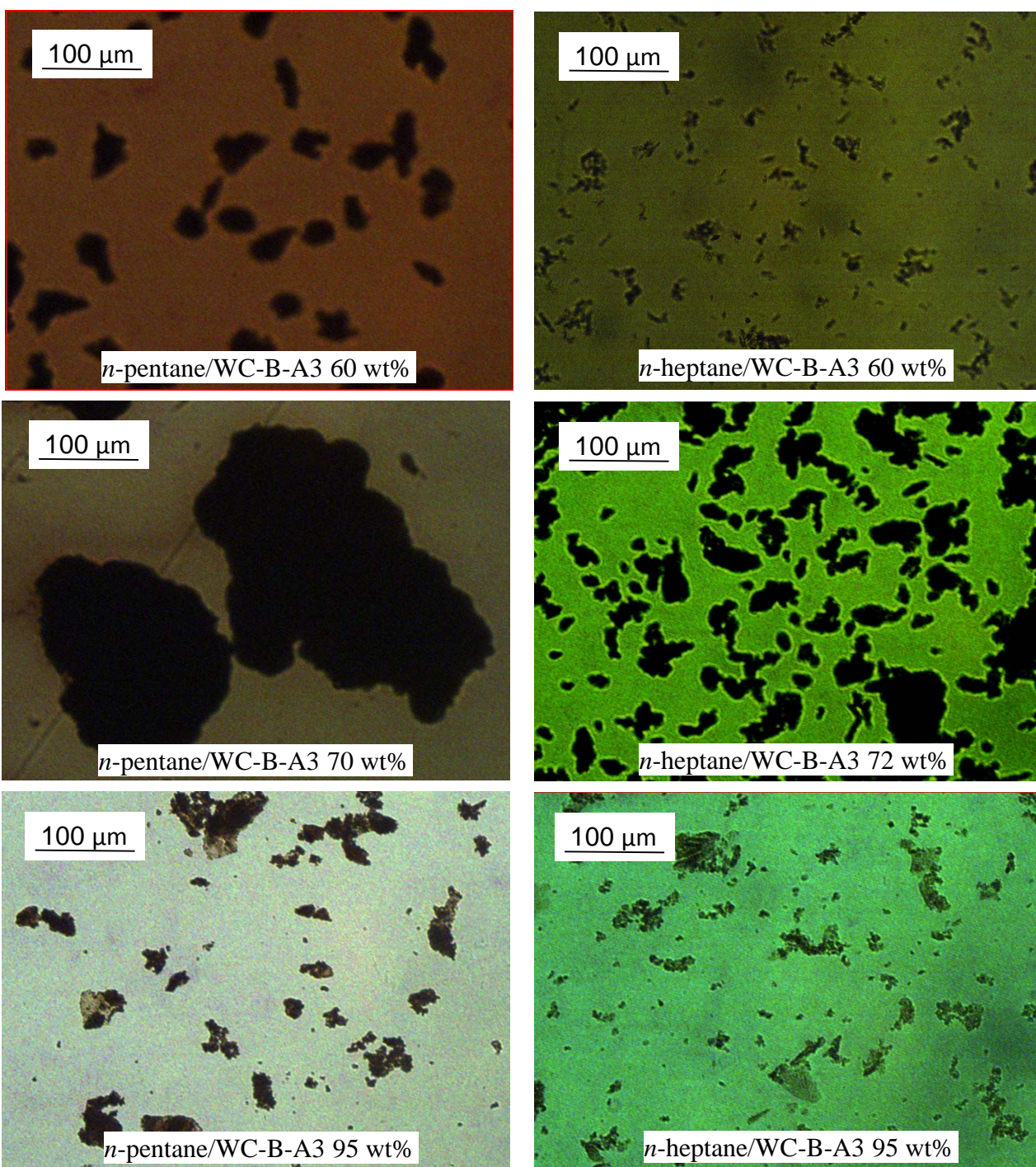
Figure 5.16. Micrographs of asphaltene flocs from WC-B-A3 bitumen diluted with *n*-pentane and *n*-heptane at solvent contents from 60 to 95 wt% at 21°C.

5.4.2 Effect of Bitumen Sample on Fractal Dimension of Asphaltene Flocs

Figure 5.17 shows the fractal dimensions of the n-heptane/WC-B-B2 mixtures at different solvent contents. The fractal dimensions follow the same trend with solvent content as observed for the n-alkane/WC-B-A3 mixtures. The fractal dimensions from the uncompacted sediment volumes are of similar magnitude. However, the fractal dimensions from the compacted sediment volume are significantly higher for the n-heptane diluted WC-B-B2 bitumen. As will be shown later, the fractal dimensions from the settling model are in good agreement with the fractal dimensions determined from the compacted sediment volume. It is not known why the fractal dimensions for the flocs from the two bitumens differ.

The large majority of the fractal dimensions determined from the compacted sediment volumes range from 2.4 to 2.8 and are consistent with most data from the literature. Daneshvar (2005) and Shafiee (2014) reported fractal dimensions of asphaltene flocs from solvent/bitumen mixtures above 2 and up to 2.3 ± 0.1, with a slight dependence on n-heptane content. Rahmani et al. (2005) determined the fractal dimensions of flocs from diluted bitumen to be between 1.30 and 1.44 based on the slope of a log-log plot of the settling velocity of individual flocs versus the floc dimension calculated from the projected area of the floc. Note, the log-log relation is derived from Equation 4-12. Such low fractal dimensions are not consistent with the micrographic images found for the flocs in this study but the reason for the discrepancy is not known.

Figure 5.17. Fractal dimension of asphaltene flocs from WC-B-B2 bitumen diluted with *n*-heptane.

5.5 Settling Rate

Settling rates were measured for the *n*-pentane/WC-B-A3, *n*-heptane/WC-B-A3 and *n*-heptane/WC-B-B2 mixtures. The first step was to confirm that the toluene insolubles settled with the flocculated asphaltenes. Then, the effects of solvent type, solvent content, and bitumen source on the settling rate were examined. As noted in Chapter 3, the settling rates were measured with the visual and sample methods over the ranges reported in Table 5.6. Note that the settling rates in *n*-pentane diluted bitumen were too rapid to use the sampling method. The same mixing speed, 195 rpm, was used for all experiments. The Reynolds number was below 0.01 in all cases, indicating creep flow.

Table 5.6. Solvent content ranges where the visual and sampling methods were used to measure the settling rate for each solvent/bitumen mixture.

Mixture	Method	Solvent Content (wt %)
n-pentane/WC-B-A3	Visual*	60.0 - 95.0
n-heptane/WC-B-A3	Sampling	60.0 - 72.0
n-heptane/WC-B-A3	Visual	72.0 - 95.0
n-heptane/WC-B-B2	Sampling	55.0 - 62.5
n-heptane/WC-B-B2	Visual	62.5 - 90.5

 * by tracking sediment height instead of upper interface

5.5.1 Asphaltene and Toluene Insolubles Settling Rate

The settling rates of both asphaltene flocs and toluene insolubles were measured for the WC-B-B2 bitumen since it had the highest toluene insoluble content. The asphaltene and toluene insoluble profiles were measured with the sampling method for the *n*-heptane/WC-B-B2 mixture at 62.5 wt% at settling times of 20 and 45 minutes as shown in Figure 5.18a and 5.18b, respectively. The plotted height is the average height of the layer. Note that the volume fraction for asphaltenes is two orders of magnitude higher than the toluene insoluble volume fraction. Similar data were obtained for the *n*-heptane/WC-B-B2 mixture at 55 wt% solvent content as shown in Figure 5.19.

The interface of the settling material was apparent as a distinct change in the volume fraction of asphaltenes or toluene insoluble from one layer to the next. The asphaltene and toluene insoluble volume fractions above the interface approached zero indicating that almost all of the material was settling. The location of the interface for the asphaltenes and the toluene insoluble was almost identical at each time, confirming that they were settling at the same rate. This result is in agreement with observations on the settling of asphaltene/water/solid flocs in froth treatment studies (Long *et al.,* 2002; Zahabi *et al.,* 2010). There is a relatively strong attraction between the asphaltenes and the inorganic solids that make up the toluene insolubles because the solids are partially coated by organic compounds (Nikakhtari *et al.*, 2014; Pal *et al.*, 2015). When asphaltenes precipitate and flocculate, they collect the toluene insoluble within the flocs. Since the asphaltenes

and toluene insolubles settle at the same rate, only the asphaltene settling rates are reported in the remainder of this thesis.
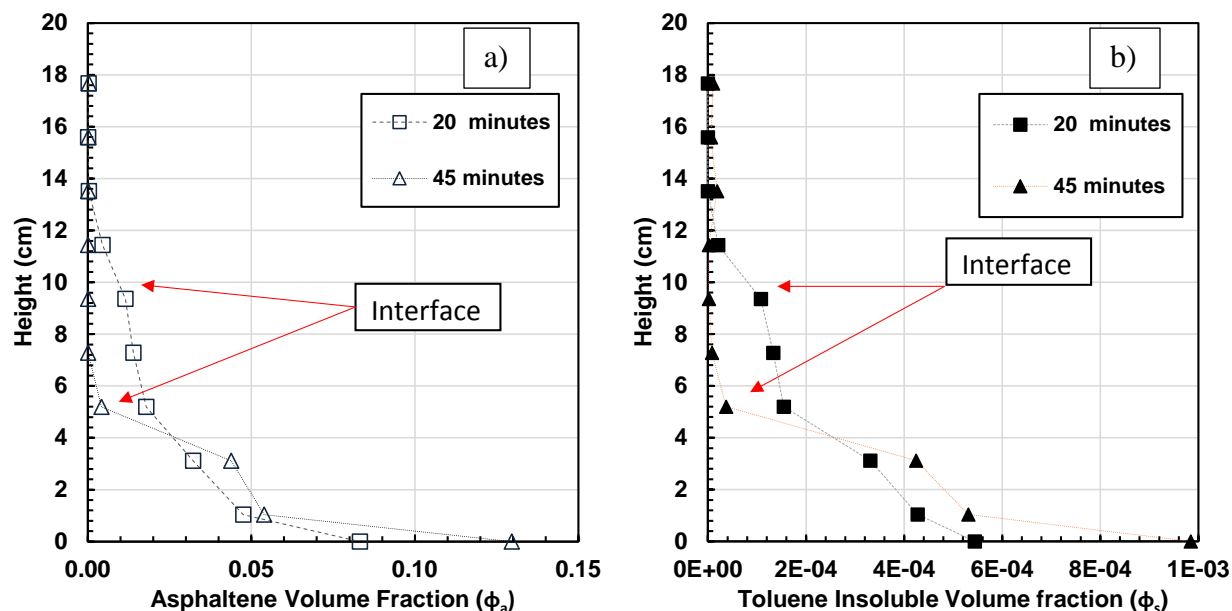
Figure 5.18. Gravimetric profile after 20 and 45 minutes settling for *n*-heptane/WC-B-B2 mixture at 62.5 wt% solvent content for: a) asphaltenes and b) toluene insolubles.
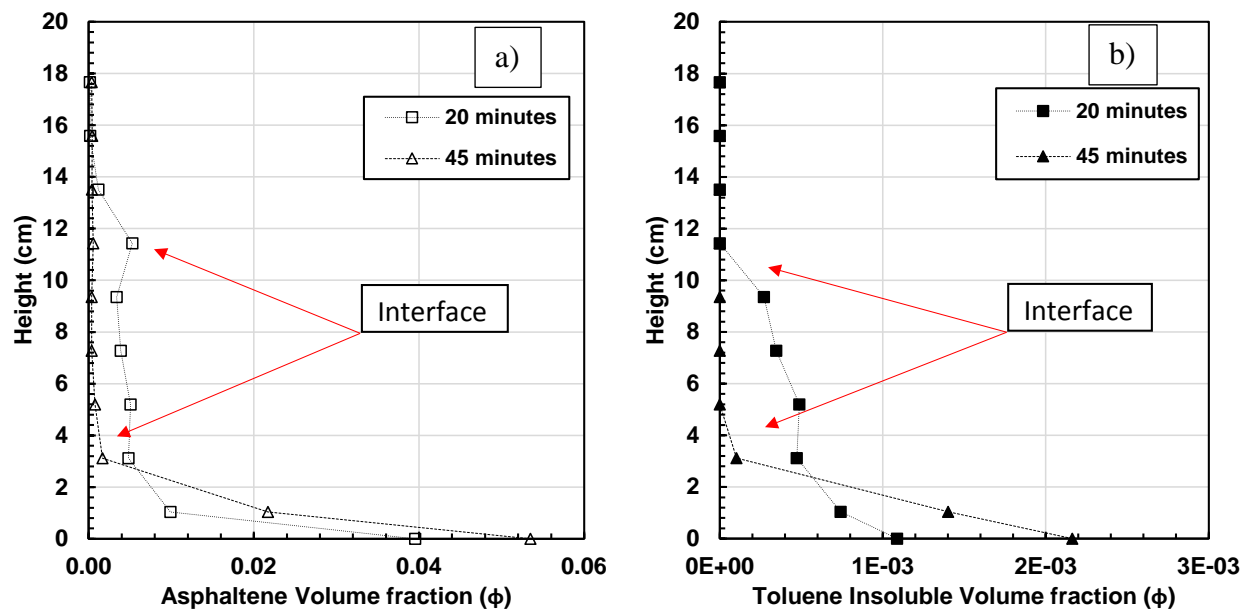
Figure 5.19. Volume fraction profiles for a) asphaltenes and b) toluene insolubles from *n*-heptane/WC-B-B2 at 55 wt% solvent content and two settling times 20 and 45 minutes.

5.5.2 Effect of Solvent Type and Content on the Settling Rate

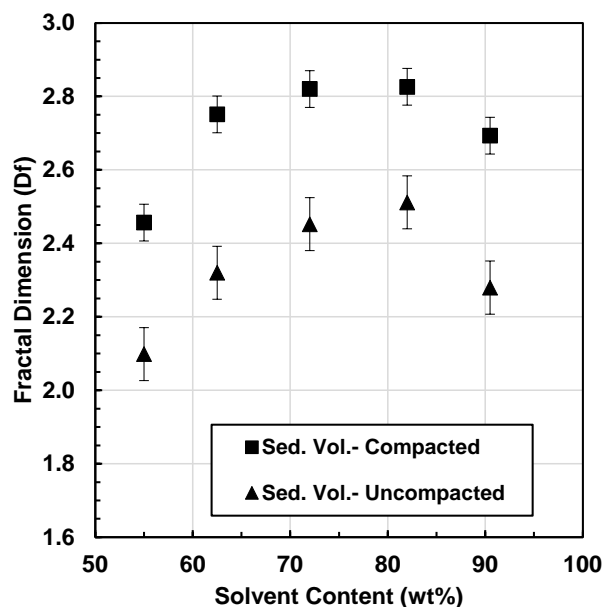The settling rates of asphaltene flocs in WC-B-A3 bitumen diluted with *n*-pentane and *n*-heptane at solvent contents from 60 and 95 wt% are shown in Figures 5.20a and 5.20b, respectively. In both cases, there was no settling below the onset of precipitation (vertical line). The settling rate increased as the solvent content increased from the onset of precipitation to a global maximum and then decreased at higher dilutions. The maxima occurred at approximately 85 wt% *n*-pentane (Figure 5.20) and 80 wt% *n*-heptane (Figure 5.20b). Note that in the *n*-heptane diluted bitumen system, there was also a local maximum just above the onset of asphaltene precipitation.

As was shown in Equation 4.12, the settling rate is proportional to the density difference between the asphaltenes and the medium, inversely proportional to the viscosity of the medium, and proportional to the floc diameter to the power of D_f-3, where D_f is the fractal dimension of the floc. Settling may be hindered and the hindering effect increased as the particle concentration increases. Solvent addition decreases the density (increases the density difference) and reduces the viscosity of the medium. Both effects will tend to increase the settling rate. Section 5.3 showed that the particles size increased from the onset of precipitation to a maximum value at 70 to 80 wt% solvent and then decreased. Section 5.4 showed that the fractal dimension reached a maximum at similar solvent contents. Both effects will tend to increase the settling rate to the global maximum and then decrease the settling rate. The global maximum approximately corresponded to the maximum particle concentration and therefore hindering may counteract some of the effect of the particle size. All of these effects except hindering cause the settling rate to increase with increasing solvent content until the maximum floc diameter is achieved. Above this maximum, the decreasing diameter tends to reduce the settling rate but the decreasing density and viscosity of the medium tend to increase the settling rate. Since the experimentally observed global maxima in the settling rates were near but not identical to the maxima in the floc sizes (Tables 5.3 and 5.4), it appears that the floc size is the most significant factor determining the settling rates. No explanation was found for the local maximum near the onset of precipitation.

The settling rate of the flocs in the *n*-pentane diluted bitumen was two orders of magnitude greater than that in the *n*-heptane diluted bitumen. Long *et al*. (2004) and Kosior *et al*. (2015) also observed

more rapid settling in bitumen froth diluted with lighter paraffinic solvents. Flocs from the *n*-pentane/WC-B-A3 mixtures were between 3 to 6 times larger than flocs from the *n*-heptane/ WC-B-A3 mixtures (see Table 5.3 and 5.4). Hence, the size of the flocs is also the main factor contributing to the difference in settling rates between the two solvents.
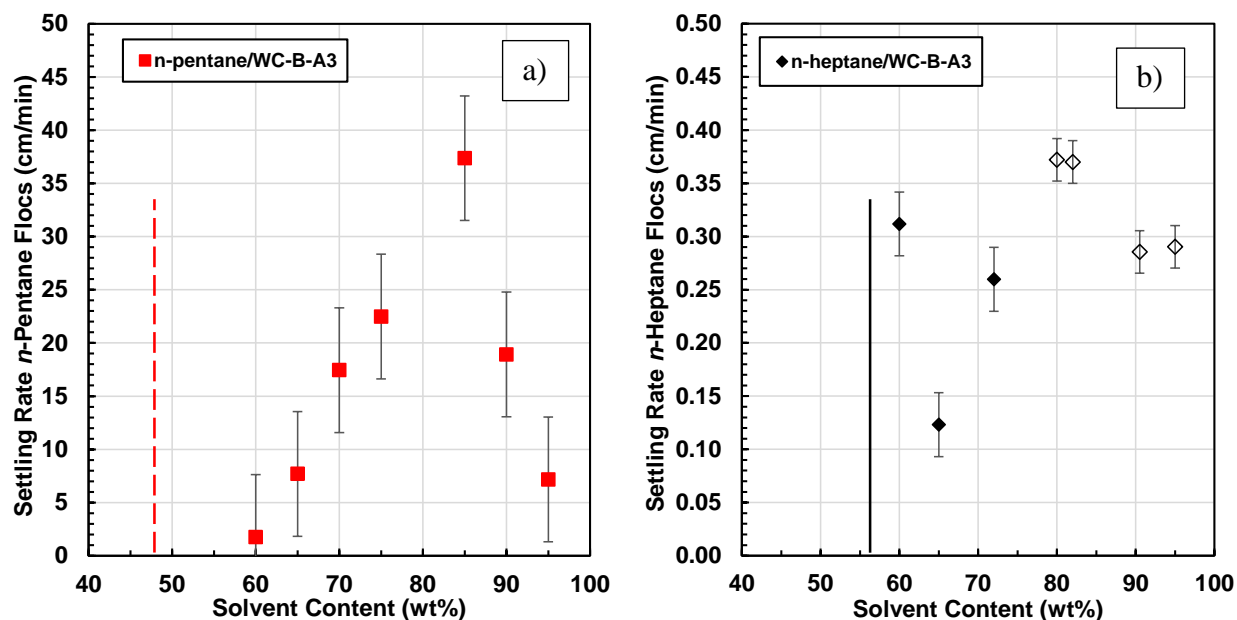
Figure 5.20. Settling rate for asphaltenes from a) *n*-pentane/WC-B-A3 and b) *n*-heptane/WC-B-A3 mixtures at 21°C. The vertical line indicates the onset of asphaltene precipitation. Closed and open symbols indicate data collected with the sampling and visual methods, respectively. Note the different y-axis scale for each plot.

5.5.3 Comparison of Settling Rate in Different Bitumens

Figure 5.21 compares the settling rate of asphaltene flocs from the *n*-heptane/WC-B-B2 and *n*-heptane/WC-B-A3 mixtures. The settling rates for both mixtures followed the same trend between 60 and 95 wt% solvent content with a maximum settling rate around 80 wt%. However, the settling rates in the *n*-heptane diluted WC-B-B2 bitumen were significantly higher than in the *n*-heptane diluted WC-B-A3 bitumen but still much lower than in *n*-pentane diluted bitumen. The main reason for the higher settling rate in WC-B-B2 bitumen is the lower porosity (higher fractal dimension) of the flocs from this oil. The higher floc size in this oil also contributes to the difference.

Relatively high settling rates were observed near the onset of precipitation for both diluted bitumens even though the average floc sizes were relatively small at this condition. This high settling rate for the diluted WC-B-B2 bitumen can be partially attributed to the presence of toluene insoluble. Near the onset of asphaltene precipitation, the ratio of toluene-insolubles to asphaltenes in the flocs is higher. Therefore, the flocs have higher density and faster settling rate. A similar trend was observed by Zahabi *et al*. (2010) for silica particles in asphaltenes precipitated with *n*-pentane from a model oil consisting of 5 wt% pitch material (O), 0.5 to 4 wt% silica, and toluene. However, this effect cannot explain the high settling rate for the diluted WC-B-A3 bitumen which contained a negligible amount of toluene insoluble.
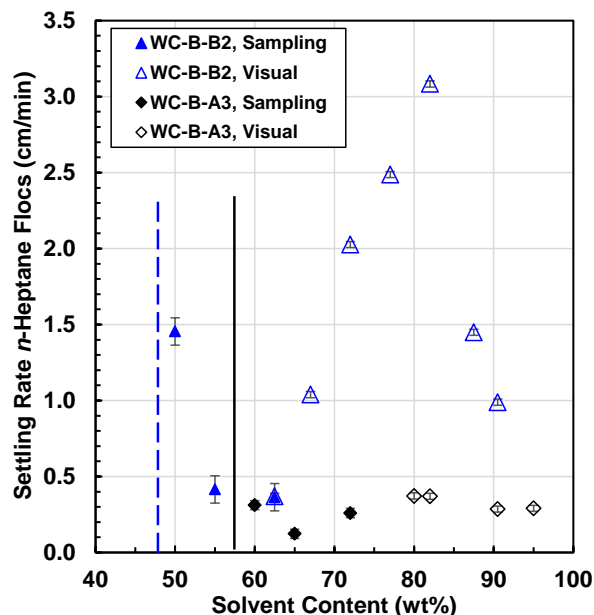
Figure 5.21. Settling rate of asphaltenes flocs in WC-B-A3 and WC-B-B2 samples diluted with *n*-heptane at 21°C. Closed and open symbols indicate data collected with the sampling and visual methods, respectively. The solid and dashed lines are the onset of precipitation for the WC-B-A3 and WC-B-B2 bitumen, respectively Note three of the WC-B-B2 points were collected by Duran (2016).

5.6 Modeling the Settling of Flocculated Asphaltenes

If the fluid density and viscosity, asphaltene density, floc size distribution, and fractal dimension are known, the settling model described in Chapter 4 can be used to predict the settling rates. In this thesis, the inputs are all known but there is significant uncertainty in the fractal dimension.

Therefore, the model was instead used to predict the fractal dimension from the other inputs and the measured settling rates. Then, the appropriate sediment volume to determine the fractal dimension was identified so that settling rates could be predicted in future.

5.6.1 Application of the Settling Model

Recall that the output of the settling model is the volume fraction profile of the asphaltene flocs. For the sampling method settling experiments, the model was simply fit to the measured profile. Note, in order to capture the formation of a sediment, the porosity of the sediment was also specified as an input to the model. For the visual method experiments, the model was fit the height of the interface marking the uppermost location of the settling flocs. Table 5.7 presents at which conditions the model fit either the asphaltene profile or the interface position.

Table 5.7. Conditions where the settling model was used to fit either the asphaltene profile or the interface.

Mixture	Model	Solvent Content (wt %)
n-heptane/WC-B-A3	Profile	60.0 -72.0
n-heptane/WC-B-A3	Interface	72.0 - 95.0
n-heptane/WC-B-B2	Profile	55.0 - 62.5
n-heptane/WC-B-B2	Interface	62.5 - 90.5

Modeling Sampling Method Data

Figure 5.22 is an example of the asphaltene volume fraction profile obtained from the sampling method for the *n*-heptane/WC-B-A3 mixture at 60 wt% after 40 minutes settling. There are two inflection points: between 12 and 10 cm height and between 6 and 4 cm height. The upper inflection point is the settling interface and the bottom inflection point is the sediment interface. Above the settling interface, the asphaltene volume fraction is zero. This zone is the solid-free supernatant. Between the two inflection points, in the settling zone, the asphaltene volume fraction is relatively constant. Below the bottom inflection point, the asphaltene volume fraction increases significantly. This zone is the sediment.
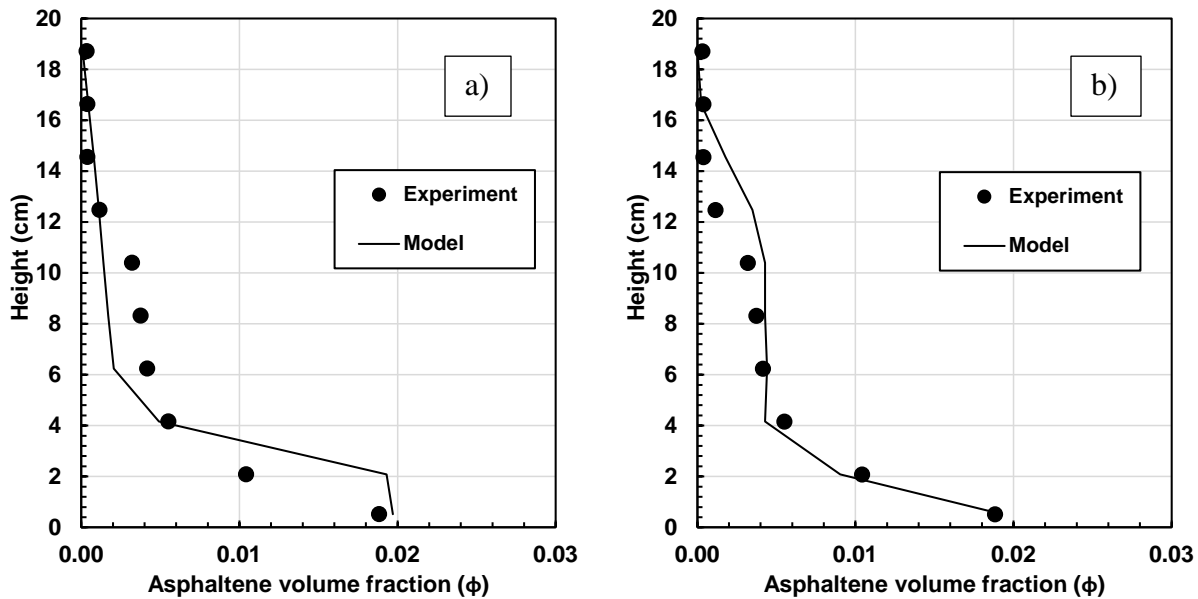
Figure 5.22. Measured and modeled asphaltene volume fractions for *n*-heptane/WC-B-A3 mixtures at 21C: a) using measured floc size distribution; b) zone settling distribution.

To model the data, the density and viscosity of the diluted bitumen were determined as shown in Section 5.2. The density of the flocs was set as the asphaltene density or, where applicable, calculated from the asphaltene and toluene insoluble densities. The measured floc size distribution was represented as a number distribution divided into 250 intervals each representing a span of 2 μm. The sediment porosity was fit using the experimental data as a function of settling time. The fractal dimension was adjusted to fit the data. The input data for the three solvent/bitumen mixtures is provided in Appendix C.

Figure 5.22a shows that, after tuning the fractal dimension, the precipitated asphaltene volume fractions calculated with the settling model were in the same order of magnitude as the experimental data. The model captured the formation of the sediment (lower interface). However, it did not predict an upper interface but rather a smooth monotonic increase of the asphaltene volume fraction with increasing depth. The model also incorrectly predicted non-zero solid volume fractions above the upper inflection point. Similar results were obtained for all of the sampling method data.

105

The reason that the model predicts a gradual volume fraction gradient is the broad floc size distribution: the larger flocs are predicted to settle rapidly while the smaller flocs are predicted to settle slowly, creating a gradient. In reality, it appears that the smaller flocs are at least partially dragged in the wake of the larger flocs. All of the flocs tend to settle at the same rate, an effect known as zone settling (Long *et al.*, 2002; McCabe *et al.*, 2001). The hindered settling method implemented in the model slows down all flocs by an equal percentage and does not account for zone settling.

To account for the zone settling, the floc size distribution was represented with the same number mean diameter but the breadth of the distribution was narrowed to ±4 μm. The new distribution was divided into 5 bins with increments of 2 μm. The frequency distribution for each bin is presented in Table 5.8. The model result using a narrower distributions for asphaltene flocs from the *n*-heptane/WC-B-A3 mixture at 60 wt% after 40 minutes settling is presented in Figure 5.22b. The model now captures both the upper and lower interface. The tuned fractal dimension was 2.95 ±0.05. The sampling method data and fitted models are provided in Appendix D.

Table 5.8. Number frequency distribution for zone settling.

Bin	Bin Diameter (μm)	Frequency (%)
1	D_{mean}-4 μm	10
2	D_{mean}-2 μm	20
3	D_{mean}	40
4	D_{mean}+2 μm	20
5	D_{mean}+4 μm	10

The average absolute relative deviation between the experimental and calculated profiles is defined as follows:

$$AARD = \frac{\sum \left| \phi_{exp} - \phi_{model} \right|}{n \, \overline{\phi}} \qquad (5\text{-}5)$$

where ϕ_{exp} are the experimental asphaltene volume fractions, ϕ_{model} are the calculated asphaltene volume fractions, n is the number of layers and $\overline{\phi}$ is the average volume fraction measured in each experiment. The AARD for the asphaltene profiles fit from the n-heptane/WC-B-A3 and n-heptane/WC-B2 mixture was 7%.

Modeling Visual Method Data

Figure 5.23 shows the position of the interface of the asphaltene flocs from the n-heptane/WC-B-A3 mixture at 80 wt% solvent content and different settling times. The free settling zone of the asphaltene flocs from this mixture was visible between 0 and 30 minutes. After 30 minutes the sedimented flocs started to compact. The zone settling floc size distribution, Table 5.8, was input into the model and the interface was identified where there was a significant change in the asphaltene solid volume fraction as was described in Section 4.6. The fractal dimension was iterated to fit the position of the interface.

Figure 5.23 shows the position of the interface for the n-heptane/WC-B-A3 mixture calculated with fractal dimensions between 2.50 and 2.55. The calculated position of the interface is lower for higher fractal dimensions because the flocs are more compact and settle faster. In this case, the best fit to the experimental data is found with a $D_f = 2.53$. Similar results were obtained all of the visual method data. The AARD for the flocs interface fit from n-heptane/WC-B-A3 and n-heptane/WC-B2 mixture was 5%. The visual method data and fitted models are provided in Appendix E.
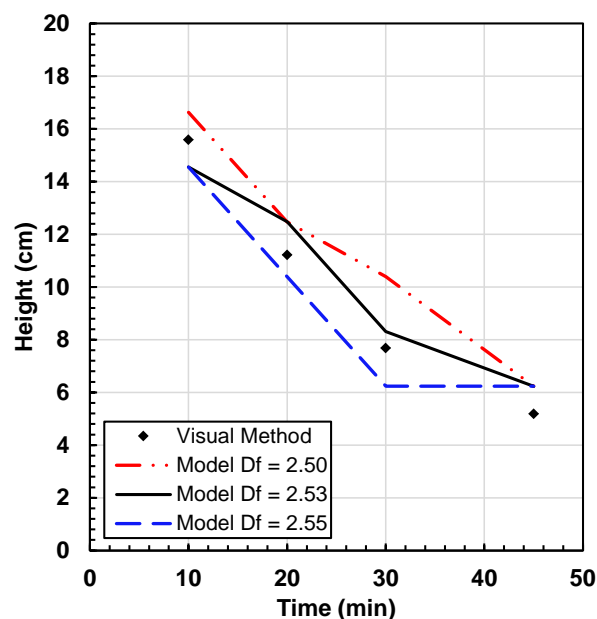
Figure 5.23. Interface position of asphaltene flocs from *n*-heptane/WC-B-A3 mixture at 80 wt% solvent content. Note the height becomes constant after 45 minutes when all of the flocs have settled to the sediment.

The settling of asphaltene flocs from *n*-pentane/WC-B-A3 mixture was too rapid to measure the height of the interface in the free settling zone. Therefore, the fractal dimension cannot be iterated to fit the position of the interface at different settling times. Instead, the fractal dimension was iterated to fit the experimental average settling rate calculated between the maximum height and the uncompacted volume, Figure 5.20. Table 5.9 shows the fitted fractal dimension and the match between the modeled and measured settling rates.

Table 5.9. Fitted fractal dimension and comparison of experimental and calculated settling rate for *n*-pentane/WC-B-A3 mixture.

n-Pentane wt%	Fitted D_f	Settling Rate, cm/min	
		Data	Model
60.0	2.80	1.8	2.6
70.0	2.75	17	17
85.0	2.80	37	26
95.0	2.80	7	9

5.6.2 Fractal Dimensions from the Settling Model.

The fractal dimension fit with the zone settling model are compared with the sediment volume method results in Figure 5.24a and 5.25b for the *n*-heptane/WC-B-A3 and *n*-heptane/WC-B-B2 mixtures, respectively. The fractal dimensions calculated from the sampling method data are the average of the fractal dimensions calculated for the same solvent content at different settling times. Note the fractal dimension did not vary systematically with time in these experiments. The fractal dimensions from the settling model closely match (AARD = 6.6%) the fractal dimension from the sediment volume method based on the compacted sediment volume. A notable exception occurred near the onset of asphaltene precipitation where the fractal dimension from the settling method increases to values close to 3 in both mixtures. These high values are not consistent with the micrographic images in Figures 5.5 and 5.16. The high fractal dimension was required to match the unexpectedly rapid settling rate just above the onset of precipitation. It is an artefact that arises because the mechanism for this high settling rate is not yet understood or accounted for in the model.
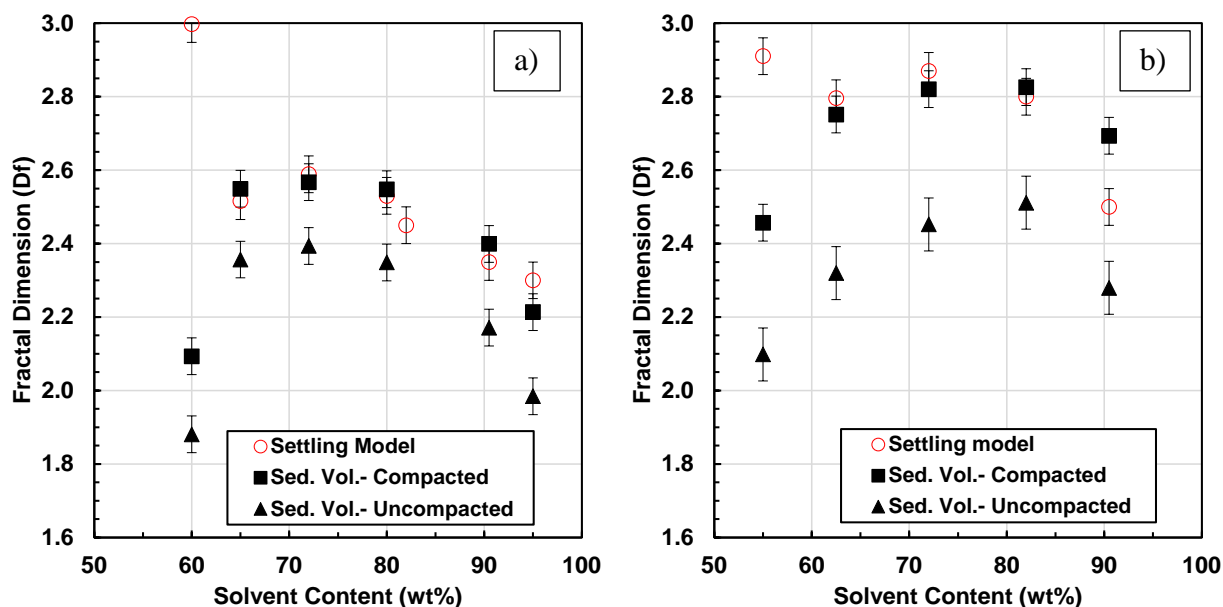
Figure 5.24. Comparison of fractal dimension of asphaltene flocs determined from settling rates and from sediment volume method for: a) *n*-heptane/WC-B-A3 mixtures; b) *n*-heptane/WC-B-B2 mixtures.

The fractal dimension from modeling the settling rates for the n-pentane/WC-B-A3 mixtures are compared with the sediment volume method in Figure 5.25. The fractal dimensions from the settling model is approximately 2.8, consistent with the fractal dimensions from the uncompacted sediment volumes up to 90 wt% n-pentane. The results diverge at 95 wt% n-pentane. The fractal dimension from the settling model remains at approximately 2.8 while the fractal dimension calculated with the sediment volume method decreases. Based on the fractal dimensions in n-heptane, a decrease in fractal dimension at high solvent content is expected and therefore the relatively high fractal dimension from the settling model may be incorrect. However, the error is greater than can be accounted for with the potential sources of error in the input data and therefore the reason for the discrepancy remains unknown.
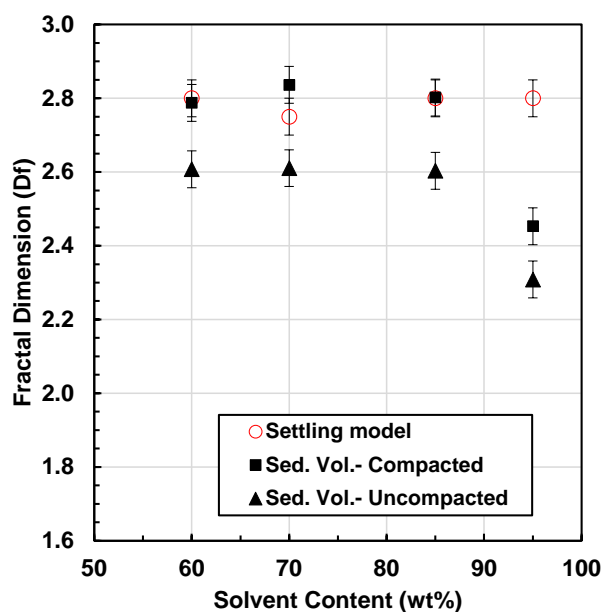
Figure 5.25. Comparison of fractal dimension of asphaltene flocs determined from settling rates and from sediment volume method for n-pentane/WC-B-A3 mixture.

In conclusion, the settling rate is best modeled as zone settling based on the number mean diameter of the asphaltene flocs. The fractal dimension of the flocs can be determined from the compacted volume of the settled flocs. The density and viscosity of the diluted bitumen can be determined from the known bitumen and solvent properties and established mixing rules. Hence, the data required to model settling are the floc size distribution, a sediment volume, and the bitumen and

solvent fluid properties. The predicted settling rates based on these are presented in Table 5.10 through Table 5.12, and Figure 5.26 and Figure 5.27. The model was able to predict the trend of the settling rate versus the solvent content with an AAD of 3.2 cm /min (16%) for the *n*-pentane/WC-B-A3 mixture, 0.05 cm/min (16%) for the *n*-heptane/WC-B-A3 mixture, and 0.2 (13%) cm/min for *n*-heptane/WC-B-B2 mixture. The main source of error for the *n*-pentane diluted bitumen is the measured settling rate because the uncertainty in the time for the sediment layer to reach the maximum height has a significant impact at short settling times (high settling rates).The main source of error for the *n*-heptane diluted bitumen is the uncertainty in the fractal dimension. Recall that the sediment volume method may not accurately account for solvent occlusion and floc deformation. The relative error is high for the *n*-heptane mixtures, particularly near the onset of precipitation, because the settling rates are low.

Table 5.10. Comparison of predicted and measured settling rate of asphaltene flocs from the *n*-pentane/WC-B-A3 mixture.

n-Pentane wt%	Settling Rate (cm/min)			
	Data	Model	AD (cm/min)	ARD (%)
60.0	1.8	2.1	0.3	15
70.0	17	17	0.4	2
85.0	37	26	11	30
95.0	7	8.1	1.1	16
Overall			3.2	16

Table 5.11. Comparison of settling rate predicted and measured of asphaltene flocs form the *n*-heptane/WC-B-A3 mixture.

n-Heptane wt%	Settling Rate (cm/min)			
	Data	Model	AD (cm/min)	ARD (%)
60.0	0.31	0.10	0.21	66
65.0	0.12	0.12	0.00	3.1
72.0	0.26	0.25	0.01	4.1
80.0	0.37	0.33	0.04	10
90.5	0.29	0.27	0.02	7.4
95.0	0.30	0.27	0.02	7.8
Overall			0.05	16

Table 5.12. Comparison of predicted and measure settling rate of flocs from the *n*-heptane/WC-B-B2 mixture.

n-Heptane wt%	Settling Rate (cm/min)			
	Data	Model	AD (cm/min)	ARD (%)
55.0	0.42	0.34	0.07	18
62.5	0.37	0.39	0.02	7
72.0	2.0	1.7	0.30	15
82.0	3.1	2.4	0.66	21
90.5	0.99	1.0	0.05	5
Overall			0.22	13
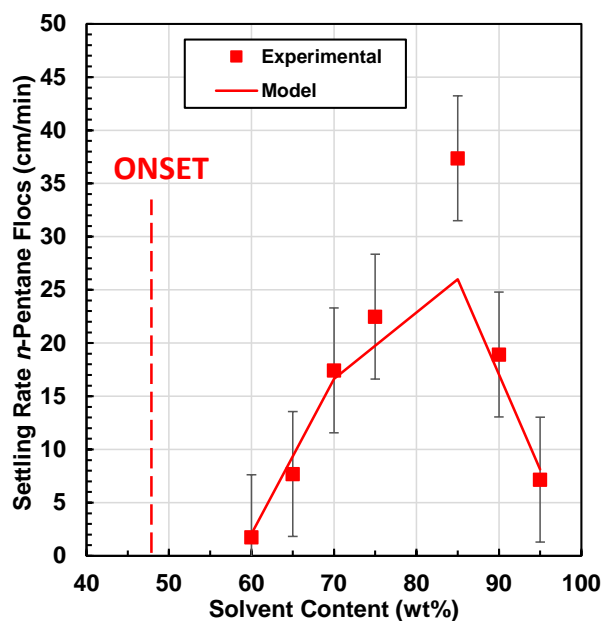
Figure 5.26. Predicted and measured settling rate of asphaltene flocs from n-pentane/WC-B-A3 mixture.
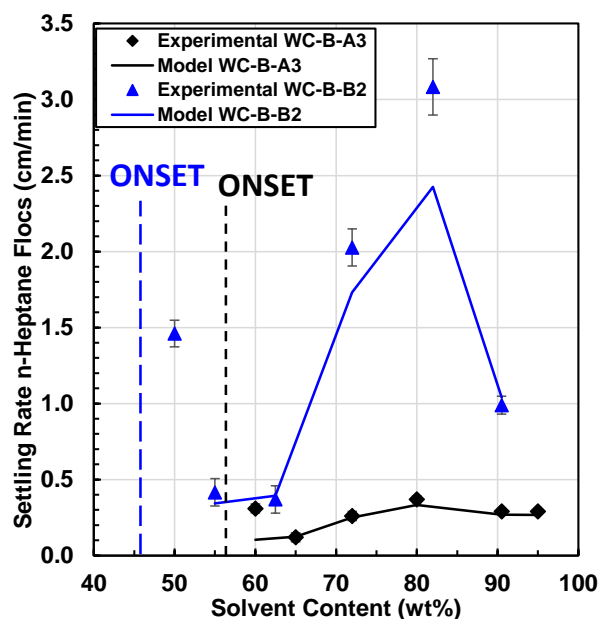
Figure 5.27. Predicted and measured settling rate of asphaltene flocs from *n*-heptane/WC-B-A3 and *n*-heptane/WC-B-B2 mixture.

5.6.3 Sensitivity of Settling Model to Input Parameters

The sensitivity of the settling model to the time step size, hindering exponent in the Richardson and Zaki equation (Equation 4-12), the fractal dimension, and the choice of mean floc diameter was evaluated.

The settling rate of asphaltene flocs from the mixture *n*-pentane/WC-B-A3 were calculated with time steps of 5, 1, 0.1 and 0.05 seconds, Figure 5.28. The predicted settling rates converged at a time step of 0.05 seconds. Note that at a time step of 0.01 seconds required too much memory in Matlab to run. Since the difference between a time step of 0.1 and 0.05 was small (AARD of 0.15% in the predicted settling rates), a time step of 0.1 seconds was selected to minimize the run time.
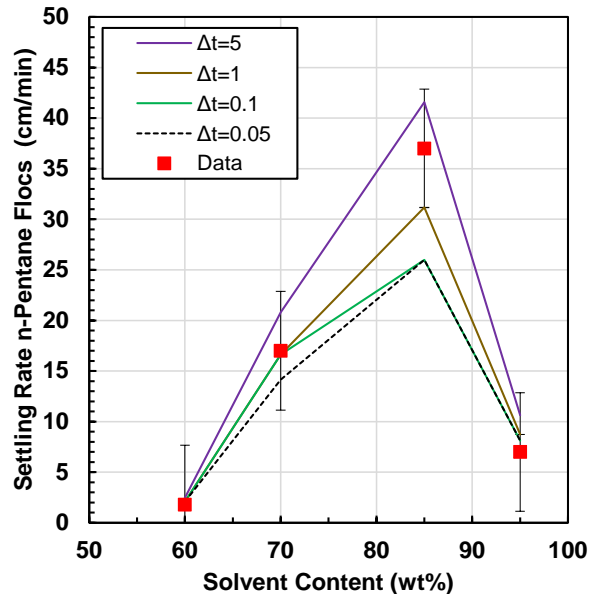
Figure 5.28. Evaluation of time step, Δt, in the predicted settling rate of flocs from the *n*-pentane/WC-B-A3.

Hindering exponents from 4 to 11 have been reported for bitumen froth and aliphatic solvent mixtures (Long *et al*., 2004; Saadatmand, 2008; Valinasab, 2006; Zahabi *et al.*, 2010). However, this exponent has not been calculated for diluted bitumen. The settling rates of the *n*-pentane/WC-B-A3, *n*-heptane/WC-B-A3 and *n*-heptane/WC-B-B2 mixtures were calculated with hindering exponents (*n*) of 0, 3, 5 and 7. The predicted settling rates for each exponent are shown in the Figure 5.28 and the AARD are presented in Table 5.10. The lowest overall AARD was for *n*=5. Therefore, the default value of *n*=4.65 was retained.
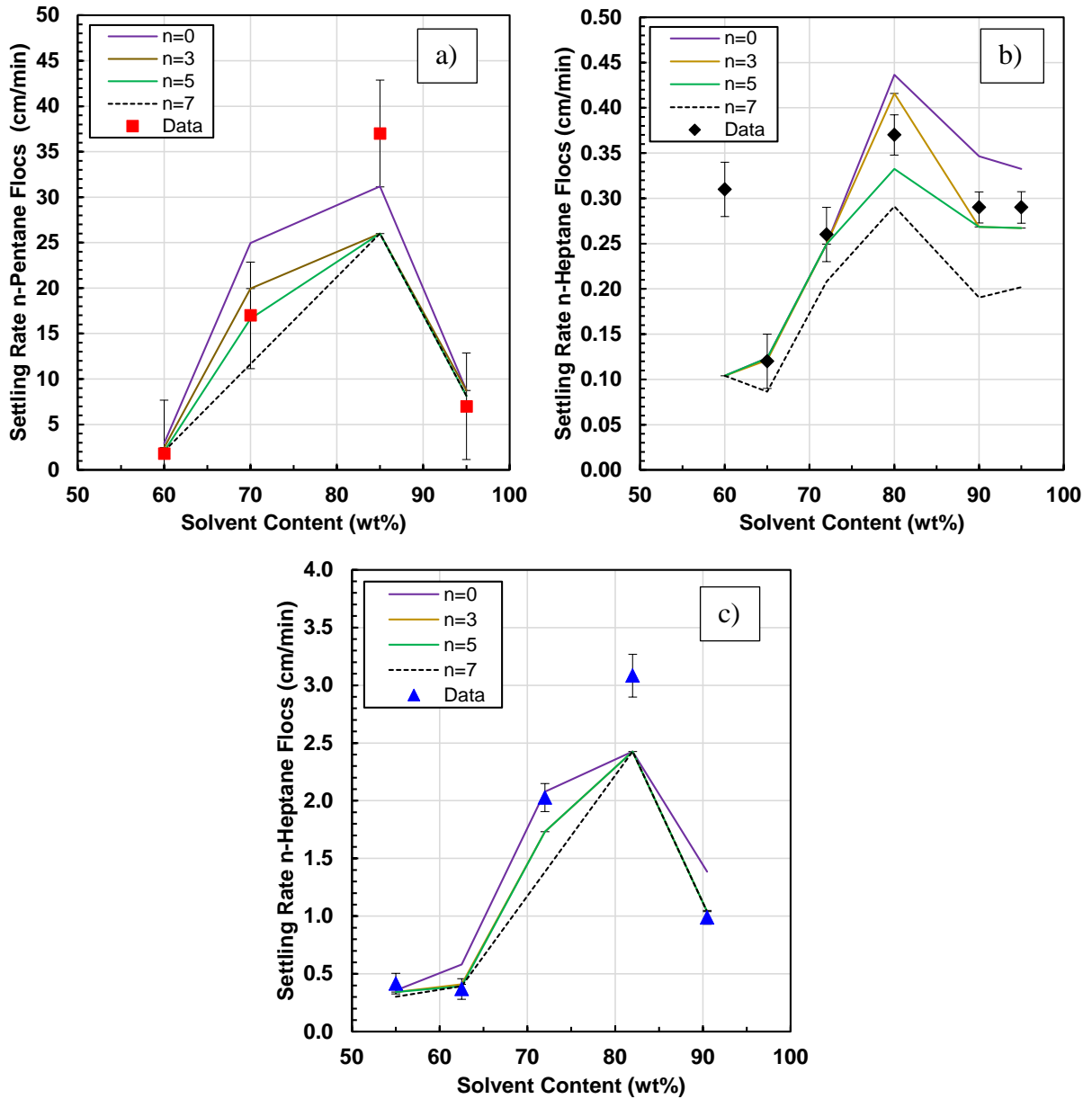
Figure 5.29. Predicted and measured settling rate of asphaltene flocs from a) *n*-pentane/WC-B-A3, b) *n*-heptane/WC-B-A3 and c) *n*-heptane/WC-B-B2 using hindering exponents n= 0, 3, 5 and 7.

Table 5.10. Calculated AARD for the settling rate of asphaltene flocs using different hindering exponents

Mixture	AARD (%)			
	n=0	*n=3*	*n=5*	*n=7*
n-pentane/WC-B-A3	27	14	13	18
n-heptane/WC-B-A3	21	17	16	33
n-heptane/WC-B-B2	38	27	16	23
Overall	29	19	15	25

The sensitivity of the predicted settling rates to the fractal dimension was determined for the three mixtures. As an example, the settling rates of asphaltene flocs from the *n*-pentane/WC-B-A3 mixture are presented in Figure 5.30. The confidence interval of the fractal dimension from the iterative model, 0.05, was used to measure the sensitivity of the predictive model. A change of ±0.05 in the input fractal dimension gives an AARD in the predicted settling rates of up to 30%. The fractal dimension is the input parameter with the greatest uncertainty and the model is very sensitive to its value. Therefore, it is recommended as the tuning parameter for fitting the model to experimental settling rates.
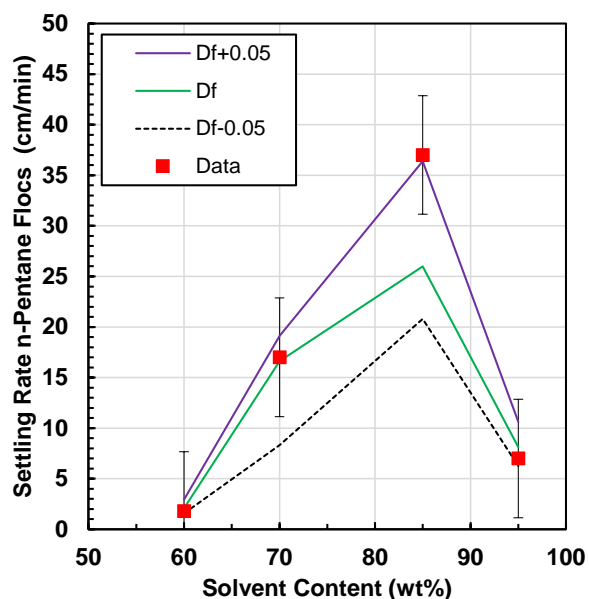
Figure 5.30. Sensitivity of predicted settling rate of asphaltene flocs from *n*-pentane/WC-B-A3, to the fractal dimension using values of ±0.05 of the fit fractal dimension.

The sensitivity of the settling rates to the choice of average diameter (number mean, area mean, and volume mean) was assessed for three mixtures using the fractal dimensions from both the compacted and the uncompacted sediment volumes as inputs. For convenience, the respective fractal dimensions are here termed the compacted and uncompacted fractal dimension. Only the results for the *n*-heptane/WC-B-B2 system are shown here but similar results were obtained for all three mixtures. Figure 5.31a and Figure 5.31b show that, when using the model with the compacted fractal dimensions, the settling rates calculated with the volume and area mean diameter, respectively, were consistently higher than the measured rates. However, the rates calculated with the uncompacted fractal dimension were consistently smaller than the measured rates. Figure 5.31c shows that, when using the model with the compacted fractal dimensions, the settling rates calculated with the number mean diameter and log mean diameter were similar and consistent with the measured settling rates. The settling rates calculated with the uncompacted fractal dimension were too low.

The sensitivity analysis shows that there the settling rates can be matched using any of the mean diameters with a fractal dimension between the compacted and uncompacted values. In other words, there is no unique combination of mean diameter and fractal dimension that best fits the data. The compacted fractal dimensions were considered to be more consistent with the micrographs. Therefore, the number mean diameter is recommended because it is simple and best matched the settling rates with the measured compacted fractal dimensions.
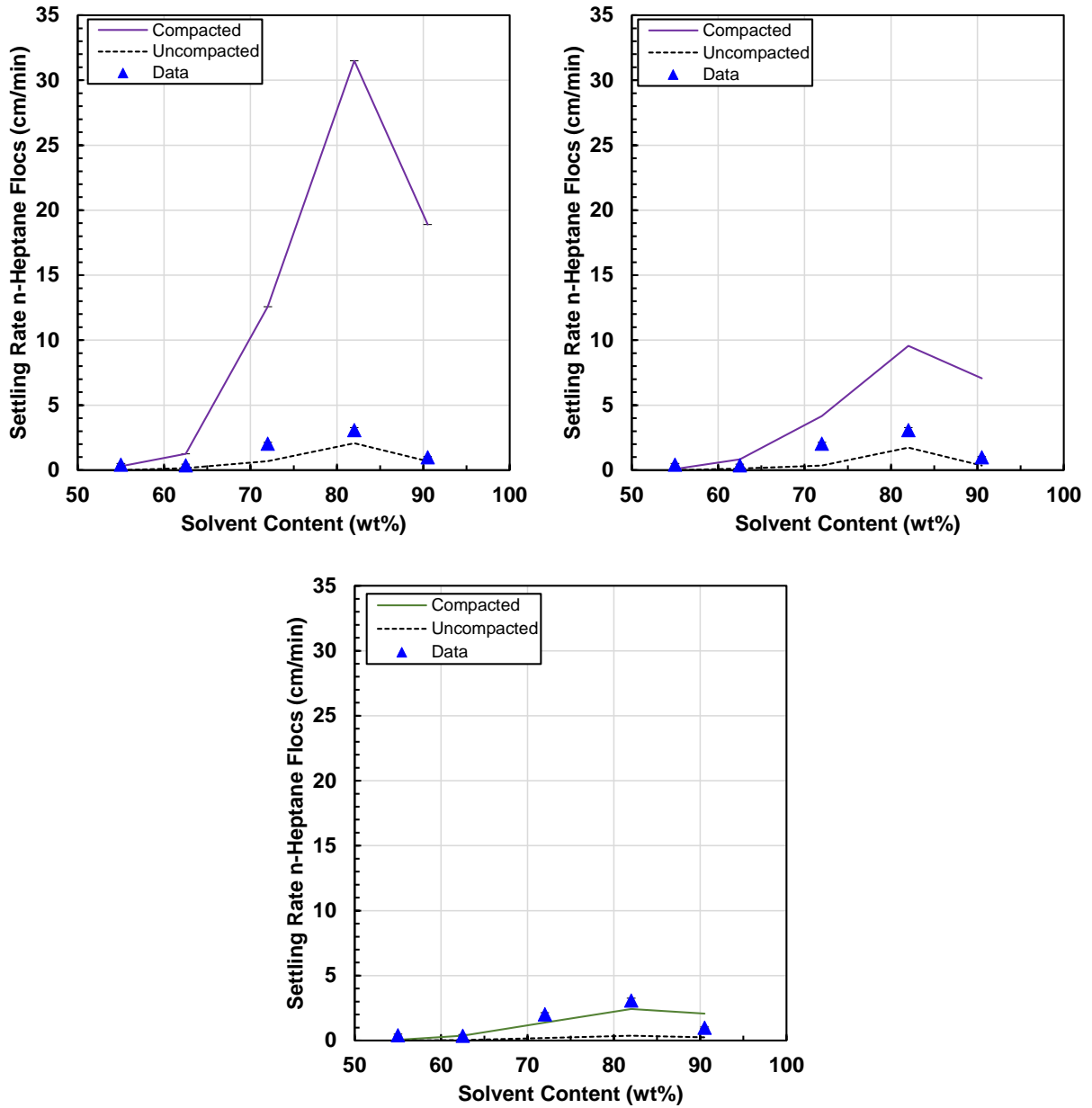
Figure 5.31. Settling rate of asphaltene flocs from the n-heptane/WC-B-B2 mixture calculated with the a) volume mean diameter, b) area mean diameter and c) number mean diameter, using compacted and uncompacted fractal dimensions.

Chapter Six: Conclusions and Recommendations

The diameter, settling rate, and fractal dimension were measured at 21°C for asphaltene flocs from three solvent/bitumen mixtures: n-pentane/WC-B-A3, n-heptane/WC-B-A3 and n-heptane/WC-B-B2. A settling model was developed to predict the settling rate of the asphaltene/solid flocs in these mixtures. The main conclusions from this study are presented below followed by recommendations for future research.

6.1 Conclusions

Asphaltene Floc Size

The asphaltenes appear to precipitate as approximately 1 μm diameter primary particles that almost instantaneously flocculate. While the flocs could be shattered at high enough shear rates they did not reflocculate. The data indicate that flocculation only occurs while the particles are coming out of solution and that the simultaneous precipitation and flocculation results in partially fused floc structures.

Two methods were used to measure the floc size distributions: the micrographic method and the FBRM method. The micrographic method provided valid, repeatable measurements for the n-pentane/WC-B-A3 and n-heptane/WC-B-A3 mixtures at solvent contents ranging from 55.0 to 95 wt% and 60.0 to 65.0 wt%, respectively. A two stage process to mix the solvent into the bitumen from Shafiee (2014) was modified to improve the reproducibility of the floc size and solvent content range for the floc size measurements with the FBRM. The measured chord length distributions were calibrated to maximum diameter distributions based on micrographic measurements at the same conditions. The FBRM provided valid, repeatable measurements for the n-pentane/WC-B-A3, n-heptane/WC-B-A3, and n-heptane/WC-B-B2 mixtures at solvent contents ranging from >95 wt%, 65.0 to 95.0 wt%, and 55.0 to 90.5 wt%, respectively.

The asphaltene floc size distributions measured with micrography and FBRM had a lognormal shape for all of the mixtures. The number mean diameters ranged from 17 to 205 μm depending on the solvent content, solvent type, and the bitumen sample. The number mean diameter of the

asphaltene flocs from the three solvent/bitumen mixtures increased from the onset of asphaltene precipitation up to a maximum at 70 to 80 wt% solvent and then decreased at higher solvent contents. The trend corresponds approximately to the concentration of precipitated asphaltenes, as expected with a flocculation process.

Asphaltene flocs from *n*-pentane/WC-B-A3 were an order of magnitude larger than asphaltene flocs from the *n*-heptane/WC-B-A3 mixture. In other words, the asphaltenes precipitate and flocculate more extensively in less compatible mixtures. The number mean diameter of the flocs from two different bitumens at the same conditions differed by 28% but a dataset consisting of only two bitumen samples was insufficient to identify the reason for the differences.

Fractal Dimension of Asphaltene Flocs

The fractal dimensions were determined using the sediment volume method based on uncompacted and compacted sediment volumes. The fractal dimension from the compacted sediment volume was consistent with the settling model results except near the onset of precipitation. The fractal dimension from the compacted sediment volume ranged from 2.10 to 2.83 depending on the solvent content, solvent type, and the bitumen sample.

The fractal dimension for all mixtures increased from the onset of asphaltene precipitation to a maximum at 70-80 wt% solvent and then decreased at higher solvent contents. Fractal dimensions were larger for asphaltene flocs from bitumen diluted with *n*-pentane than diluted with *n*-heptane. The fractal dimension of the asphaltene flocs from the WC-B-B2 oil were larger than those from the WC-B-A3 oil. The results suggest that higher asphaltene particle concentrations and poorer solubility lead to more compact flocs.

Settling Rates of Asphaltene/Solid Flocs

The settling rate of asphaltene/solid flocs was measured with the sediment and visual method. The settling rates from each method were in excellent agreement at conditions where both methods could be applied. The visual method is simpler to perform but could only be used at conditions

where the interface was visible (generally at solvent contents above 70 wt%). The sampling method was used when the interface was not visible but could not be used for rapid settling rates.

The toluene insolubles settled at the same rate as the asphaltene, as expected with co-flocculated material. The settling rates of n-heptane asphaltene flocs from the WC-B-A3 sample were between 0.1 and 0.4 cm/min and for the WC-B-B2 sample between 0.4 and 3 cm/min. The settling rates for both samples are too slow for industrial processes (Abel, 2017). However, settling rates of n-pentane flocs from WC-B-A3 sample were between 2 and 38 cm/min. The higher end of these settling rates are suitable for a commercial separation process.

The settling rate of the flocs from the n-pentane/WC-B-A3 and n-heptane/WC-B-A3 mixtures increased as the solvent content increased from the onset of asphaltene precipitation up to 80 wt% solvent and then decreased at higher solvent contents. The trend in the settling rate corresponds to the trends in the diameter and fractal dimension of the asphaltene flocs. The setting rate of the flocs from the n-pentane/WC-B-A3 mixture was two orders of magnitude faster than the settling rate of asphaltenes form the n-heptane/WC-B-A3 mixture. The difference is mainly attributed to the higher number mean diameter of the flocs in n-pentane. The flocs in n-pentane also had a higher fractal dimension (lower porosity).

The settling rate of asphaltene flocs from n-heptane/WC-B-B2 was relatively high at n-heptane contents just above the onset of asphaltene precipitation. The settling rate decreases as the n-heptane content increased to 62.5 wt% and then increased at higher n-heptane contents as observed with the WC-B-A3 bitumen. The toluene insoluble content of the WC-B-B2 bitumen was higher than the WC-B-A3 bitumen. Hence, the density of the flocs closer to the onset of asphaltene precipitation was higher, increasing the settling rate.

Settling Model

A settling model was developed based on the Stokes' law modified for the hindered settling of polydisperse particles. The model inputs are the fluid density and viscosity, asphaltene density, and the floc size distribution and fractal dimension. To model the zone settling of the asphaltene

flocs, the floc size distribution was reset to a narrow range of values around the number mean diameter. The model predicted the settling rates to within 15% except near the onset of precipitation. The reason the model fails near the onset was not established.

6.2 Recommendations for Future Work

There was not enough characterization information of the bitumen samples, such as molecular weight and SARA composition, to find correlations between bitumen properties and the settling rate, floc size and structure of the asphaltene flocs. It is recommended to do a full characterization of the samples and then, follow the methodology developed in this thesis to estimate the settling rate, floc size and fractal dimension of asphaltene flocs. In addition, more bitumen samples with different properties are required to develop meaningful correlations.

The main challenge in this thesis was to find an accurate method to measure the diameter of the asphaltene flocs. For future work, it is recommended to develop a method to automatize the measurement of the particle size from micrographs. For instance, the perimeter of independent flocs can be determined using software such as Matlab or ImageJ. Also, the Particle Vision and Measurement Technology (PVM) is a promising technology that could be used in diluted bitumen to measure the floc size distribution. The main advantage of this technique is that it takes pictures *in-situ*, avoiding offline analysis and sampling problems. This approach could improve the measurements closer to the onset of asphaltene precipitation. However, this technique has not been tested in diluted bitumen. It is also recommended to evaluate non-integer calibrations for the FBRM method. In this thesis, calibrations for the FBRM method were performed using integer calibration exponents (γ of either -1 or 0). It may be possible to obtain a consistent calibration for all of the mixtures with a calibration exponent between -1 and 0.

The settling rate and concentration profile of asphaltene flocs could be measured with non-intrusive methods for faster and more convenient measurements. For example, the settling rate of water/asphaltene/solid flocs in paraffinic froth treatment has been measured with ultrasonic methods (Kosior *et al.,* 2016). The concentration profile could be measured with Magnetic Resonance Imaging, Nuclear Magnetic Resonance, or X-ray methods.

Finally, to improve the settling model, a more rigorous approach to modeling band settling is required that accounts for the wake effect that causes small flocs settle at the same rate as larger particles. As a first approach, the exponent n in the Richardson and Zaki equation could be made a function of the size of the floc. Note that Allen (2003) speculated that the exponent may be a function of both the shape and size of the floc.

References

Abel, K. (2017). *Personal Communication. IOSI Stewarship meeting.* Edmonton.

Adeyinka, O., & Speirs, B. (2010). Processes and systems for solvent extraction of bitumen from oil sands. *US Patent App. 13*. Retrieved from http://www.google.com/patents/US20130001136

AER. (2015). *ST98-2016 Alberta's Energy Reserves 2015 and Supply Demand Outlook 2015-2024.* Calgary. Retrieved from http://www.aer.ca/documents/sts/ST98/ST98-2015.pdf

Agrawal, P., Schoeggl, F. F., Satyro, M. A., Taylor, S. D., & Yarranton, H. (2012). Measurement and modeling of the phase behavior of solvent diluted bitumens. *Fluid Phase Equilibria*, *334*, 51–64. https://doi.org/10.1016/j.fluid.2012.07.025

Agrawala, M., & Yarranton, H. (2001). An Asphaltene Association Model Analogous to Linear Polymerization. *Industrial & Engineering Chemistry Research*, *40*(21), 4664–4672. https://doi.org/10.1021/ie0103963

Akbarzadeh, K., Alboudwarej, H., Svrcek, W. Y., & Yarranton, H. (2005). A generalized regular solution model for asphaltene precipitation from n-alkane diluted heavy oils and bitumens. *Fluid Phase Equilibria*, *232*(1–2), 159–170. https://doi.org/10.1016/j.fluid.2005.03.029

Alboudwarej, H., Akbarzadeh, K., Beck, J., Svrcek, W. Y., & Yarranton, H. (2003). Regular solution model for asphaltene precipitation from bitumens and solvents. *AIChE Journal*, *49*(11), 2948–2956. https://doi.org/10.1002/aic.690491124

Allen, T. (2003). *Powder sampling and particle size determination* (First). Amsterdan.

Arya, A., Liang, X., von Solms, N., & Kontogeorgis, G. M. (2017). Modeling of Asphaltene Precipitation from Crude Oil with the Cubic Plus Association Equation of State. *Energy & Fuels*, acs.energyfuels.6b02767. https://doi.org/10.1021/acs.energyfuels.6b02767

Barnea, E., & Mizrahi, J. (1973). A generalized approach to the fluid dynamics of particulate systems. *The Chemical Engineering Journal*, *5*(2), 171–189. https://doi.org/10.1016/0300-9467(73)80008-5

Barrera, D. M., Ortiz, D. P., & Yarranton, H. (2013). Molecular weight and density distributions of asphaltenes from crude oils. *Energy and Fuels*, *27*(5), 2474–2487. https://doi.org/10.1021/ef400142v

Baydak, E. (2016). Personal Communication.

Bowman, C. (1967). MOLECULAR AND INTERFACIAL PROPERTIES OF ATHABASCA TAR SANDS. *7th World Petroleum Congress*, *3*, 583–604.

Boxall, J. A., Koh, C. A., Sloan, E. D., Sum, A. K., & Wu, D. T. (2010). Measurement and calibration of droplet size distributions in water-in-Oil emulsions by particle video microscope and a focused beam reflectance method. *Industrial and Engineering Chemistry Research*, *49*(3), 1412–1418. https://doi.org/10.1021/ie901228e

BP. (2014). *BP Energy Outlook 2035*. Retrieved from http://www.bp.com/en/global/corporate/about-bp/energy-economics/energy-outlook.html

Brandt, A. R., Englander, J., & Bharadwaj, S. (2013). The energy efficiency of oil sands extraction: Energy return ratios from 1970 to 2010. *Energy*, *55*, 693–702. https://doi.org/10.1016/j.energy.2013.03.080

Burya, Y. G., Yudin, I. K., Dechabo, V. a, Kosov, V. I., & Anisimov, M. a. (2001). Light-scattering study of petroleum asphaltene aggregation. *Applied Optics*, *40*(24), 4028–4035. https://doi.org/10.1364/AO.40.004028

Calles, J. A., Dufour, J., Marugán, J., Peña, J. L., Giménez-Aguirre, R., & Merino-García, D. (2008). Properties of asphaltenes precipitated with different n-Alkanes. A study to assess the most representative species for modeling. *Energy and Fuels*, *22*(2), 763–769. https://doi.org/10.1021/ef700404p

Castellanos, O., Modaresghazani, J., Satyro, M. A., & Yarranton, H. W. (2011). Modeling the phase behavior of heavy oil and solvent mixtures. *Fluid Phase Equilibria*, *304*(1–2), 74–85. https://doi.org/10.1016/j.fluid.2011.02.011

Castellanos, O., Sánchez-Lemus, M. C., Schoeggl, F., Satyro, M. A., Taylor, S. D., & Yarranton, H. W. (2014). Deep-vacuum fractionation of heavy oil and bitumen, part I: Apparatus and standardized procedure. *Energy and Fuels*, *28*(5), 2857–2865. https://doi.org/10.1021/ef500489y

Chacón-Patiño, M. L., Blanco-Tirado, C., Orrego-Ruiz, J. A., Gómez-Escudero, A., & Combariza, M. Y. (2015). High resolution mass spectrometric view of asphaltene-SiO2 interactions. *Energy and Fuels*, *29*(3), 1323–1331. https://doi.org/10.1021/ef502335b

Clain, P., Ndoye, F. T., Delahaye, A., Fournaison, L., Lin, W., & Dalmazzone, D. (2015). Particle size distribution of TBPB hydrates by focused beam reflectance measurement

(FBRM) for secondary refrigeration application. *International Journal of Refrigeration*, *50*(0), 19–31. https://doi.org/10.1016/j.ijrefrig.2014.10.016

Coulson, J. M., Richardson, J. F., Backhurst, J. R., & Harker, J. H. (1999). *Coulson and Richardson's Chemical Engineering. Fluid Flow, Heat Transfer and Mass Transfer.* (6th editio). Elsevier.

Czarnecki, J., Radoev, B., Schramm, L. L., & Slavchev, R. (2005). On the nature of Athabasca Oil Sands. *Advances in Colloid and Interface Science*, *114–115*, 53–60. https://doi.org/10.1016/j.cis.2004.09.009

Dai, Q., & Chung, K. H. (1995). Bitumen sand interaction in oil and processing, *74*(12), 1858–1864.

Daneshvar, S. (2005). *Asphaltene flocculation in diluted bitumen*. University of Calgary.

Dang-Vu, T., Jha, R., Wu, S., Tannant, D. D., Masliyah, J., & Xu, Z. (2009). Effect of Solid Wettability on Processability of Oil Sands Ores, (April), 2628–2636. https://doi.org/10.1021/ef9000117

Duran, J. (2016). Personal communication. Calgary.

Elimenech, N., Gregory, J., Jia, X., & Williams, R. (1998). Experimental techniques for aggregation studies. In *Particle deposition & aggregation. Measuring, modeling and simulation.* (pp. 263–289).

Feder, J. (1988). *Fractals*. New York: Plenum Press.

Fenistein, D., & Barré, L. (2001). Experimental measurement of the mass distribution of petroleum asphaltene aggregates using ultracentrifugation and small-angle X-ray scattering. *Fuel*, *80*(2), 283–287. https://doi.org/10.1016/S0016-2361(00)00072-7

Fenistein, D., Barre, L., Broseta, D., Espinat, D., Livet, A., Roux, J. N., & Scarsella, M. (1998). Viscosimetric and neutron scattering study of asphaltene aggregates in mixed toluene / heptane solvents. *Langmuir*, *14*(5), 1013–1020. https://doi.org/10.1021/la9709148

Ferworn, K., Svrcek, W., & Mehrotra, A. (1993). Measurement of asphaltene particle size distributions in crude oils diluted with n-heptane. *Industrial & Engineering Chemistry Research*, *32*(5), 955–959. https://doi.org/10.1021/ie00017a026

Gray, M. R. (1994). *Upgrading Petroleum Residues and Heavy Oil and*.

Gray, M. R. (2015). *Upgrading Oilsands Bitumen and Heavy Oil*.

Greaves, D., Boxall, J., Mulligan, J., Montesi, A., Creek, J., Dendy Sloan, E., & Koh, C. A. (2008). Measuring the particle size of a known distribution using the focused beam reflectance measurement technique. *Chemical Engineering Science*, *63*(22), 5410–5419. https://doi.org/10.1016/j.ces.2008.07.023

Heath, A. R., Fawell, P. D., Bahri, P. A., & Swift, J. D. (2002). Estimating average particle size by focused beam reflectance measurement (FBRM). *Particle and Particle Systems Characterization*, *19*(2), 84–95. https://doi.org/10.1002/1521-4117(200205)19:2<84::AID-PPSC84>3.0.CO;2-1

Hirschberg, A., DeJong, L. N. J., Schipper, B. a., & Meijer, J. G. (1984). Influence of Temperature and Pressure on Asphaltene Flocculation. *Society of Petroleum Engineers Journal*, *24*(3), 283–293. https://doi.org/10.2118/11202-PA

Hooshiar, A., Uhlik, P., Ivey, D. G., Liu, Q., & Etsell, T. H. (2012). Clay minerals in nonaqueous extraction of bitumen from Alberta oil sands. *Fuel Processing Technology*, *96*, 183–194. https://doi.org/10.1016/j.fuproc.2011.10.010

Hooshiar, A., Uhlik, P., Liu, Q., Etsell, T. H., & Ivey, D. G. (2012). Clay minerals in nonaqueous extraction of bitumen from Alberta oil sands. *Fuel Processing Technology*, *94*(1), 80–85. https://doi.org/10.1016/j.fuproc.2011.10.008

Jarvis, P., Jefferson, B., & Parsons, S. A. (2005). Measuring floc structural characteristics. *Reviews in Environmental Science and Biotechnology*, *4*(1–2), 1–18. https://doi.org/10.1007/s11157-005-7092-1

Johnston, K. A., Schoeggl, F. F., Satyro, M. A., Taylor, S. D., & Yarranton, H. W. (2017). Phase behavior of bitumen and n- pentane. *Fluid Phase Equilibria*, *442*, 1–19. https://doi.org/10.1016/j.fluid.2017.03.001

Kaminsky, H. a. W., Etsell, T. H., Ivey, D. G., & Omotoso, O. (2008). Characterization of heavy minerals in the Athabasca oil sands. *Minerals Engineering*, *21*(4), 264–271. https://doi.org/10.1016/j.mineng.2007.09.011

Kosior, D., Ngo, E., & Dabros, T. (2016). Determination of the Settling Rate of Aggregates Using the Ultrasound Method during Paraffinic Froth Treatment. *Energy & Fuels*, *30*(10), 8192–8199. https://doi.org/10.1021/acs.energyfuels.6b01714

Lasentec. (2002). FBRM control interface version 6.0 user manual.

Li, M., Wilkinson, D., & Patchigolla, K. (2005). Determination of non-spherical particle size distribution from chord length measurements. Part 2: Experimental validation. *Chemical Engineering Science*, *60*(18), 4992–5003. https://doi.org/10.1016/j.ces.2005.04.019

Li, X. Y., & Logan, B. E. (2001). Permeability of fractal aggregates. *Water Research*, *35*(14), 3373–3380. https://doi.org/10.1016/S0043-1354(01)00061-6

Li, Z., & Firoozabadi, A. (2010). Modeling asphaltene precipitation by n-alkanes from heavy oils and bitumens using cubic-plus-association equation of state. *Energy and Fuels*, *24*(2), 1106–1113. https://doi.org/10.1021/ef9009857

Long, Y., Dabros, T., & Hamza, H. (2002). Stability and settling characteristics of solvent-diluted bitumen emulsions. *Fuel*, *81*(15), 1945–1952. https://doi.org/10.1016/S0016-2361(02)00132-1

Long, Y., Dabros, T., & Hamza, H. (2004). Structure of water/solids/asphaltenes aggregates and effect of mixing temperature on settling rate in solvent-diluted bitumen. *Fuel*, *83*(7–8), 823–832. https://doi.org/10.1016/j.fuel.2003.10.026

Mandelbrot, B. (1977). *Fractals: form, change and dimension*. San Francisco.

Mandelbrot, B. (1983). *The fractal geometry of nature*. New York.

Maqbool, T., Balgoa, A. T., & Fogler, H. S. (2009). Revisiting Asphaltene Precipitation from Crude Oils : A Case of Neglected Kinetic Effects. *Energy and Fuels*, (9), 3681–3686. https://doi.org/10.1021/ef800706c.(8)

Maqbool, T., Raha, S., Hoepfner, M. P., & Fogler, H. S. (2011). Modeling the aggregation of asphaltene nanoaggregates in crude oil-precipitant systems. *Energy and Fuels*, *25*(4), 1585–1596. https://doi.org/10.1021/ef1014132

Masliyah, J., Zhou, Z. J., Xu, Z., Czarnecki, J., & Hamza, H. (2004). Understanding Water-Based Bitumen Extraction from Athabasca Oil Sands. *The Canadian Journal of Chemical Engineering*, *82*(4), 628–654. https://doi.org/10.1002/cjce.5450820403

McCabe, W., Smith, J., & Harriot, P. (2001). *Unit operations of chemical engineering.* (6th editio).

McKenna, A. M., Donald, L. J., Fitzsimmons, J. E., Juyal, P., Spicer, V., Standing, K. G., … Rodgers, R. P. (2013). Heavy petroleum composition. 3. Asphaltene aggregation. *Energy and Fuels*, *27*(3), 1246–1256. https://doi.org/10.1021/ef3018578

McKenna, A. M., Marshall, A. G., & Rodgers, R. P. (2013). Heavy petroleum composition. 4. Asphaltene compositional space. *Energy and Fuels*, *27*(3), 1257–1267. https://doi.org/10.1021/ef301747d

Merino-Garcia, D., Murgich, J., & Andersen, S. I. (2004). Asphaltene Self-Association: Modeling and Effect of Fractionation With A Polar Solvent. *Petroleum Science and Technology*, *22*(7–8), 735–758. https://doi.org/10.1081/LFT-120038710

Mitchell, D. L., & Speight, J. G. (1972). The Solubility of Aspahtlenes in hydrocarbon solvents. *Energy & Fuels*, *52*(2), 149–152.

Mostowfi, F., Indo, K., Mullins, O. C., & McFarlane, R. (2009). Asphaltene nanoaggregates studied by centrifugation. *Energy and Fuels*, *23*(3), 1194–1200. https://doi.org/10.1021/ef8006273

Mullins, O. C. (Schlumberger-D. R., Sheu, E. Y., Hammami, A., & Marshall, A. G. (2007). *Asphaltenes, Heavy Oils, and Petroleomics. Chemistry & …*. https://doi.org/10.1007/0-387-68903-6

Nikakhtari, H., Vagi, L., Choi, P., Liu, Q., & Gray, M. R. (2013). Solvent screening for non-aqueous extraction of Alberta oil sands. *The Canadian Journal of Chemical Engineering*, *91*(6), 1153–1160. https://doi.org/10.1002/cjce.21751

Nikakhtari, H., Wolf, S., Choi, P., Liu, Q., & Gray, M. (2014). Migration of fine solids into product bitumen from solvent extraction of Alberta oil sands. *Energy & Fuels*, *28*, 2925–2932. Retrieved from http://pubs.acs.org/doi/abs/10.1021/ef500021y

Nomura, M., Rahimi, P., & Koseoglu, O. (2004). *Heavy Hydrocarbon Resources: characterization, upgrading and utilization*.

Osacky, M., Geramian, M., Ivey, D. G., Liu, Q., & Etsell, T. H. (2013). Mineralogical and chemical composition of petrologic end members of Alberta oil sands. *Fuel*, *113*, 148–157. https://doi.org/10.1016/j.fuel.2013.05.099

Pal, K., Nogueira Branco, L. D. P., Heintz, A., Choi, P., Liu, Q., Seidl, P. R., & Gray, M. R. (2015). Performance of solvent mixtures for non-aqueous extraction of Alberta oil sands. *Energy & Fuels*, *29*(4), 2261–2267. https://doi.org/10.1021/ef502882c

Panuganti, S. R., Tavakkoli, M., Vargas, F. M., Gonzalez, D. L., & Chapman, W. G. (2013). SAFT model for upstream asphaltene applications. *Fluid Phase Equilibria*, *359*, 2–16.

https://doi.org/10.1016/j.fluid.2013.05.010

Podgorski, D. C., Corilo, Y. E., Nyadong, L., Lobodin, V. V., Bythell, B. J., Robbins, W. K., … Rodgers, R. P. (2013). Heavy petroleum composition. 5. Compositional and structural continuum of petroleum revealed. *Energy and Fuels*, *27*(3), 1268–1276. https://doi.org/10.1021/ef301737f

Powers, D. P., Sadeghi, H., Yarranton, H., & Van Den Berg, F. G. A. (2016). Regular solution based approach to modeling asphaltene precipitation from native and reacted oils: Part 1, molecular weight, density, and solubility parameter distributions of asphaltenes. *Fuel*, *178*, 218–233. https://doi.org/10.1016/j.fuel.2016.03.027

Rahmani, N., Dabros, T., & Masliyah, J. (2004). Evolution of asphaltene floc size distribution in organic solvents under shear. *Chemical Engineering Science*, *59*(3), 685–697. https://doi.org/10.1016/j.ces.2003.10.017

Rahmani, N., Dabros, T., & Masliyah, J. H. (2005a). Fractal structure of asphaltene aggregates. *Journal of Colloid and Interface Science*, *285*(2), 599–608. https://doi.org/10.1016/j.jcis.2004.11.068

Rahmani, N., Dabros, T., & Masliyah, J. H. (2005b). Settling properties of asphaltene aggregates. *Energy and Fuels*, *19*(3), 1099–1108. https://doi.org/10.1021/ef0496707

Ramos-Pallares, F., Schoeggl, F. F., Taylor, S. D., Satyro, M. A., & Yarranton, H. W. (2016). Predicting the Viscosity of Hydrocarbon Mixtures and Diluted Heavy Oils Using the Expanded Fluid Model. *Energy and Fuels*, *30*(5), 3575–3595. https://doi.org/10.1021/acs.energyfuels.5b01951

Ramos-Pallares, F., Taylor, S. D., Satyro, M. A., Marriot, R. A., & Yarranton, H. (2016). Prediction of Viscosity for Characterized Oils and Their Fractions Using the Expanded Fluid Model. *Energy and Fuels*, *30*(9), 7134–7157. https://doi.org/10.1021/acs.energyfuels.6b01419

Rastegari, K., Svrcek, W. Y., & Yarranton, H. (2004). Kinetics of Asphaltene Flocculation. *Industrial & Engineering Chemistry Research*, *43*, 6861–6870. https://doi.org/10.1021/ie049594v

Richardson, J. F., & Zaki, W. N. (1954). Sedimentation and fluidisation: Part I. *Transactions of the Institution of Chemical Engineers*, *32*, S82–S100. https://doi.org/10.1016/S0263-

8762(97)80006-8

Rogak, S. N., & Flagan, R. C. (1990). Stokes drag on self-similar clusters of spheres. *Journal of Colloid And Interface Science*, *134*(1), 206–218. https://doi.org/10.1016/0021-9797(90)90268-S

Romanova, U. G., Yarranton, H. W., Schramm, L. L., & Shelfantook, W. E. (2004). Investigation of oil sands froth treatment. *Canadian Journal of Chemical Engineering*, *82*(4), 710–721. https://doi.org/10.1002/cjce.5450820410

Saadatmand, M. (2008). *Investigation of rag layers from oil sand froth*. University of Calgary.

Saryazdi, F., Motahhari, H., Schoeggl, F. F., Taylor, S. D., & Yarranton, H. (2013). Density of hydrocarbon mixtures and bitumen diluted with solvents and dissolved gases. *Energy and Fuels*, *27*(7), 3666–3678. https://doi.org/10.1021/ef400330j

Schümann, H., Khatibi, M., Tutkun, M., Pettersen, B. H., Yang, Z., & Nydal, O. J. (2015). Droplet Size Measurements in Oil–Water Dispersions: A Comparison Study Using FBRM and PVM. *Journal of Dispersion Science and Technology*, *36*(10), 1432–1443. https://doi.org/10.1080/01932691.2014.989569

Seifried, C. M., Crawshaw, J., & Boek, E. S. (2013). Kinetics of asphaltene aggregation in crude oil studied by confocal laser-scanning microscopy. *Energy and Fuels*, *27*(4), 1865–1872. https://doi.org/10.1021/ef301594j

Shafiee, M. (2014). *Kinetics of asphaltene precipitation and flocculation from diluted bitumen*. University of Calgary. Retrieved from http://scholar.google.com/scholar?hl=en&btnG=Search&q=intitle:No+Title#0

Speight, J. (1998). *Petroleum Chemistry and Refining*.

Speight, J. (1999). *The Chemistry and Technology of Petroleum* (3th ed.).

Speight, J. (2007). *The Chemistry and Technology of Petroleum* (fourth).

Speight, J. (2013). *Heavy and extra-heavy oil upgrading technologies*.

Sztukowski, D. M., & Yarranton, H. (2004). Characterization and interfacial behavior of oil sands solids implicated in emulsion stability. *Journal of Dispersion Science and Technology*, *25*(3), 299–310. https://doi.org/10.1081/DIS-120037692

Tan, X., Vagi, L., Liu, Q., Choi, P., & Gray, M. R. (2016). Sorption equilibrium and kinetics for cyclohexane, toluene, and water on Athabasca oil sands solids. *The Canadian Journal of*

Chemical Engineering, *94*(2), 220–230. https://doi.org/10.1002/cjce.22389

Tang, P., & Raper, J. A. (2002). Modeling the settling behavior of fractal aggregates-a review. *Powder Technology*, *123*, 114–125.

Ting, D., Hirasaki, G. J., & Chapman, W. G. (2003). Modeling of Asphaltene Phase Behavior with the SAFT Equation of State. *Petroleum Science and Technology*, *21*(June 2014), 647–661. https://doi.org/10.1081/LFT-120018544

Tu, Y., O'Carroll, J. B., Kotlyar, L. S., Sparks, B. D., Ng, S., Chung, K. H., & Cuddy, G. (2005). Recovery of bitumen from oilsands: Gelation of ultra-fine clay in the primary separation vessel. *Fuel*, *84*(6 SPEC. ISS.), 653–660. https://doi.org/10.1016/j.fuel.2004.03.020

Valinasab, M. (2006). *Bitumen extracion and froth treatment*. University of Calgary.

Wallace, D., Tipman, R., Komishke, B., Wallwork, V., & Perkins, E. (2004). Fines / Water Interactions and Consequences Oil Sands Extractability, *82*(August), 667–677.

Wang, J. X., & Buckley, J. S. (2001). A Two-Component Solubility Model of the Onset of Asphaltene Flocculation in Crude Oils A Two-Component Solubility Model of the Onset of Asphaltene Flocculation in Crude Oils. *Energy & Fuels*, *15*(4), 1004–1012. https://doi.org/10.1021/ef010012l

Wang, S., Liu, Q., Tan, X., Xu, C., & Gray, M. R. (2013). Study of Asphaltene Adsorption on Kaolinite by X-ray Photoelectron Spectroscopy and Time-of-Flight Secondary Ion Mass Spectroscopy. *Energy Fuels*, *27*(5), 2465–2473. https://doi.org/10.1021/ef4001314

Wiehe, I., Yarranton, H., Akbarzadeh, K., Rahimi, P., & Teclemariam, A. (2005). The Paradox of Asphaltene Precipitation with normal paraffins, *19*, 1261–1267.

Woodfield, D., & Bickert, G. (2001). An improved permeability model for fractal aggregates settling in creeping flow. *Water Research*, *35*(16), 3801–3806. https://doi.org/10.1016/S0043-1354(01)00128-2

Xu, R. (2000). *Particle characterization: Light scattering methods*. Dordrecht.

Yan, Y., & Masliyah, J. H. (1993). Solids-stabilized oil-in-water emulsions : scavenging of emulsion droplets by fresh oil addition, *15*, 123–132.

Yarranton, H. (2005). Asphaltene Self-Association. *Journal of Dispersion Science and Technology*, *26*(1), 5–8. https://doi.org/10.1081/DIS-200040234

Yarranton, H. W., Ortiz, D. P., Barrera, D. M., Baydak, E. N., Barré, L., Frot, D., … Oake, J.

(2013). On the size distribution of self-associated asphaltenes. *Energy and Fuels*, *27*(9), 5083–5106. https://doi.org/10.1021/ef400729w

Yarranton, H. W., & Satyro, M. A. (2009). Expanded fluid-based viscosity correlation for hydrocarbons. *Industrial and Engineering Chemistry Research*, *48*(7), 3640–3648. https://doi.org/10.1021/ie801698h

Yarranton, H. W., van Dorp, J. J., Verlaan, M. L., & Lastovka, V. (2012). Wanted Dead or Live : Crud de Cockta ail Viscos sity : A Ps omponen nt Method to o Predict t the Visc cosity of Dead Oils s , Live Oi ils , and M Mixtures. *Spe 160314*, (May), 1–22.

Yudin, I. K., Nikolaenko, G. L., Gorodetskii, E. E., Kosov, V. I., Melikyan, V. R., Markhashov, E. L., … Briolant, Y. (1998). Mechanisms of asphaltene aggregation in toluene–heptane mixtures. *Journal of Petroleum Science and Engineering*, *20*(3–4), 297–301. https://doi.org/10.1016/S0920-4105(98)00033-3

Zahabi, A., Gray, M. R., Czarnecki, J., & Dabros, T. (2010). Flocculation of silica particles from a model oil solution: effect of adsorbed asphaltenes. *Energy & Fuels*, *24*(6), 3616–3623. https://doi.org/10.1021/ef100079j

Zawala, J., Dabros, T., & Hamza, H. (2012). Settling properties of aggregates in paraffinic froth treatment. *Energy and Fuels*, *26*(9), 5775–5781. https://doi.org/10.1021/ef300885t

Zhao, S., Kotlyar, L. S., Sparks, B. D., Woods, J. R., Gao, J., & Chung, K. H. (2001). Solids contents, properties and molecular structures of asphaltenes from different oilsands. *Fuel*, *80*(13), 1907–1914. https://doi.org/10.1016/S0016-2361(01)00044-8

Appendix A: Expanded Fluid Model

The Expanded Fluid viscosity model was used to calculate the viscosity of the supernatant from bitumen diluted with *n*-alkanes. The basic principle of the model is that the fluidity of a fluid increases as the fluid expands; that is, viscosity (the inverse of fluidity) decreases as the density decreases. Yarranton and Satyro (2009) proposed the following relationship between viscosity and density:

$$\mu - \mu_0 = 0.165\left(\exp(c_{2,mix}\beta_{mix}) - 1\right)$$

(A-0-1)

where μ is the viscosity of the fluid in mPa.s formulated as a departure from diluted gas viscosity μ_0, $c_{2,mix}$ is a parameter specific for each mixture which quantifies the response of the viscosity of the fluid to the expansion from the compressed state, and β_{mix} is the correlation parameter between the density and the viscosity given by:

$$\beta_{mix} = \frac{1}{\exp\left[\left(\frac{\rho^*_{s,mix}}{\rho_{mix}}\right)^{0.65} - 1\right] - 1}$$

(A-0-2)

where ρ_{mix} is the density of the mixture and $\rho^*_{s,mix}$ is the pressure-dependent compressed state density of the fluid given by:

$$\rho^*_{s,mix} = \frac{\rho^0_{s,mix}}{\exp(-c_3 P)}$$

(A-0-3)

where $\rho^0_{s,mix}$ is the compressed state density of the mixture in a vacuum. Since all of the experiments in this thesis were performed at atmospheric pressure, the pressure dependency was not considered and $\rho^*_{s,mix} = \rho^0_{s,mix}$. The mixing rules for the mixture parameters $\rho^0_{s,mix}$ and $c_{2,mix}$ were taken from Ramos-Pallares *et al*. (2016) and are given by:

$$\rho_{s,mix}^0 = \left(\sum_i^{nc} \sum_j^{nc} \frac{w_i w_j}{2} \left(\frac{1}{\rho_{s,i}^0} + \frac{1}{\rho_{s,j}^0} \right) (1 - \alpha_{ij}) \right)^{-1}$$

(A-0-4)

$$\frac{c_{2,mix}}{\rho_{s,mix}^0} = \sum_i^{nc} \sum_j^{nc} \frac{w_i w_j}{2} \left(\frac{c_{2,i}}{\rho_{s,i}^0} + \frac{c_{2,j}}{\rho_{s,j}^0} \right) (1 - \alpha_{ij})$$

(A-0-5)

where w is the mass composition and α_{ij} is the viscosity interaction parameter. The subscript i and j stand for each component in the mixture. The interaction parameter is given by (Ramos-Pallares *et al.*, 2016):

$$\alpha_{ij} = \alpha_{ij}^0 - \Delta\alpha_{ij}$$

(A-0-6)

where α_{ij}^0 is the reference value and $\Delta\alpha_{ij}$ is the departure function.

The reference value was correlated to the normalized specific gravity defined as follows:

$$\Delta SG_{norm} \leq 0.165 : \quad \alpha_{ij}^0 = 0.021 \tag{A-7}$$

$$\Delta SG_{norm} > 0.165 : \quad \alpha_{ij}^0 = 0.038304 - 0.10478 \Delta SG_{norm} \tag{A-8}$$

where

$$\Delta SG_{norm} = \frac{2|SG_i - SG_j|}{SG_i + SG_j} \tag{A-9}$$

and SG is the specific gravity of components i and j.

The departure function was correlated to the normalized difference in the hydrogen/carbon ratio ($\Delta(H/C)_{norm}$) of the paired components as follows:

$$\Delta(H/C)_{norm} \leq 0.25: \quad \Delta\alpha_{ij} = 0.02756 - 0.1103\Delta(H/C)_{norm}$$

(A-0-7)

$$\Delta(H/C)_{norm} > 0.25: \quad \Delta\alpha_{ij} = 0$$

(A-0-8)

where

$$\Delta(H/C)_{norm} = \frac{2\left|(H/C)_i - (H/C)_j\right|}{(H/C)_i + (H/C)_j}$$

(A-0-9)

and *(H/C)* is the hydrogen/carbon ratio of the components *i* and *j*.

A.1 Bitumen Viscosity Predictions

The viscosity of the diluted oil after asphaltene precipitation was required. Therefore a pseudo-component approach was selected so that the removal of asphaltenes could be accounted for. The approach for bitumen viscosity predictions is presented in Figure A.1. The bitumen was divided into maltene and asphaltene fractions and each was characterized separately. The maltene fraction was characterized into pseudo-components defined from distillation assay and the asphaltenes were characterized as a single pseudo-component for viscosity modeling purposes. Details of the characterization of maltenes and asphaltenes are provided below.
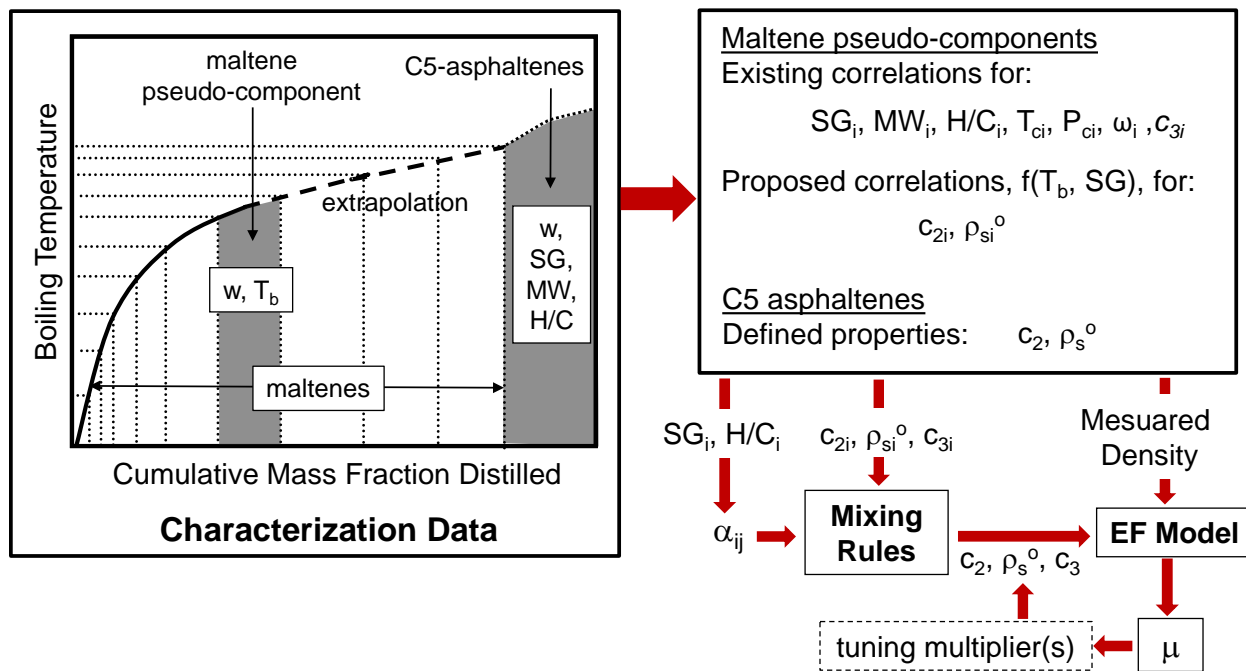
Figure A.1 Schematic of characterization procedure for predicting crude oil viscosity adapted from Ramos-Pallares *et al.* (2016).

Maltenes

The maltene fraction was completely characterized by a Gaussian extrapolation of the distillation data to the end of the fraction. Then, the fraction was divided into 14 pseudo-components as described by Ramos-Pallares *et al.* (2016). They reported the physical properties of the pseudo-components such as specific gravity, molecular weight, H/C critical properties and EF parameters in the supporting information.

Asphaltenes

Asphaltenes were represented as a single pseudo-component with defined properties calculated from the calculated maltene properties and whole crude oil properties. The EF asphaltene model parameters were taken from Ramos-Pallares *et al.* (2016).

A.2 Supernatant Viscosity Prediction

To calculate the viscosity of the supernatant, it was assumed that only asphaltenes precipitate whereas maltenes remain solubilized. The amount of asphaltenes that remained in solution was calculated from the corresponding yield curve and used to adjust the composition of the whole fluid (maltenes and solubilized asphaltenes). Once the composition of the fluid was adjusted, its viscosity was predicted using the same approach presented in Figure A.1. Note, the maltene boiling point distribution, and therefore their physical properties and EF model parameters do not change as asphaltenes precipitate. EF model parameters for solubilized asphaltenes also remain constant as recommended by Ramos-Pallares *et al.* (2016).

It was found that the calculated supernatant viscosity after removing the asphaltenes was within 5% of the viscosity calculated with the asphaltenes. Therefore, for convenience, all further viscosity calculations were performed on the whole oil, neglecting any asphaltene precipitation.

Note, the pseudo-component properties and parameters for the WC-B-A3 sample were not available. Instead, the EF parameters of the WC-B-A3 bitumen were calculated by fitting its viscosity data. The viscosity of the diluted WC-B-A3 was calculated with the EF model considering two pseudo-components: the bitumen and the solvent. The effect of asphaltene precipitation was again neglected.

Appendix B: Floc Number Size Distributions

This appendix presents the floc size distribution of the *n*-pentane/WC-B-A3, *n*-heptane/WC-B-A3 and *n*-heptane/WC-B-B2 mixtures, measured as explained in Chapter 3.
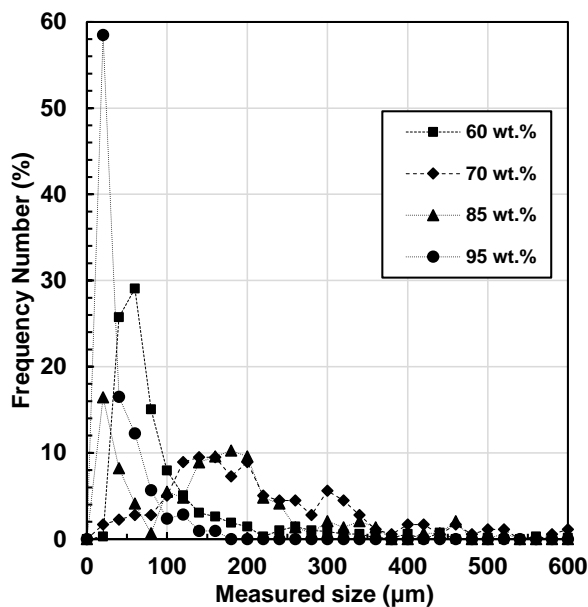
Figure B.1. Number Frequency Distribution for WC-B-B3 bitumen diluted with *n*-pentane at 60, 70, 85 and 95 wt% solvent content**.**
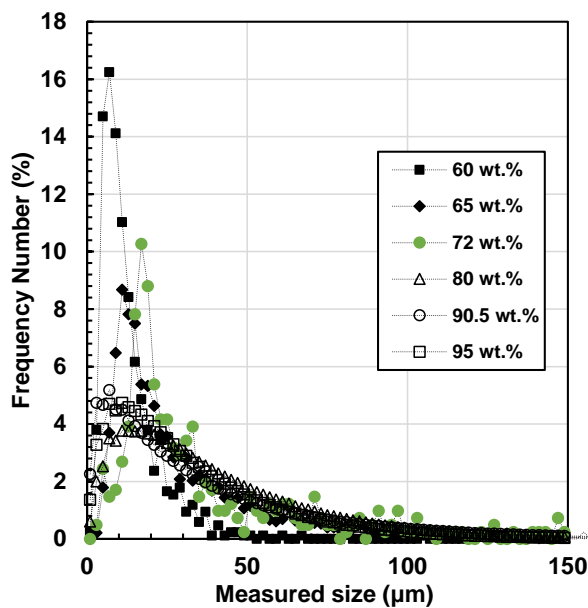
Figure B.2. Number Frequency Distribution for WC-B-B3 bitumen diluted with *n*-heptane at 60, 65, 72, 80, 90.5 and 95 wt% solvent content**.**
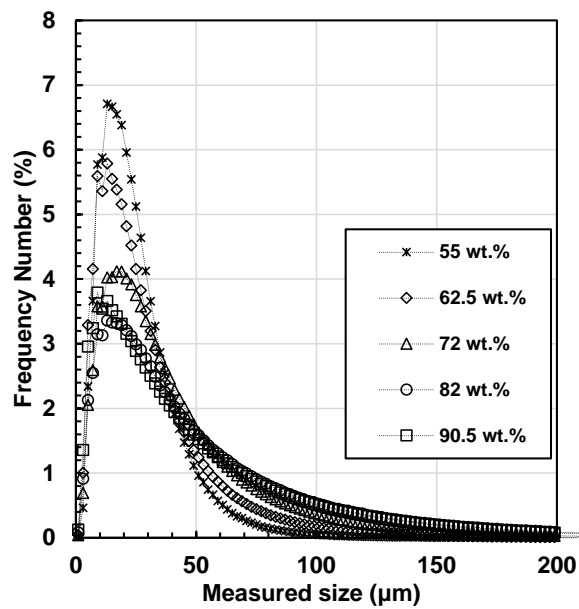
Figure B.3. Number Frequency Distribution for WC-B-B2 bitumen diluted with *n*-heptane at 55, 62.5, 72, 80, 82 and 90.5 solvent content**.**

Appendix C: Settling Model Input Data

This appendix presents the inputs used to calculate the settling rate using the settling model. The input data consist of two matrices for each system the physical properties and the experimental solid volume fraction data. This appendix does not include the floc size distributions of asphaltenes presented in Appendix B.

Table C.1. Input data for the settling model of the system *n*-pentane/WC-B-A3.

Solvent content (wt%)	Time (s)	Viscosity (mPa s)	Density (kg/m^3)	Asphaltene mass (g)	Asphaltene density (kg/m^3)	Primary particle diameter (μm)	Sediment porosity (φ)
60	60	1.1910	750.44	6.4607	1200	1	0.1077
60	300	1.1910	750.44	6.4607	1200	1	0.1077
60	600	1.1910	750.44	6.4607	1200	1	0.1077
60	1200	1.1910	750.44	6.4607	1200	1	0.1077
70	60	0.6630	711.55	6.2644	1200	1	0.1044
70	180	0.6630	711.55	6.2644	1200	1	0.1044
70	300	0.6630	711.55	6.2644	1200	1	0.1044
70	600	0.6630	711.55	6.2644	1200	1	0.1044
85	12	0.3685	666.53	3.4182	1200	1	0.1096
85	24	0.3685	666.53	3.4182	1200	1	0.1096
85	36	0.3685	666.53	3.4182	1200	1	0.1096
85	60	0.3685	666.53	3.4182	1200	1	0.1096
95	12	0.2625	639.05	1.1643	1200	1	0.0539
95	36	0.2625	639.05	1.1643	1200	1	0.0539
95	60	0.2625	639.05	1.1643	1200	1	0.0539
95	120	0.2625	639.05	1.1643	1200	1	0.0539

Table C.2. Input data for the settling model of the system *n*-heptane/WC-B-A3.

Solvent content (wt%)	Time (s)	Viscosity (mPa s)	Density (kg/m³)	Asphaltene mass (g)	Asphaltene density (kg/m³)	Primary particle diameter (μm)	Sediment porosity (φ)
60	1200	2.2665	791.35	0.7366	1200	1	0.0120
	2400	2.2665	791.35	0.7366	1200	1	0.0193
	3600	2.2665	791.35	0.7366	1200	1	0.0266
	7200	2.2665	791.35	0.7366	1200	1	0.0484
65	1200	1.7111	776.57	2.0032	1200	1	0.0332
	3600	1.7111	776.57	2.0032	1200	1	0.0493
	7200	1.7111	776.57	2.0032	1200	1	0.0734
	10800	1.7111	776.57	2.0032	1200	1	0.0975
72	1200	1.2102	756.81	2.7661	1200	1	0.0545
	2400	1.2102	756.81	2.7661	1200	1	0.0651
	3600	1.2102	756.81	2.7661	1200	1	0.0756
	5400	1.2102	756.81	2.7661	1200	1	0.0915
80	600	0.8499	734.96	3.3196	1200	1	0.0510
	1200	0.8499	734.96	3.3196	1200	1	0.0510
	1800	0.8499	734.96	3.3196	1200	1	0.0510
	2700	0.8499	734.96	3.3196	1200	1	0.0510
82	600	0.7825	729.61	3.1788	1200	1	0.0432
	1140	0.7825	729.61	3.1788	1200	1	0.0432
	1800	0.7825	729.61	3.1788	1200	1	0.0432
	2700	0.7825	729.61	3.1788	1200	1	0.0432
90.5	648	0.5642	707.56	1.7087	1200	1	0.0187
	1392	0.5642	707.56	1.7087	1200	1	0.0187
	1926	0.5642	707.56	1.7087	1200	1	0.0187
	2760	0.5642	707.56	1.7087	1200	1	0.0187
95	540	0.4805	696.28	0.8825	1200	1	0.0108
	1080	0.4805	696.28	0.8825	1200	1	0.0108
	1860	0.4805	696.28	0.8825	1200	1	0.0108
	2700	0.4805	696.28	0.8825	1200	1	0.0108

Table C.3. Experimental solid volume fraction for the mixture *n*-heptane/WC-B-A3 at 60 wt% solvent content, at different settling times.

	Settling Time (minutes)			
Layer	20	40	60	120
1	0.0013	0.0003	0.0002	0.0003
2	0.0021	0.0004	0.0002	0.0004
3	0.0030	0.0004	0.0002	0.0004
4	0.0033	0.0011	0.0002	0.0004
5	0.0037	0.0032	0.0003	0.0004
6	0.0036	0.0037	0.0003	0.0004
7	0.0035	0.0042	0.0025	0.0004
8	0.0041	0.0055	0.0070	0.0005
9	0.0065	0.0104	0.0157	0.0241
10	0.0114	0.0188	0.0281	0.0479

Table C.4. Experimental solid volume fraction for the mixture *n*-heptane/WC-B-A3 at 65 wt% solvent content, at different settling times.

	Settling Time (minutes)			
Layer	20	60	120	180
1	0.0025	0.0001	0.0008	0.0000
2	0.0088	0.0001	0.0007	0.0000
3	0.0100	0.0005	0.0008	0.0000
4	0.0107	0.0098	0.0000	0.0000
5	0.0107	0.0126	0.0001	0.0000
6	0.0114	0.0124	0.0004	0.0000
7	0.0111	0.0135	0.0131	0.0000
8	0.0114	0.0233	0.0042	0.0330
9	0.0158	0.0340	0.0423	0.0519
10	0.0357	0.0443	0.0766	0.0967

Table C.5. Experimental solid volume fraction for the mixture *n*-heptane/WC-B-A3 at 72 wt% solvent content, at different settling times.

	Settling Time (minutes)			
Layer	**20**	**40**	**60**	**90**
1	0.0001	0.0000	0.0002	0.0000
2	0.0074	0.0000	0.0003	0.0000
3	0.0120	0.0000	0.0003	0.0000
4	0.0134	0.0045	0.0003	0.0000
5	0.0143	0.0110	0.0003	0.0000
6	0.0130	0.0132	0.0002	0.0000
7	0.0151	0.0147	0.0190	0.0079
8	0.0152	0.0291	0.0423	0.0477
9	0.0354	0.0478	0.0654	0.0628
10	0.0547	0.0669	0.0720	0.0930

Table C.6. Input data for the settling model of the system *n*-heptane/WC-B-B2.

Solvent content (wt%)	Time (s)	Viscosity (mPa s)	Density (kg/m³)	Asphaltene mass (g)	Asphaltene density (kg/m³)	Primary particle diameter (µm)	Sediment porosity (φ)
55	180	1.8898	808.30	1.3604	1249	1	0.0671
55	1200	1.8898	808.30	1.3604	1249	1	0.0671
55	1800	1.8898	808.30	1.3604	1249	1	0.0671
55	2700	1.8898	808.30	1.3604	1249	1	0.0671
55	3600	1.8898	808.30	1.3604	1249	1	0.0671
62.5	180	1.3143	785.29	3.7837	1210	1	0.1300
62.5	1200	1.3143	785.29	3.7837	1210	1	0.1300
62.5	1800	1.3143	785.29	3.7837	1210	1	0.1300
62.5	2700	1.3143	785.29	3.7837	1210	1	0.1300
62.5	3600	1.3143	785.29	3.7837	1210	1	0.1300
62.5	1200	1.3143	785.29	3.7837	1210	1	0.1300
62.5	2700	1.3143	785.29	3.7837	1210	1	0.1300
72	180	0.7521	747.43	4.9943	1207	1	0.0730
72	360	0.7521	747.43	4.9943	1207	1	0.0730
72	600	0.7521	747.43	4.9943	1207	1	0.0730
82	180	0.6493	729.95	3.8772	1205	1	0.0800
82	360	0.6493	729.95	3.8772	1205	1	0.0800
82	600	0.6493	729.95	3.8772	1205	1	0.0800
90.5	180	0.4982	705.83	1.9716	1205	1	0.0250

| 90.5 | 360 | 0.4982 | 705.83 | 1.9716 | 1205 | 1 | 0.0250 |
| 90.5 | 600 | 0.4982 | 705.83 | 1.9716 | 1205 | 1 | 0.0250 |

Table C.7. Experimental solid volume fraction for the mixture *n*-heptane/WC-B-B2 at 55 wt% solvent content, at different settling times.
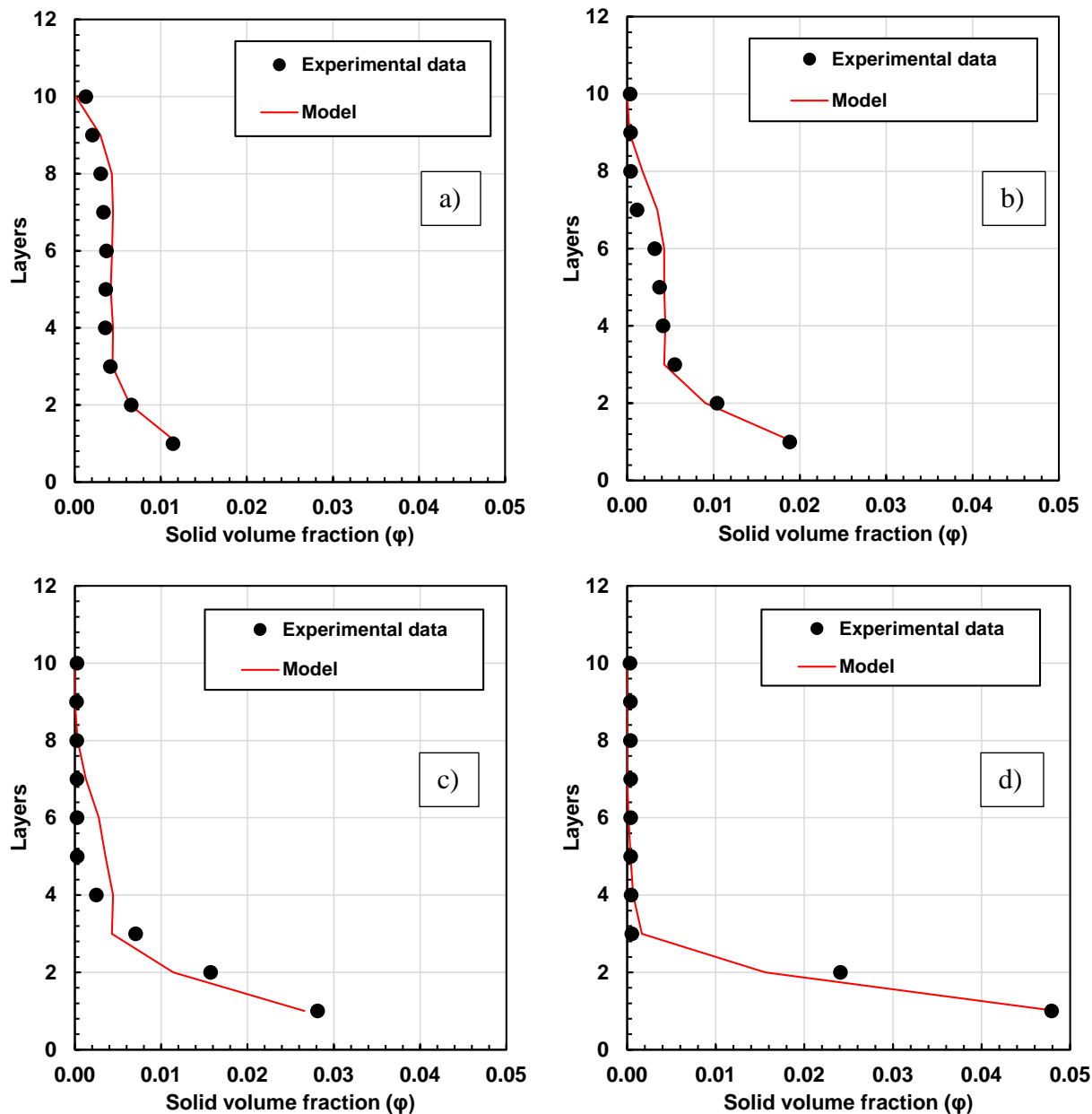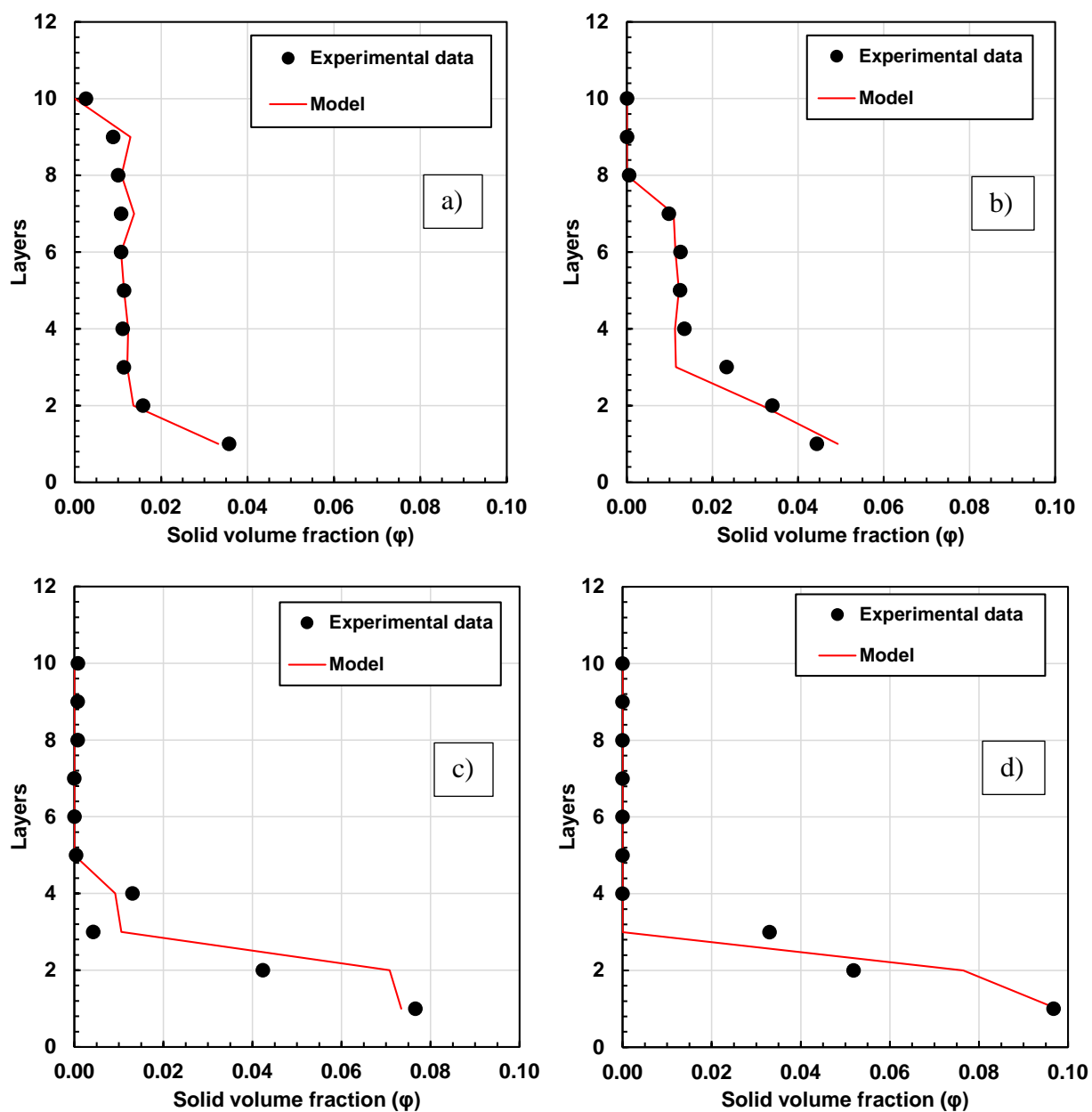
	Settling Time (minutes)				
Layer	**10**	**20**	**30**	**45**	**60**
1	0.0010	0.0001	0.0004	0.0003	0.0015
2	0.0038	0.0002	0.0003	0.0004	0.0017
3	0.0045	0.0012	0.0004	0.0004	0.0017
4	0.0049	0.0053	0.0004	0.0005	0.0019
5	0.0050	0.0037	0.0017	0.0004	0.0018
6	0.0050	0.0042	0.0006	0.0004	0.0019
7	0.0053	0.0056	0.0028	0.0008	0.0018
8	0.0055	0.0053	0.0059	0.0018	0.0101
9	0.0074	0.0106	0.0208	0.0231	0.0285
10	0.0363	0.0489	0.0529	0.1055	0.0917

Table C.8. Experimental solid volume fraction for the mixture *n*-heptane/WC-B-B2 at 62.5 wt% solvent content, at different settling times.

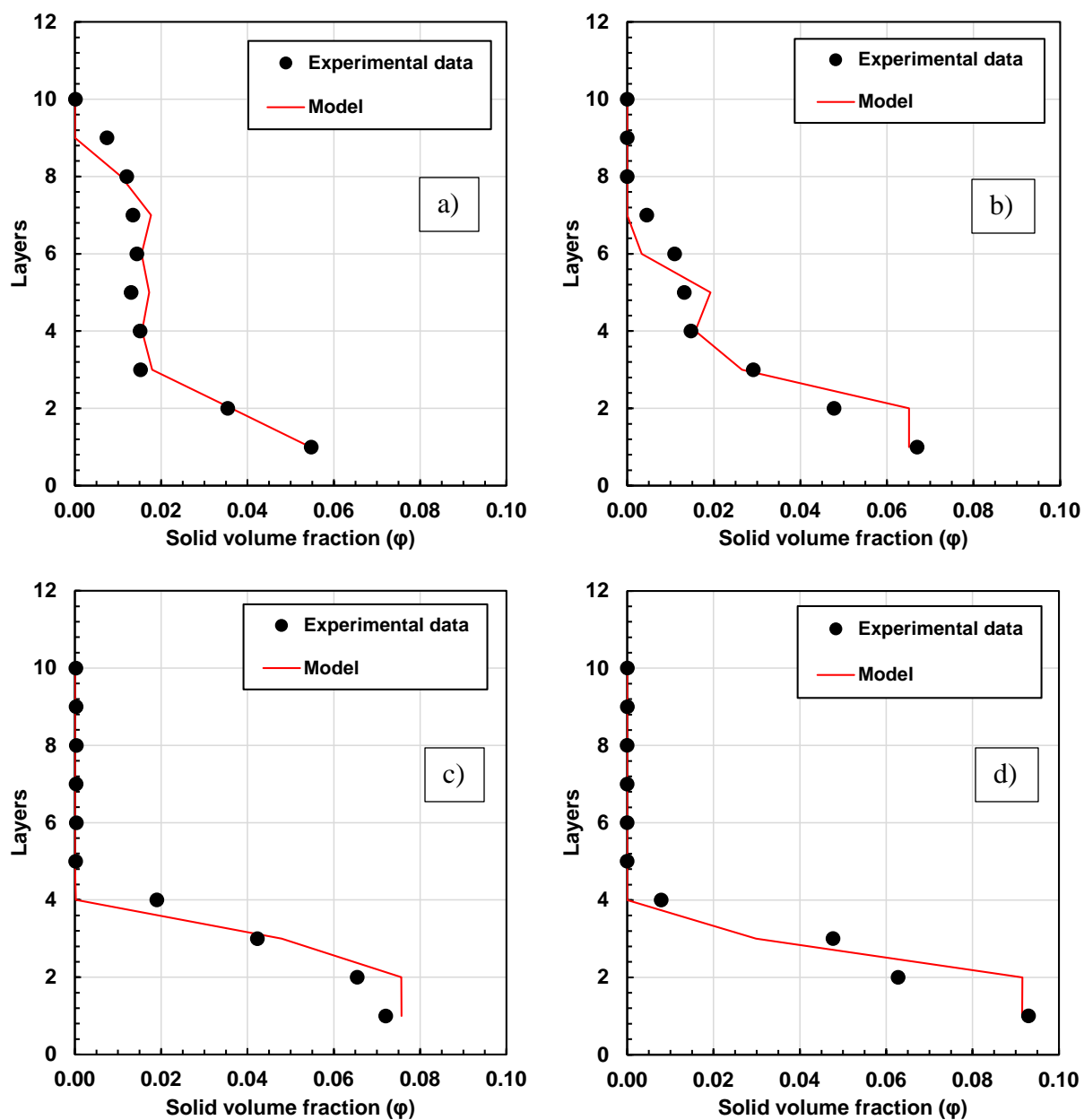|	**Settling Time (minutes)**						
Layer	**10**	**20_1**	**30**	**45_1**	**60**	**20_2**	**45_2**
1	0.0003	0.0002	0.0001	0.0003	0.0005	0.0002	0.0001
2	0.0076	0.0000	0.0001	0.0002	0.0005	0.0002	0.0002
3	0.0149	0.0003	0.0002	0.0001	0.0005	0.0003	0.0001
4	0.0105	0.0045	0.0002	0.0001	0.0004	0.0020	0.0002
5	0.0090	0.0116	0.0002	0.0001	0.0005	0.0120	0.0002
6	0.0150	0.0141	0.0014	0.0001	0.0004	0.0152	0.0004
7	0.0119	0.0180	0.0270	0.0042	0.0010	0.0116	0.0006
8	0.0156	0.0325	0.0400	0.0442	0.0429	0.0308	0.0410
9	0.0291	0.0480	0.0558	0.0544	0.0636	0.0473	0.0605
10	0.0948	0.1078	0.1480	0.3154	0.1400	0.2022	0.2290

Appendix D: Profiles fit with settling model

This appendix presents the solid volume fraction profiles of asphaltene floc with the settling model.
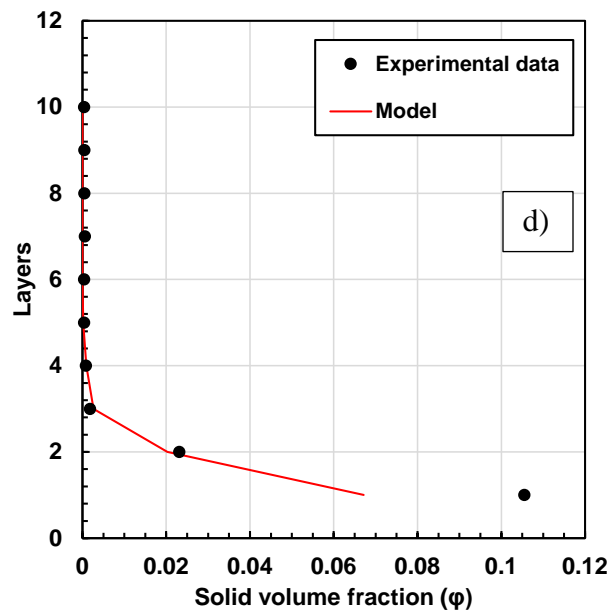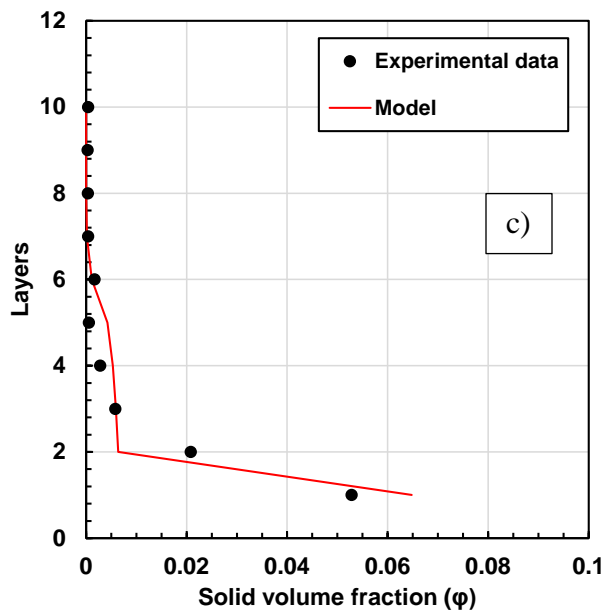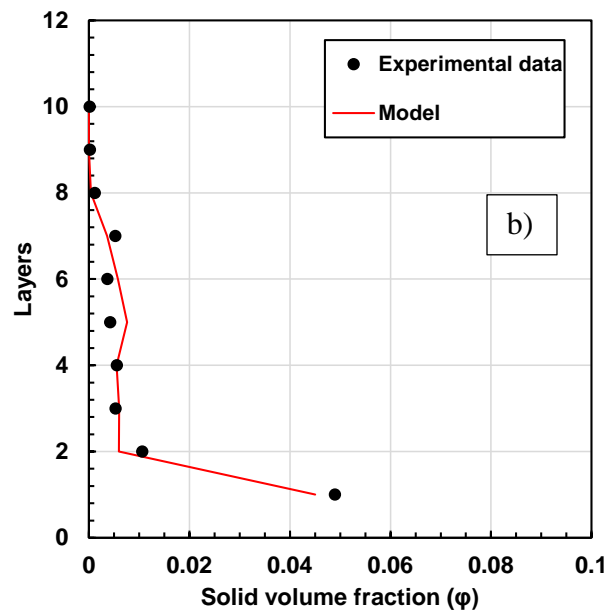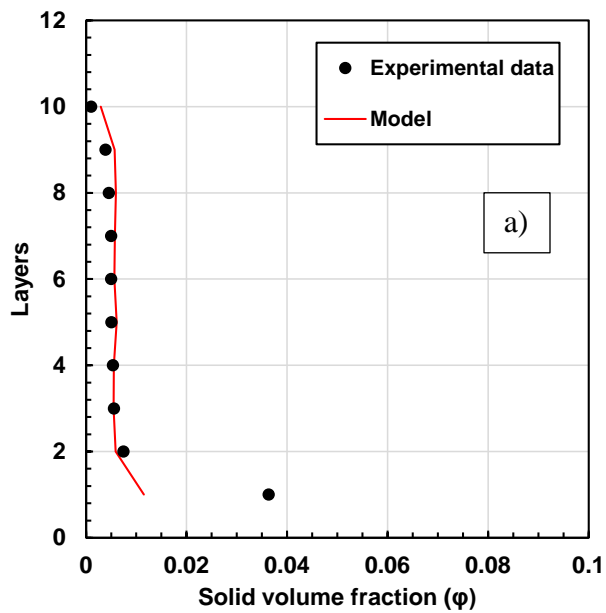

Figure D.1. Fit asphaltene volume fraction profile with the settling model for the mixture *n*-heptane/WC-B-A3 at 60 wt% solvent content after a) 20, b)40, c)60 and d)120 minutes of settling time.
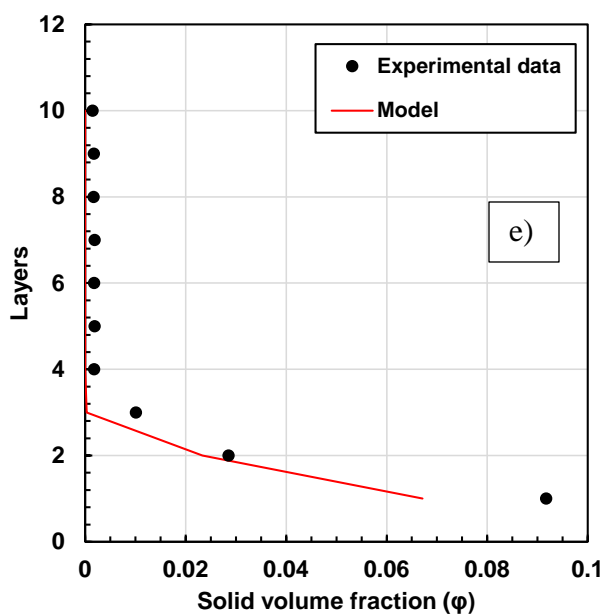
**Figure D.2.** Fit asphaltene volume fraction profile with the settling model for the mixture *n*-heptane/WC-B-A3 at 65 wt% solvent content after a) 20, b)60, c)120 and d)180 minutes of settling time.

**Figure D.3.** Fit asphaltene volume fraction profile with the settling model for the mixture *n*-heptane/WC-B-A3 at 72 wt% solvent content after a) 20, b)40, c)60 and d)90 minutes of settling time.

Figure D.4. Fit asphaltene volume fraction profile with the settling model for the mixture *n*-heptane/WC-B-B2 at 55 wt% solvent content after a) 10, b) 20, c) 30, d) 45 and e) 60 minutes of settling time.
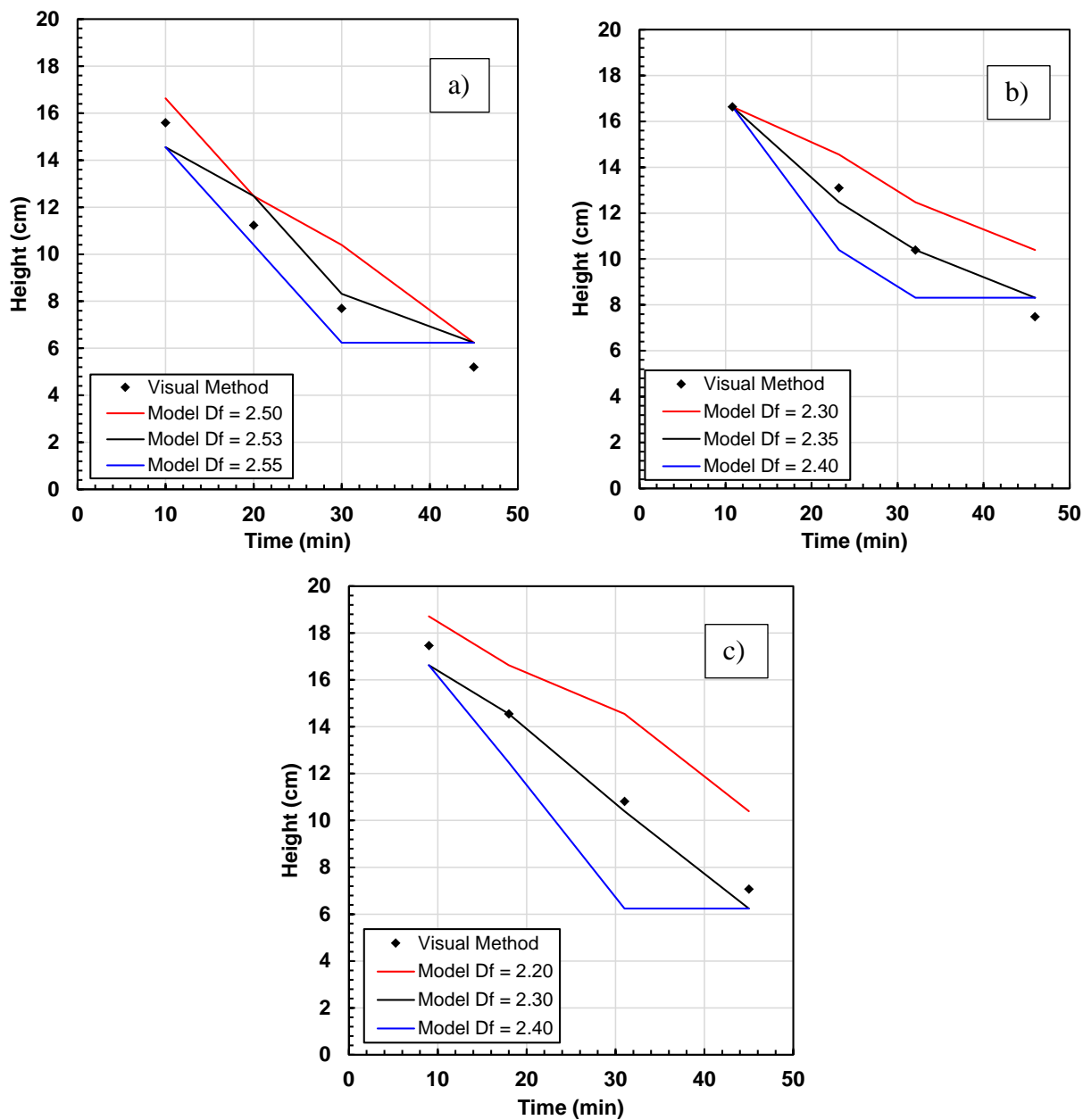
Figure D.5. Fit asphaltene volume fraction profile with the settling model for the mixture *n*-heptane/WC-B-B2 at 62.5 wt% solvent content after a) 10, b) 20_1, c) 30, d) 45_1, e) 60, f) 20_2 and g) 45_2 minutes of settling time.
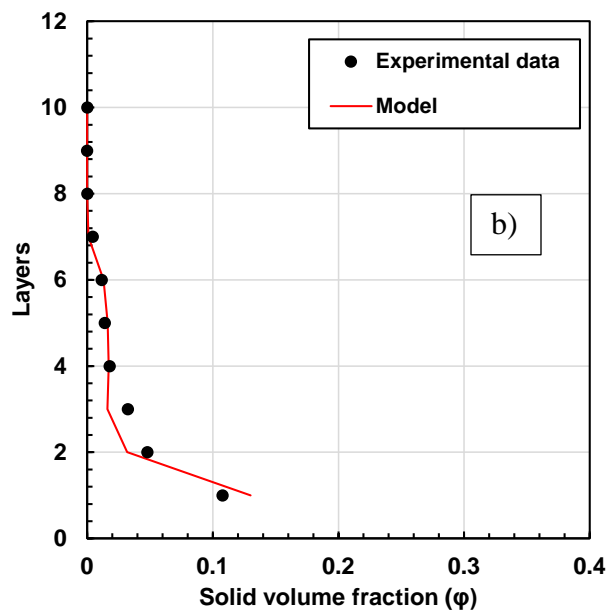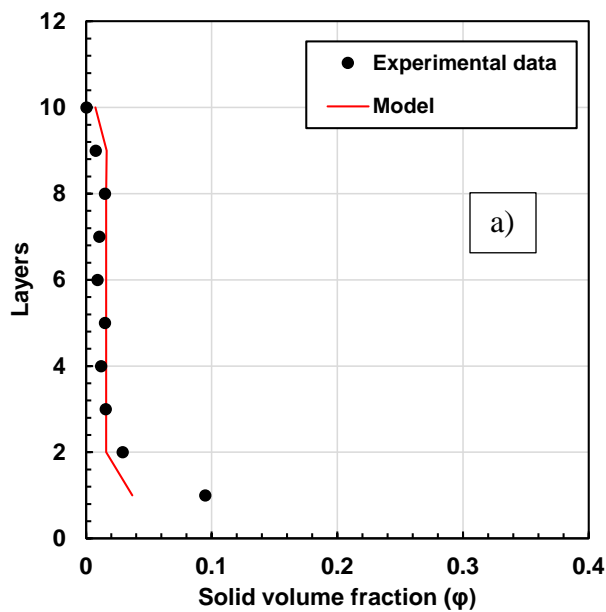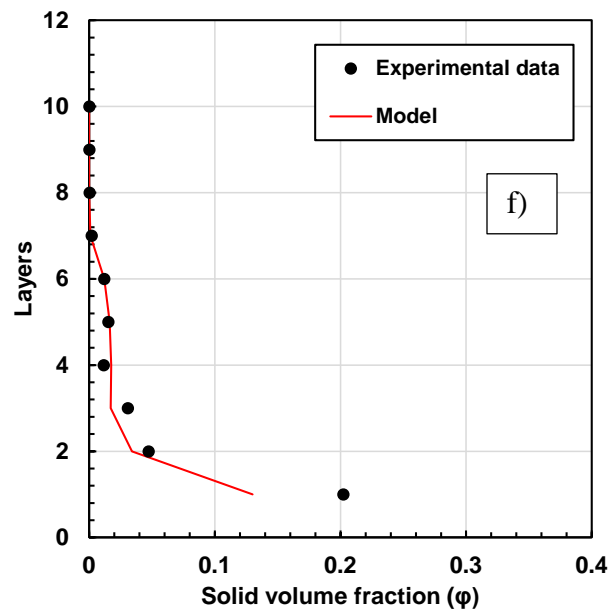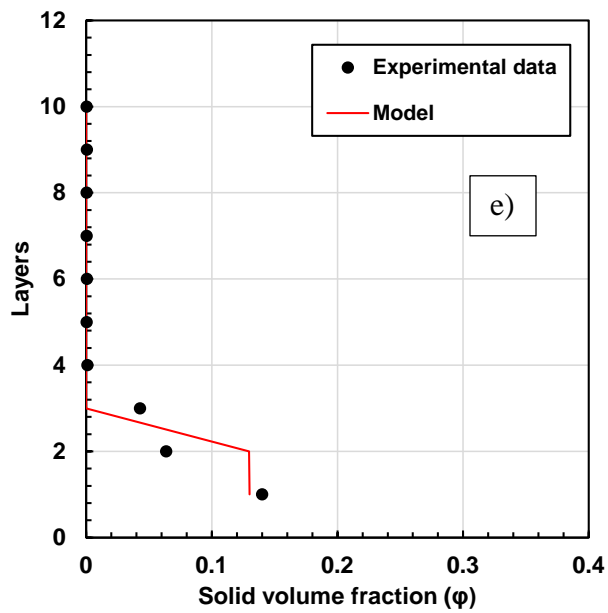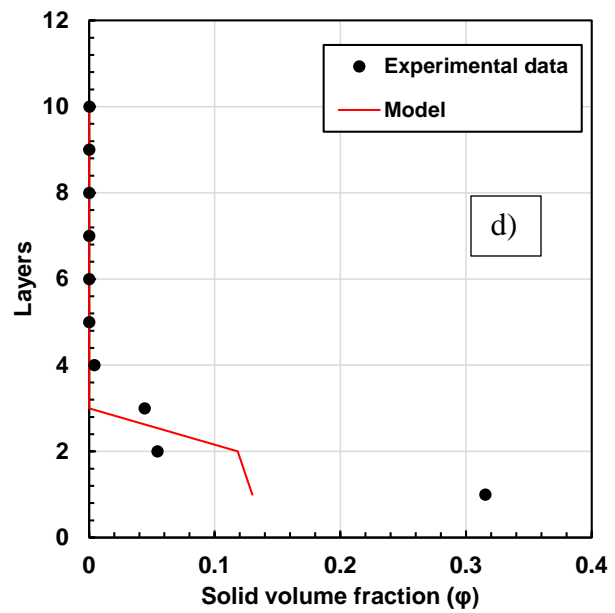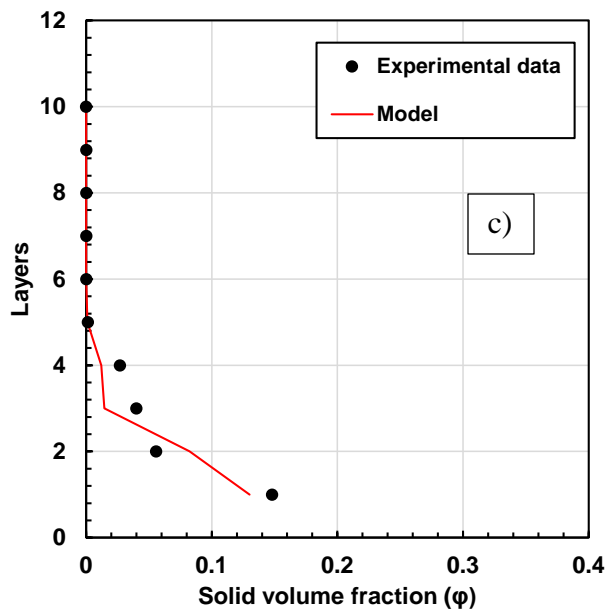
Appendix E: Model Fitting to Interface Position

This appendix presents the fit interface positions of the asphaltene flocs, calculated with the settling model.

Figure E.1. Fit asphaltene floc interface position for the mixture *n*-heptane/WC-B-A3 at a) 80, b) 90.5 and c) 95 wt% solvent content.
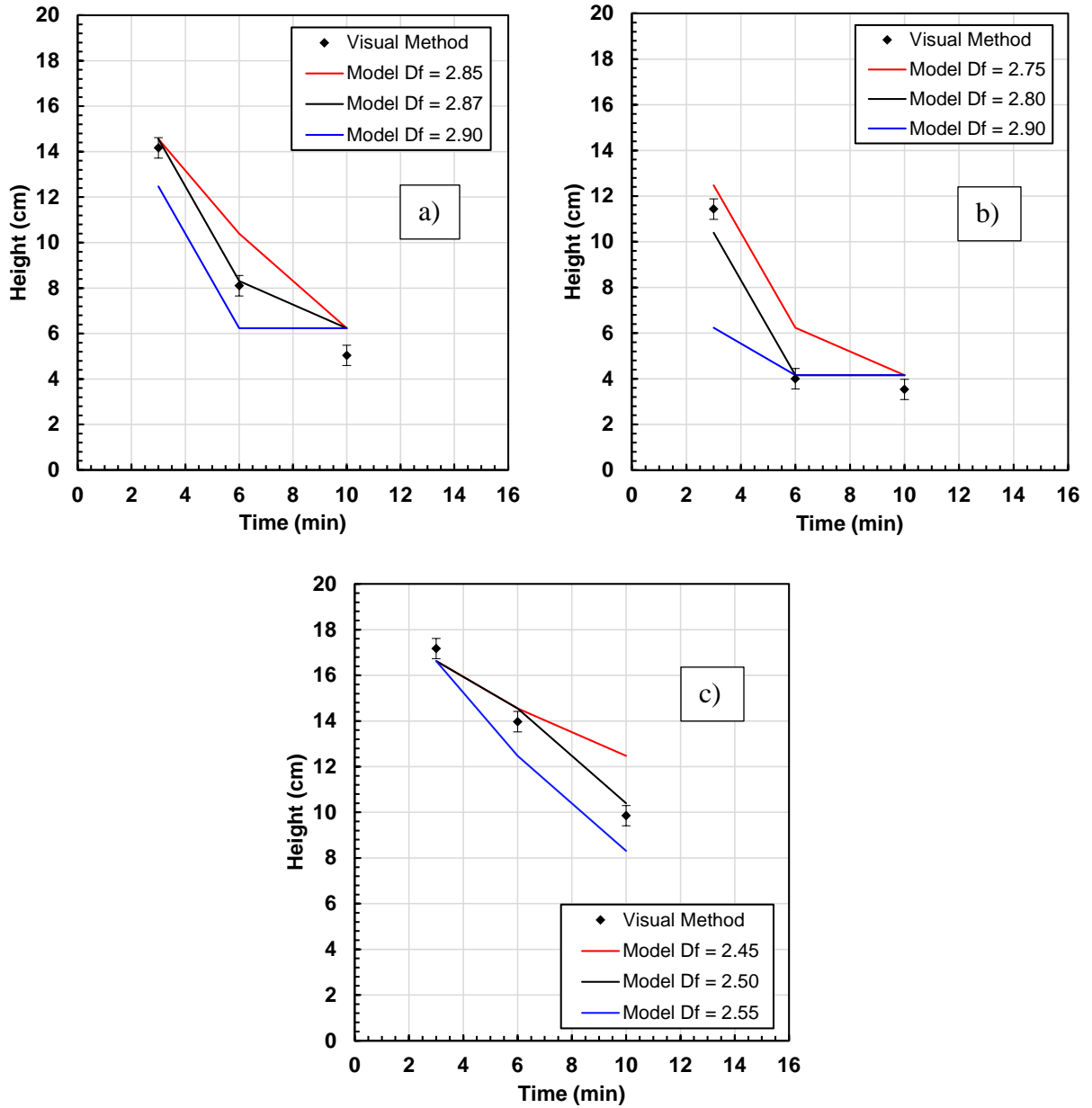
Figure E.2. Fit asphaltene floc interface position for the mixture *n*-heptane/WC-B-B2 at a) 72, b) 82 and c) 90.5 wt% solvent content.